Alma Mater Studiorum – Università di Bologna

Dipartimento di Fisica e Astronomia "Augusto Righi"
Laurea Magistrale in Fisica del Sistema Terra

Convection-permitting simulations for the attribution of extreme precipitation events in Emilia-Romagna

Presentata da:

Beatrice Albo

Relatore:
Prof. Federico Porcù

Correlatori:

Dott. Giuseppe Zappa
Dott. Paolo Stocchi

Anno Accademico 2024 - 2025
Appello V

Abstract

The work presented in this thesis analyzes the impact of anthropogenic climate change on the extreme precipitation events that struck Emilia-Romagna and Northern Adriatic coast between April 30 and May 4, 2023, and from September 17 to 20, 2024.

To this end, a novel extreme event attribution methodology is implemented, combining the storyline approach with spectral nudging and the pseudo-global warming (PGW) technique. The events are simulated using the high-resolution convection-permitting model MOLOCH (1.8 km) under both the present-day (factual) climate and a hypothetical pre-industrial (counterfactual) scenario in absence of global warming. The pre-industrial simulations are obtained by applying a thermodynamic perturbation derived from high-resolution (9 km) global climate simulations produced within the Destination Earth project, which provide the large-scale atmospheric conditions used in the storyline framework. The analysis focuses on identifying the added value of MOLOCH for the simulation of the events, on isolating the thermodynamic contribution of climate change, and evaluating how increased temperature and atmospheric moisture content can intensify extreme precipitation.

The results highlight substantial differences between the two analyzed events. The May 2023 event, dominated by well-defined dynamical drivers and orographic forcing, shows a linear increase in precipitation in the factual simulation, primarily attributable to the intensification of moisture fluxes toward the affected area. In contrast, the September 2024 event, characterized by intense convective activity, presents a more complex response, appearing to be linked to the interaction between higher moisture fluxes and thermodynamic instability. In this case, the increase in precipitation emerges clearly only in the high-resolution, convection-permitting simulations, highlighting the importance of explicit convection representation for an accurate attribution of extreme events.

Contents

Chapter 1

Introduction

1.1 Climate change and its impact on extreme events

In recent decades, atmospheric science has experienced a significant evolution with the aim of improving the understanding of the effects of anthropogenic global warming on climate dynamics. The state of the Earth system exhibits its own variability over long timescales, driven by internal oscillations and natural external forcings, which can play a prominent role in modulating climate trends over years or decades. However, the influence of such natural variability is typically small compared to the warming that can be attributed to human activities (Intergovernmental Panel on Climate Change (IPCC), 2023).

Over recent decades, the rise in global mean surface air temperature (GSAT), which is a standard indicator of global warming, has emerged as a major scientific and societal challenge. It is unequivocal that human influence, through greenhouse gas emissions, industrial activities and land-use changes such as deforestation, has resulted in a measurable warming of the atmosphere, ocean, and land. Confidence in this assessment has increased in recent years, supported by the availability of improved observational datasets and the development of climate models that are increasingly sophisticated in their ability to reproduce the historical evolution of the global climate system. Since the pre-industrial period (1850–1900), the increase in global mean surface air temperature has been primarily driven by these anthropogenic factors. The accumulation of greenhouse gases is estimated to have contributed between 1.0 °C and 2.0 °C to this trend, an effect that has been partially offset by the cooling influence of anthropogenic aerosols. Natural variability and solar factors instead had a negligible impact on global temperatures, ranging only between -0.1 °C and +0.1 °C (Intergovernmental Panel on Climate Change (IPCC), 2023).

According to recent assessments, these anthropogenic emissions are the primary driver behind the observed increase in the frequency and intensity of hot extremes, as well as

the corresponding decrease in cold extremes on a global scale. Beyond temperature shifts, human influence has significantly contributed to the rise in near-surface specific humidity and the intensification of extreme precipitation events observed across many land regions. This phenomenon is governed by a fundamental thermodynamic constraint known as the Clausius–Clapeyron relationship; as the atmosphere warms, its capacity to hold water vapour increases by approximately 7% per degree Celsius of warming. This mechanism provides additional moisture and energy to storms and flood-producing systems, aggravating their impact.

In addition, human activity has been identified as the dominant cause of large-scale environmental changes since the mid-20th century, including the loss of Arctic sea-ice, the reduction in Northern Hemisphere spring snow cover, widespread glacier retreat, the increase in ocean heat content, and the accelerating rise in global mean sea level (Intergovernmental Panel on Climate Change (IPCC), 2023).

In the context of climate change research, it is essential to distinguish between thermodynamic and dynamical responses of the climate system to warming. While thermodynamic changes associated with warming and increased atmospheric moisture are robust and well understood, larger uncertainties remain regarding changes in atmospheric circulation, both in observations, theory and models. Dynamical aspects of the climate system are more strongly influenced by internal variability and are therefore more difficult to distinguish from natural background fluctuations. Also, at regional scale the confidence is even lower because of the model sensitivity and parameterizations (Shepherd, 2016).

This distinction between thermodynamic and dynamical contributions is particularly important for understanding changes in extreme precipitation. According to the framework proposed by O'Gorman, changes in precipitation rates during extreme events under climate change depend on both thermodynamic factors, such as air saturation linked to temperature, and dynamical factors, including vertical motion, moisture convergence and large-scale circulation patterns. Moreover, extreme precipitation events are not solely controlled by local temperature increases, but are strongly influenced by the advection of water vapour from oceanic regions, for example through atmospheric rivers. Increases in sea surface temperatures act as a primary driver of extreme precipitation by enhancing moisture availability, thereby contributing to more intense and frequent precipitation extremes under favourable atmospheric conditions of instability (O'Gorman, 2015).

Despite the complexity of these processes and the uncertainties associated with circulation changes and regional variability, precipitation extremes tend to intensify under climate warming, although with substantial regional variability. These regional differences reflect the complex interplay between thermodynamic forcing and circulation changes, highlighting the importance of studying extreme precipitation events (EPEs), as they represent the most direct way in which society experiences the impacts of climate change. They are often short-lived and spatially localized but capable of causing severe flooding, landslides, and widespread damage, as well as disrupting critical infrastructure and causing large economic losses, particularly in agriculture and urban environments. The

severity of the damage observed in recent years is illustrated, for example, by hundreds of fatalities and economic losses exceeding €17 billion in Spain in 2024 (Barriopedro et al., 2025), as well as by the estimated €8.8 billion associated with the 2023 Emilia-Romagna floods (Scoccimarro, Borrelli, Sangelantoni, et al., 2025). This further demonstrates that research on extreme precipitation is not merely an issue of academic importance, but also a critical tool for public safety and risk reduction.

Future projections studies indicate a further amplification of climate extremes under continued global warming. For example, a global mean temperature increase of 1.5°C is projected to be reached in the near term (2021–2040) across almost all scenarios. With increasing warming, it is nearly certain that hot extremes and heatwaves will become more frequent, intense, and persistent worldwide, while cold extremes will continue to decline, with particularly severe consequences for human health (Intergovernmental Panel on Climate Change (IPCC), 2023).Increasing global temperatures provide a thermodynamic background that favors the intensification of the hydrological cycle. In this context, there is high confidence that extreme precipitation events will intensify across most regions, even where mean seasonal rainfall may decrease. An overall increase in precipitation variability is expected, with future climatic conditions characterized by fewer rainy days, enhanced drought conditions, and a higher likelihood of short-duration, localized, and intense precipitation events. The intensity of such extremes is influenced by increasing atmospheric moisture availability and may, at local scales, exceed Clausius–Clapeyron expectations. This intensification is projected to substantially increase flood risk, with event-based studies suggesting that, in a climate warmer by 3°C, accumulated precipitation during extreme events could be up to twice that of the pre-industrial climate (Lenderink et al., 2025).

In this context, understanding the mechanisms governing extreme precipitation remains a central challenge in climate science. Changes in such events arise from a complex interplay between thermodynamic factors, linked to increasing atmospheric moisture, and dynamical processes, including circulation patterns, moisture transport, and vertical motion, whose responses to climate change are often masked by strong internal variability, particularly at the regional scale.

This complexity highlights the need for targeted, event-based analyses that adopt a meteorological perspective to investigate extreme precipitation within a climate framework. By combining an attribution methodology with detailed meteorological analyses of the atmospheric processes driving high-impact events, this work aims to contribute to a more robust understanding of how and why extreme precipitation is changing, with particular focus on May 2023 and September 2024 floods in Emilia-Romagna, and to assess the implications of these changes in a warming climate.

1.2 Recent precipitation events and flooding in Emilia-Romagna (2023 - 2024)

Within this wider framework of climate change and increasing hydroclimatic extremes, the Mediterranean region is highly vulnerable, as extreme precipitation events constitute a major source of weather-related damage (Campos et al., 2025). This pronounced sensitivity is closely linked to rising Mediterranean Sea surface temperatures, which is identified as a primary driver of energy supply for storm systems, as said before. Elevated sea surface temperatures (SST) enhance evaporation and atmospheric moisture availability, thereby intensifying low-pressure systems, thermodynamic instability and favouring the development of more intense precipitation events.
For these reasons, this study wants to investigate extreme precipitation events that have recently affected Italy, with a particular focus on the Emilia-Romagna region. Recent studies based on the Cyclone Density Persistence (CDP) index have shown that the Italian Peninsula exhibits some of the highest levels of cyclonic activity in the Mediterranean, especially over the Tyrrhenian and Ionian sectors. However, Emilia-Romagna is not among the regions where Mediterranean cyclones most frequently develop; rather, its orography makes it particularly favourable for intercepting and accumulating the moisture fluxes associated with such systems (Scoccimarro, Borrelli, Sangelantoni, et al., 2025).

The analysis focuses on two case studies: the first phase of May 2023 flood, which occurred from 30 April to 4 May 2023 (1^{st} event), and the 2^{nd} event that took place more than one year later, between 17 and 21 September 2024, associated with the remnants of a storm that impacted large parts of Europe. The primary drivers of these events are the regional orography and the persistence of cyclonic systems over the Mediterranean basin, factors that make the Italian territory a key target for the study of extreme precipitation events.

The 2023 event caused one of the most devastating floods in recent Italian history, leading to more than 36,000 displacements, 15 fatalities, a lot of landslides, hundreds closed roads and severe damages affecting infrastructure, rivers and ecosystems (Wu, Hartmuth, and Wernli, 2026). This event was classified as extremely rare, with an estimated return period of about 500 years. It was triggered by the Mediterranean cyclone "Minerva", which originated over North Africa and moved northward toward central Italy, where it remained quasi-stationary throughout the duration of the event. This prolonged stationarity led to a persistent blocking configuration, which represents a defining feature of the event. Unlike short-lived convective extremes characterized by intense hourly rainfall peaks, this event was not dominated by particularly strong hourly precipitation intensities. Instead, the severe impacts resulted from sustained and continuous precipitation over several consecutive days, driven by the persistent advection of moist air from the Adriatic Sea toward the Po Valley. This configuration is rela-

tively typical of the Emilia-Romagna region and explains why it's frequently affected by long-lasting precipitation events. In these cases, the so-called "cul-de-sac effect" occurs, whereby moisture is effectively trapped over the region by the Apennine chain, limiting its dispersion and confining the water vapour flux within a semi-enclosed geographical basin that is open primarily to south-easterly flows (Scoccimarro, Borrelli, Sangelantoni, et al., 2025).

In September 2024, the Emilia-Romagna region was affected by another severe precipitation event. Over a four-day period, the region received rainfall amounts equivalent to approximately three months of climatological precipitation (Foraci et al., 2024). This event was associated with Storm Boris, which was first identified over the Gulf of Genoa on 11 September and subsequently led to record-breaking precipitation across large parts of central Europe. During the first stage of the storm rainfall totals equivalent to two to five times the average September precipitation were recorded over wide areas of Poland, the Czech Republic, and Austria, causing widespread flooding and severe impacts on local communities (CIMA Foundation, 2025). After producing severe impacts across central Europe, the system became partially blocked over eastern Europe before undergoing a retrograde motion toward northern Italy. There, its persistence over the region, together with the presence of the Adriatic Sea with high SST, favoured sustained moisture transport and led to intense precipitation over Emilia-Romagna. Sea surface temperature anomaly played a key role in amplifying this event, with an estimated return periods exceeding 200 years. Indeed, during August 2024, the average Mediterranean SST reached the pick of 28.7°C (Copernicus Climate Change Service, 2024), and at the time of Boris' formation, large portions of the Tyrrhenian, Ionian, and Adriatic Seas exhibited anomalies exceeding +3.5°C, with peaks above +4.5°C in the central–northern Adriatic (Figure 1.1) (Foraci et al., 2024).
This event differed substantially from the May 2023 flood in terms of its dominant precipitation processes. While the 2023 event was associated with persistent large-scale forcing, the 2024 episode was characterized by intense convective activity, with very high precipitation peaks reached over short time scales, in some cases within only a few hours. The primary driver of this behaviour was the exceptionally warm post-summer sea surface conditions, which enhanced thermodynamic instability and favoured the development of localized but highly intense convective systems. As a consequence, rainfall during the 2024 event was shorter-lived but more spatially heterogeneous and locally extreme.

Although locally higher rainfall intensities and peak river levels were observed compared to May 2023, the overall extent of flooding and associated damage was smaller. This difference is largely explained by a antecedent soil moisture conditions, as soils were generally drier following the summer period and thus able to absorb a larger fraction of the rainfall, in contrast to the highly saturated conditions preceding the 2023 event (Foraci et al., 2024).

Nevertheless, according to recent studies the area affected by extreme precipitation totals exceeding 100 mm was approximately 18% larger respect to a pre-industrial cli-

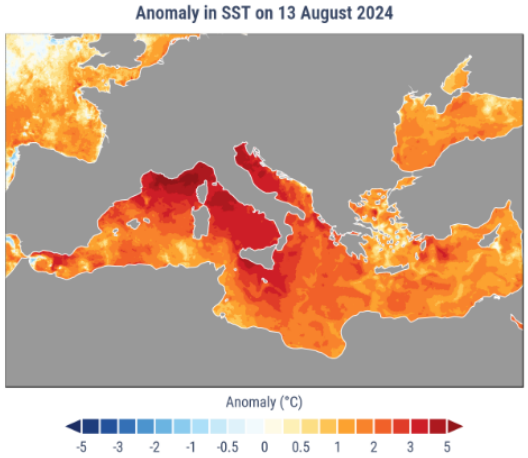

Figure 1.1: Daily Mediterranean Sea Surface Temperature anomaly (°C) on 13 August 2024, relative to the average for the 1991–2020 reference period. Source: https://climate.copernicus.eu/esotc/2024/european-ocean

mate, consistent with the influence of ongoing global warming on the spatial footprint of extreme rainfall events (Mélanie Athanase, Sánchez-Benítez, Monfort, et al., 2024).

1.3 Attribution approaches for extreme precipitation events

Within the scientific community, there has been a growing need to quantify the impact of climate change on individual extreme weather and climate events through attribution studies, as unprecedented events may arise both from natural variability and from externally forced deviations of the climate system (Shepherd, 2016). These studies differ from traditional statistical analyses of climatological trends, as they focus on local extremes associated with individual events in order to better characterize their intensity, frequency of occurrence, and spatial and temporal variability. Extreme events are therefore no longer treated as isolated anomalies, but rather as phenomena that are strongly modulated by global warming.

The underlying premise is that each extreme event must be assessed on a case-by-case basis because, although it is well established that a warmer atmosphere can favour the occurrence of extreme events, each event exhibits unique characteristics. Therefore, the primary objective of attribution studies is to provide robust physical evidence of the link between extreme events and climate change, and this also represents the main objective of the study presented. Traditionally, attribution research has developed along different approaches which help to isolate thermodynamic forcing and distinguish them from the

dynamic ones, evaluate impact and damages locally and work on prevention, bridging the gap between scientific research and real-world decision-making (European Digital Twin Earth (DESTINe), 2024).

The attribution approach relies on the comparison of two hypothetical scenarios: a "factual" scenario representing current climate conditions, and a "counterfactual" scenario describing a world without climate change, for instance by removing greenhouse gas forcing or sea surface temperature anomalies. The counterfactual climate is generated through model simulations, and statistical robustness—particularly for rare events with long return periods—is achieved using large ensemble simulations with global climate models (GCMs). A key limitation of this method is its sensitivity to uncertainties in dynamical conditions, as it assumes that events within the same category share similar underlying dynamics. Moreover, the coarse spatial resolution of global models limits their ability to adequately represent small-scale processes and convective systems (Garderen, Feser, and Shepherd, 2021).

1.3.1 Overview of probabilistic attribution approaches

In the context of attribution studies, a preliminary distinction must be made between probabilistic and deterministic approaches. The former are often referred to as risk-based approaches and focus on estimating the extent to which anthropogenic climate change has influenced a given class of events that are meteorologically similar to the event under investigation, while treating natural variability as background noise. Within this framework, the impact of climate change is quantified in terms of changes in the frequency or intensity of a given category of events, typically defined using specific physical thresholds and spatial or temporal averaging (Shepherd, 2016). The selection of these thresholds can significantly influence the results, leading to different assessments of the signal.

This type of approach primarily aims to minimize false-alarm errors by focusing on the estimation of risk, which indicates whether the studied climate change signal constitutes a necessary cause for the occurrence of an event belonging to a given class, without addressing whether that cause is also sufficient. Consequently, while risk-based approaches are fundamental for risk management policies and long-term planning, they are less suitable for the investigation of localized extreme events and for providing a detailed physical understanding of the processes involved (Shepherd, 2016). In addition, analogue-based methods represent a conditional attribution approach that provides a conceptual bridge between probabilistic and deterministic approaches (Barriopedro et al., 2025). This technique is based on the identification, within historical observations or climate model simulations, of circulation analogues characterized by atmospheric patterns similar to those associated with the extreme event under analysis. Attribution is performed by comparing sets of analogues representative of present-day (factual) and past (counterfactual) climate conditions, typically using similarity metrics applied to large-scale circulation fields such as sea-level pressure or geopotential height (Faranda

et al., 2024). The main advantage of this method compared to the previously described approach is that it preserves similar atmospheric circulation between the two scenarios, thereby allowing the thermodynamic component and the contribution of warming to be isolated, reducing dynamical uncertainty and increasing the signal-to-noise ratio (Barriopedro et al., 2025).

An important contribution to this methodology is provided by the ClimaMeter platform, which delivers rapid analyses of extreme events shortly after their occurrence. This enables extremes to be contextualized in terms of their intensity, persistence, and predictability, in direct relation to the associated atmospheric dynamics and circulation patterns. However, a key limitation of this approach is its reduced reliability when applied to unprecedented events, because the statistical robustness of the results is limited by the relatively small number of analogs. Moreover, the results are sensitive to the choice of the reference period used to identify analogues and to the spatial domain over which the events are occurred (Faranda et al., 2024).

1.3.2 Storyline-based attribution approaches

Storyline-based methods are deterministic approaches that focus on the causal chain of physical processes leading to the occurrence of a specific extreme event as it actually unfolded, explicitly accounting for the contribution of natural climate variability. Attribution is performed in a conditional manner, in that the presence of anthropogenic warming is taken as given and the aim is to provide a refined estimate of its contribution. Specifically, these methods seek to assess how a particular event and the physical processes characterizing it have been influenced by the thermodynamic conditions associated with climate change, which are already well established. Therefore, the main advantage of this approach—similarly to analogue-based methods—is its ability to isolate the thermodynamic response of the system to warming by conditioning on event-specific dynamical configurations. This is again accompanied by a reduction in internal variability. However, these methods provide only partial attribution, as they do not address whether the dynamical conditions that led to a specific extreme event were themselves influenced by climate change (Shepherd, 2016).

Pseudo-global warming studies

Within the storyline framework, the Pseudo–Global Warming (PGW) approach is an event-oriented method used to explore how specific extreme events evolve under different climate states. Instead of running long-term continuous simulations, PGW focuses on "re-running" an observed historical event—typically a past (cooler), present-day, and future (warmer) scenario—to isolate the impact of thermodynamic changes (Lenderink et al., 2025).

The core of the method lies in applying thermodynamically consistent perturbations to the atmospheric initial and lateral boundary conditions of a specific event. These perturbations are typically derived from the mean climate change signal projected by Global Climate Models (GCMs), calculated as the difference in variables such as temperature, specific humidity, and sea surface temperatures between a future period and a historical baseline. It is important to emphasize that these perturbations represent a mean warming signal and are not event-specific, allowing to investigate how a fixed circulation pattern responds to a warmer background state.

While some implementations use spectral nudging to constrain the large-scale atmospheric circulation and keep it aligned with observations across scenarios, this is not an inherent requirement of the PGW approach. In many cases, the combination of prescribed boundary conditions and the short time horizon of the simulations provides enough constraint to maintain the invariance of the large-scale flow. This focused approach allows for a robust separation of the forced thermodynamic signal from internal variability, a task that remains challenging for next-generation Storm Resolving Earth System Models (GSRMs) and regional Convection Permitting Models (CPMs) when limited by simulation length (Lenderink et al., 2025).

Within this context, the PGW approach enables high-resolution simulations at relatively modest computational cost, making it well suited for event-based analyses that focus on individual extreme events rather than long continuous climate simulations.

Dynamical downscaling

Although the PGW approach can be applied at any scale, its application to extreme precipitation in this study necessitates dynamical downscaling as a specific technical choice rather than an intrinsic requirement of the method. GCMs generally struggle to accurately simulate rainfall frequency, intensity, and the timing of the diurnal cycle due to their coarse spatial resolution (about 100 km) and reliance on parameterized convection. These global models often fail to resolve the local forcing agents—such as complex orography, coastlines, and land–surface heterogeneity—that are critical for the development and evolution of localized extremes.

In this framework, dynamical downscaling serves to translate the large-scale climate information, modified by the PGW signal, into physically consistent regional responses. This is achieved by using the output of a GCM or reanalysis to drive a Regional Climate Model (RCM) or a Convection-Permitting Model (CPM) over a nested, smaller domain at higher spatial resolution (Fig. 1.2). The information flux is strictly unidirectional, moving from the GCM to the nested model, and for physical consistency, the nesting ratio is typically constrained to not exceed a value of 12 (Giorgi, 2019).

By operating at kilometer-scale resolution, this nested configuration allows for the explicit representation of deep convection, enabling a detailed investigation of the spatiotemporal characteristics of rainfall and associated phenomena like wind gusts, hail,

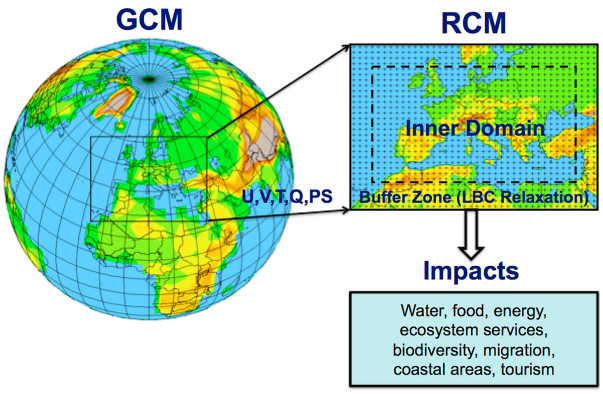

Figure 1.2: Schematic illustration of dynamical downscaling from a Global Climate Model (GCM) to a nested Regional Climate Model (RCM). Source: https://doi.org/10.1029/2018JD030094

and lightning (Lenderink et al., 2025). Consequently, downscaling captures how extreme events are modulated by local-scale processes that remain unresolved in global models but are critical for real-world impacts. Ultimately, this approach provides a more detailed representation of regional climate variability by transforming a broad, non-event-specific warming signal into a realistic local-scale response tailored to the physical requirements of the event under study.

Spectral nudging storyline method

Spectral nudging is a climate modelling technique recently developed within storyline-based attribution approaches. It represents a key added value of these methods compared to probabilistic approaches, as it allows the large-scale atmospheric circulation to be constrained, thereby enabling a focused assessment of the purely thermodynamic impacts of climate change. This method consists of constraining the simulated atmosphere to closely follow the observed large-scale circulation during a given event, thus allowing the same meteorological situation to be reproduced under different levels of global warming (Campos et al., 2025).

In this regard, the lower levels of the atmosphere are left free to respond to the imposed warming and to evolve dynamically, enabling the investigation of the physical processes governing local-scale dynamics. The general principle is that the realistic large-scale state provided by reanalysis data is followed by the global climate model (GCM), while at smaller spatial scales the model develops additional detail to better represent high-resolution weather patterns. An important advantage of this approach is its selectivity, as it reduces inconsistencies among datasets across different simulated scenarios, while leaving only selected fields within the boundary layer unconstrained (Garderen, Feser, and Shepherd, 2021).

Typically, synoptic-scale fields such as vorticity and divergence are constrained (nudged) over high tropospheric levels, while targeting only large horizontal scales on the order of 1000 km (Mélanie Athanase, Sánchez-Benítez, Monfort, et al., 2024). This configuration allows researchers to compare the same extreme event across different climate states, thereby providing deeper insight into how global warming modulates local weather extremes (Garderen, Feser, and Shepherd, 2021). As a result, the physical interpretation of climate change impacts becomes more intuitive beyond the scientific community, contributing to improved understanding and more effective impact prevention.

Destination Earth project

Destination Earth is a European Union initiative launched in 2022 with the objective of developing a digital twin of the Earth system, aimed at advancing the understanding of climate change and its impacts. As such, it represents a valuable resource for the present work, as it provides a physically consistent framework to assess whether and to what extent climate change influences the three extreme events studied and their characteristics.

One of the core components of the DestinE programme is the Climate Digital Twin for Adaptation, developed by ECMWF, which delivers kilometre-scale climate simulations at global, regional, and national scales over multi-decadal periods. These simulations reproduce pre-industrial climate conditions (around 1950), present-day conditions (2017–2024), and future scenarios corresponding to a global warming level of +2°C relative to pre-industrial levels (Destination Earth, 2024). This enables the investigation of counterfactual and factual scenarios, addressing "what-if" questions regarding how specific extreme events—such as floods or heatwaves—would have unfolded under different climatic backgrounds.

The Climate Digital Twin simulations are based on the coupled IFS–FESOM modelling system, which combines the Integrated Forecasting System (IFS) with the Finite Element Sea Ice–Ocean Model (FESOM), ensuring a physically consistent representation of atmosphere–ocean interactions. The simulations combine kilometre-scale atmospheric and oceanic modelling, with spatial resolutions of approximately 5–10 km for the for atmospheric, land, ocean and sea-ice components, representing a substantial advance over traditional global climate models that typically operate at resolutions of order 100 km. The considerable computational requirements of these high-resolution, multi-decadal simulations are addressed through the use of European high-performance computing infrastructures within the EuroHPC framework, including flagship supercomputers such as LUMI in Finland and Leonardo in Italy (European Digital Twin Earth (DESTINe), 2024).

In this context, large-scale atmospheric conditions are constrained to realistic states derived from reanalysis products such as ERA5, while smaller-scale processes, including convection and orographically induced precipitation, are allowed to evolve freely

according to the high-resolution model physics. This configuration aligns with the storyline attribution approach, in which the dynamical conditions associated with an event are held fixed and the response of local-scale processes to changes in thermodynamic forcing—particularly greenhouse gas concentrations and sea surface temperatures—is isolated.

By enabling the direct comparison of the same events under real and hypothetical climate conditions, the Destination Earth framework provides a powerful tool for attribution studies that complements and extends traditional probabilistic approaches, offering physically grounded insight into how climate change modulates local extreme events and their impacts.

1.4 Aims and research questions

This study aims to investigate the connection between anthropogenic climate change and specific extreme precipitation events. In particular, the primary objective is understanding the impact of climate change on the extreme precipitation events that have affected Emilia – Romagna in 2023 and 2024. Thermodynamic amplification as a key mechanism in Mediterranean flood events and, while traditional climatology has focused on average statistics and trends, high-resolution, physically consistent storyline simulations offer a robust framework for event-based attribution (Campos et al., 2025). This research proposes an event-based attribution study through a counterfactual question: "Would these events have emerged and evolved in the same way in a climate without global warming?".

A key contribution of this work lies in its methodological approach, which combines a storyline-based framework with the pseudo-global warming (PGW) technique and high-resolution simulations using the MOLOCH convection-permitting regional climate model. This allows the same extreme event to be analyzed under different thermodynamic climate states while maintaining comparable large-scale dynamical conditions. Despite recent advances in global storyline experiments within the Destination Earth project, the explicit resolution of convective processes is essential for accurately representing precipitation extremes and their variability, since they are poorly represented in coarser global models. This aspect is particularly important in regions characterized by complex topography, such as the Emilia-Romagna region, where orographic effects must be taken into account. To generate the thermodynamic scenarios, the study uses data from the European Destination Earth (DestinE) project, which provides high-resolution climate simulations for the pre-industrial and present-day periods. By comparing these scenarios, thermodynamic deltas are calculated and then applied to MOLOCH simulations to create the "factual" and "counterfactual" scenarios, which are essential for the attribution analysis. Consequently, a primary research question was to identify the limitations of spectrally-nudged DestinE simulations with parameterized convection, and to determine whether the climate change response is altered by convective processes.

Building on this framework, the study investigates how extreme precipitation responds to warming across events characterized by different dominant physical mechanisms. In particular, one of the central questions addressed in this study concerns whether the climate change signal manifests consistently in convective events compared to those primarily driven by large-scale dynamical features, such as atmospheric blocking or quasi-stationary circulation. This comparative perspective is motivated by the well-established robustness of the thermodynamic contribution to extreme precipitation under warming, contrasted with the larger uncertainty surrounding the role of atmospheric circulation and dynamical variability. Special attention is given to convective extremes for which the sensitivity of precipitation intensity to temperature remains more uncertain and strongly dependent on local-scale processes. The inclusion of the 2024 flood event, marked by intense deep convection and a quasi-stationary cut-off low, provides an ideal context for evaluating the added value of convection-permitting simulations.

In summary, the thesis seeks to introduce a new methodology to isolate the thermodynamic contribution of climate change to extreme events, assess whether changes in temperature and humidity are sufficient to explain their intensity, or whether dynamical processes also play a critical role. Although natural variability continues to influence individual events, it offers a more detailed understanding of the physics of high-impact weather events and their societal implications.

Chapter 2

Methods, models and data

This chapter presents the methodologies applied to the case studies presented in this thesis. The primary tool used for the analysis of extreme events is the MOLOCH model, which is described in Section 2.1. The following paragraphs outline the approach adopted for the attribution study, which includes a factual simulation (referred to the present climate) and a counterfactual one (referred to a pre-industrial climate) for each event analysed. The whole procedure adopted to generate these simulations, including the specific model configuration, is detailed in Section 2.2. Section 2.3 describes the datasets used for model evaluation, while Section 2.4 introduces the diagnostic methodologies applied in the analysis.

2.1 The convection-permitting model MOLOCH

MOLOCH (Modello Locale in Hybrid Coordinates) is a high-resolution, non-hydrostatic model designed to provide detailed atmospheric simulations and mesoscale weather forecasting, with its primary advantage being the explicit resolution of convective processes (ISAC-CNR, 2012). Originally developed for research purposes at the Institute of Atmospheric Sciences and Climate (ISAC) of the Italian National Research Council (CNR), MOLOCH is now employed for both operational forecasting and research activities at several national centers (Mariani et al., 2015).

2.1.1 Model dynamics and physical parameterizations

MOLOCH integrates a set of fully compressible dynamical equations and includes parameterizations for boundary-layer turbulence, radiation, soil physics, and cloud microphysics. It typically operates at grid spacings of 1–4 km, allowing the explicit representation of deep convection without the need for convective parameterization (Malguzzi et al., 2006). The prognostic variables include pressure p, absolute temperature T, specific

humidity q, the horizontal (u,v) and vertical (w) components of wind velocity, turbulent kinetic energy (TKE), and five microphysical water species. These variables are represented in latitude and longitude on a rotated Arakawa C-type grid, and this requires the interpolation of the model fields from the rotated grid to the geographical grid during the post-processing phase.

The set of equations solved by the model includes the three momentum equations (Eq. 2.1, 2.2, 2.3), the continuity equation (Eq. 2.4), the equation expressing the first law of thermodynamics (Eq. 2.5), and the equation of state for a perfect gas (Eq. 2.6):

$$\frac{Du}{Dt} - \frac{uv\tan\phi}{a} + \frac{uw}{a} = -\frac{1}{\rho}\frac{\partial p}{\partial x} + 2\Omega v\sin\phi - 2\Omega w\cos\phi + F_{rx} \tag{2.1}$$

$$\frac{Dv}{Dt} + \frac{u^2\tan\phi}{a} + \frac{vw}{a} = -\frac{1}{\rho}\frac{\partial p}{\partial y} - 2\Omega u\sin\phi + F_{ry} \tag{2.2}$$

$$\frac{Dw}{Dt} - \frac{u^2+v^2}{a} = -\frac{1}{\rho}\frac{\partial p}{\partial z} - g + 2\Omega u\cos\phi + F_{rz} \tag{2.3}$$

$$\frac{1}{\rho}\frac{D\rho}{Dt} + \nabla\cdot\mathbf{U} = 0 \tag{2.4}$$

$$c_v\frac{DT}{Dt} + p\frac{D\alpha}{Dt} = J \tag{2.5}$$

$$\frac{1}{\rho} = \frac{R_d T}{p} \tag{2.6}$$

The equations are expressed in a spherical coordinate system (λ, ϕ, z), where λ is longitude, ϕ is latitude, and z is the vertical distance above the Earth's surface, while the unit vectors i, j, k are directed eastward, northward, and upward, respectively (Holton and Hakim, 2012).

MOLOCH resolves the atmosphere using hybrid vertical levels, employing the ζ (*zita*) coordinate as a terrain-following hybrid vertical coordinate that imposes a lower boundary condition (ISAC-CNR, 2012). This coordinate system is particularly suitable for high-resolution simulations, as it closely follows the underlying orography in the lower layers (the so-called *sigma* levels) and transitions through a smooth transformation to standard pressure levels with increasing altitude, eventually approaching horizontal surfaces where the influence of the terrain becomes negligible (Figure 2.1). The ζ coordinate is defined as follows:

$$\zeta = H\left(1 - e^{-\frac{z-h\left(1-\frac{\xi}{H}\right)}{H}}\right) \tag{2.7}$$

where h denotes the orographic height ($h < z < \infty$), $H = \frac{R_d T_0}{g}$ is the tropospheric scale height, R_d is the specific gas constant for dry air, g is the acceleration due to gravity, and T_0 is a reference temperature (Davolio, Buzzi, and Malguzzi, 2006).

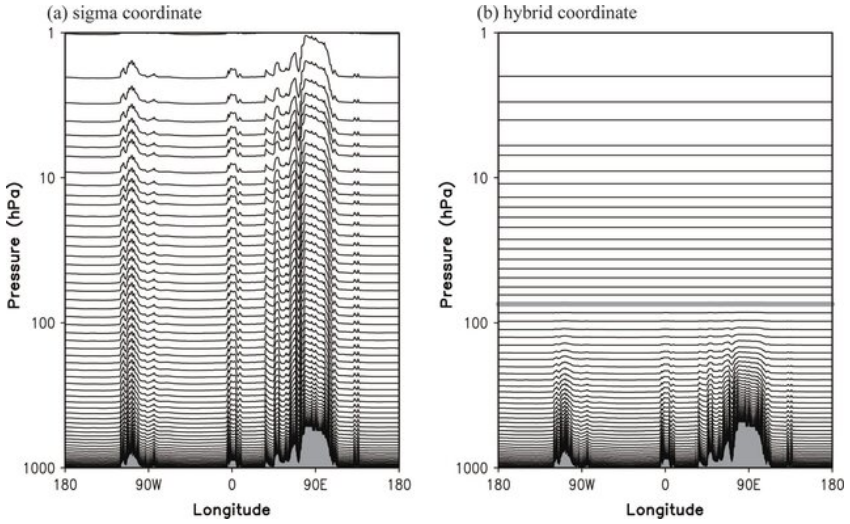

Figure 2.1: Vertical profile of coordinate surface versus pressure for the (a) sigma and (b) hybrid vertical coordinates. Topographic elevations are shaded light gray. Adapted from (Koo and Hong, 2013)

The dynamical equations are integrated in time using a semi-implicit scheme, since an implicit scheme for vertically propagating acoustic waves is adopted, while the remaining terms are treated with explicit time-splitting schemes. Three-dimensional advection is computed using the Eulerian Weighted Average Flux (EWAF) scheme, while horizontal second-order diffusion and a weak divergence damping are included to prevent the accumulation of energy at the smallest resolved spatial scales (ISAC-CNR, 2012).

The soil model of MOLOCH uses 4-6 layers, whose depths (from a few cm to more than 1 m) increasing moving downward. The soil model computes surface energy, momentum, water and snow balances, heat and water vertical transfer, vegetation effects at the surface (evapo-transpiration, interception of precipitation, wilting effects etc.) and in the soil (extraction of water by roots). It takes into account the observed geographical distribution of different soil types and soil physical parameter. The soil model includes also treatment of water freezing and melting processes within the ground.
The entire MOLOCH code is written in Fortran 90. It is designed to be a flexible, state-of-the-art atmospheric simulation system that is portable and efficient on available parallel computing platforms.

2.2 Experimental setup

This study combines the advantages of the pseudo–global warming (PGW) framework and the spectrally-nudged storyline approach to estimate the impact of climate change on extreme events. For each event, both factual and counterfactual simulations are performed, representing the occurrence of the event under present-day and pre-industrial climate conditions, respectively, using the high-resolution convection-permitting model MOLOCH. The counterfactual simulations are constructed by extracting the thermodynamic perturbation from the "storyline" simulations from the Destination Earth Digital Twin for Adaptation. In this way, the imposed perturbation does not correspond to a generic atmospheric cooling but rather to an event-specific thermodynamic modification. In addition, the high-resolution MOLOCH simulations themselves apply spectral nudging to ERA5 dynamical fields, thereby ensuring consistency in the large-scale circulation. The event is thus simulated under different climate states while maintaining comparable large-scale dynamical conditions. By combining spectral nudging, high-resolution convection-permitting modelling, and PGW-based perturbations derived from large-scale climate information, this framework enables the isolation of the thermodynamic contribution of climate change while preserving the observed synoptic-scale dynamics.

2.2.1 Factual simulations: choice of initial and boundary conditions

Factual simulations consist in high-resolution (1.8 km) simulations of observed weather extremes under "real", present-day, climate conditions. The simulations are performed with MOLOCH to explicitly resolve mesoscale and convective processes, while large-scale atmospheric conditions are constrained through spectral nudging and driven by external datasets. The use of spectral nudging preserves the large-scale circulation while allowing small-scale processes to develop freely within the high-resolution model. Therefore, the choice of initial and lateral boundary conditions plays a crucial role in the experimental setup, as these fields constrain the large-scale atmospheric circulation. Two types of datasets produced by the European Centre for Medium-Range Weather Forecasts (ECMWF) were considered as boundary and initial conditions: the operational analyses and the ERA5 reanalysis data. A schematic representation of the foregoing methodological procedure is presented in Figure 2.2.

Operational analyses are near-real-time products generated by operational meteorological centres to provide the most accurate current state of the atmosphere for the intialisation of daily weather forecasts. At ECMWF, these analyses are produced within the Integrated Forecasting System (IFS) and represent a key component of the operational weather prediction chain. They are obtained through a process of data assimilation, which combines a wide range of meteorological observations with short-range model forecasts (background) to estimate the best possible atmospheric state (European

Centre for Medium-Range Weather Forecasts (ECMWF), 2025). This process is implemented using a four-dimensional variational data assimilation system (4D-Var), which performs a statistically consistent interpolation in space and time between observations and the background atmospheric state. Operational analyses are produced continuously and made available four times per day (00, 06, 12, and 18 UTC), with output fields every six hours and a horizontal resolution of approximately 10 km (Andersson and Thépaut, 2008).

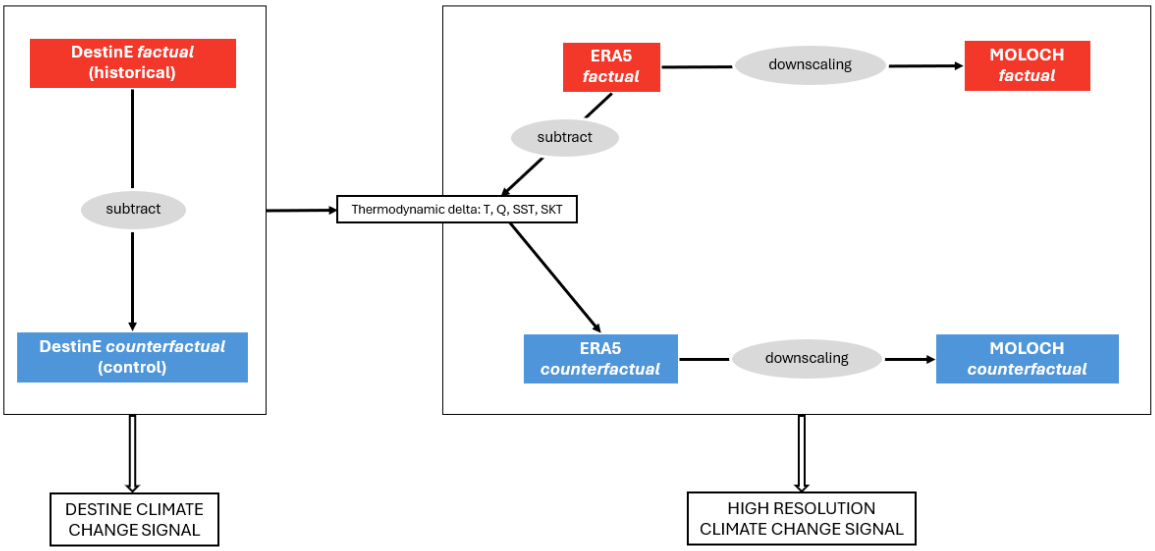

Figure 2.2: Schematic representation of the methodological approach to counterfactual modeling and signal processing.

The reanalysis datasets provide a temporally consistent reconstruction of the past state of the atmosphere, ocean, and land surface. These data are produced retrospectively by assimilating all available historical observations within a fixed numerical model and data assimilation system, thereby ensuring internal consistency over long time periods. ERA5 is the fifth-generation atmospheric reanalysis developed by ECMWF and is produced within the Copernicus Climate Change Service (C3S). It covers the period from January 1940 to the present and continues to be extended forward in near real time. This dataset provides hourly estimates of a large number of atmospheric, land, and oceanic climate variables, which are distributed on a regular global grid with a horizontal resolution of approximately 31 km. The reanalysis is generated using a four-dimensional variational data assimilation (4D-Var) scheme combined with model forecasts from cycle CY41R2 of the ECMWF Integrated Forecast System (IFS). The vertical discretization consists of 137 hybrid sigma–pressure model levels, with the top level located at 0.01 hPa.

By combining vast amounts of historical observations with advanced modelling and data assimilation techniques, ERA5 delivers a physically coherent and homogeneous representation of the Earth system (European Centre for Medium-Range Weather Forecasts (ECMWF), 2025).

While operational analyses are generally more suitable for real-time applications and short-range forecasts, reanalysis products are more appropriate for climate-oriented studies. In the present work, both datasets were tested as sources of initial and boundary conditions. From a purely technical perspective, performing dynamical downscaling from a higher-resolution dataset would be advantageous, as it would reduce the resolution jump from approximately 30 km to 10 km, and potentially improve the representation of mesoscale and convective processes. However, tests showed that the benefit of using the operational analyses depended on the event and it was not always robust. Therefore, the results presented in this thesis are based on simulations driven by ERA5 data, which has two main benefits. First, it maintains methodological consistency with the Destination Earth spectrally nudged storylines, which also used nudging towards ERA5. Second, it enables a simple approach to create an ensemble of simulations, as motivated and justified in Section 2.4.2.

2.2.2 Counterfactual simulations: computation and implementation of the climate perturbation

Counter-factual simulations of the weather extremes consist in MOLOCH simulations of the same events, but initialised from plausible pre-industrial thermodynamic climate conditions. As previously mentioned, the pre-industrial conditions are generated by subtracting from ERA5 a thermodynamic climate change perturbation extracted from the storyline simulations of the Destination Earth Digital Twin for Climate Change Adaptation (Climate DT).

Within Destination Earth, three global atmosphere-ocean coupled models (ICON, IFS-NEMO and IFS-FESOM) have been run at resolutions ranging between 5 and 10 km for the different Earth-system components (atmosphere, land, ocean and sea ice). Multi-decadal simulations are produced to cover the recent past (from 1990) and possible future evolutions of the climate up to 2050 (Destination Earth, 2024). In addition, "storyline simulations" have been run at 9km resolution with only the IFS-FESOM model using the spectral nudging technique to maintain a similar large-scale circulation to that from ERA5 for the period 2017-2023. In particular, the IFS-FESOM historical (present-climate) experiments simulate the events of 2017-2023 under real "factual" climate conditions, i.e. observed GHG concentrations. The control (past-climate) experiments simulates the same meteorological events, thanks to the spectral nudging, but with a GHG forcing approximately corresponding to that of the 1940s and a global-mean temperature 1 degree cooler (John, Beyer, Marylou Athanase, et al., 2026).

The thermodynamical climate change perturbation is constructed as the difference between the present-day (historical) and past-climate (control) IFS-FESOM spectrally-nudged simulations. The difference is calculated for a set of selected thermodynamic surface and atmospheric variables: air temperature, specific humidity, sea surface temperature (SST), and skin temperature, with the latter being a measure of temperature at the Earth's surface.

The resulting signal thus contains the difference values for each variable, expressed as a function of hour, space, and vertical level. Since it represents the difference between present and past climates, it corresponds to a positive quantity associated with the warming induced by climate change over recent decades. Accordingly, this signal is subtracted from the corresponding fields from ERA5, in order to generate the "cooled" boundary conditions to run the counter-factual MOLOCH simulations. Here, the methodology is presented considering ERA5 data as input but, the procedure is identical when operational analyses are used instead, merely requiring adjustments to the spatial and temporal resolutions.

The application of this signal is not straightforward due to differences in the horizontal and vertical grids between IFS-FESOM and ERA5. As a first step, the warming signal from the IFS-FESOM storyline simulations was remapped using belinear interpolation from the Destination Earth horizontal grid (9km) to the ERA5 grid (25km). Second, for each grid point, the vertical grid of IFS-FESOM is interpolated on the vertical grid of ERA5, but this is more critical since the vertical discretizations adopted by the two datasets differ substantially. As described in the previous section, ERA5 resolves the atmosphere using 137 hybrid vertical levels, of which only the lowest 113 levels (from the 25th level downward) are considered here, neglecting the upper free atmosphere. In contrast, the Destination Earth simulations are provided on 19 standard pressure levels (see Section 2.4). It was therefore necessary to interpolate the temperature and humidity warming signals, which are three-dimensional variables, onto the hybrid vertical levels used by MOLOCH.

The pressure in hPa corresponding to each hybrid level of ERA5 is defined by the following relation:

$$p_k = A_k + B_k \times p_s \tag{2.8}$$

where k is the vertical hybrid level index, ranging from 25 to 137. The coefficients A_k and B_k are model constants that define the vertical coordinate and are fixed on the model grid, being independent of time and horizontal position. They allow the effective pressure to be computed for each level at each point of the three-dimensional grid (European Centre for Medium-Range Weather Forecasts, 2015). Here p_s denotes the local surface pressure, explicitly extracted at each spatial point and temporal instant, in order to account for its variability. This ensures that the effective pressure associated with each hybrid level is computed consistently with the local atmospheric state at each time step, allowing the thermodynamic perturbation to be applied in a physically coherent manner.

At this stage, the three-dimensional (temperature and specific humidity) signals are interpolated onto the pressure levels corresponding to the hybrid levels of ERA5 at that grid point. The fields are interpolated using an interpolation function defined in logarithmic pressure space, mapping from the logarithm of the standard pressure levels to the logarithm of the effective pressure on the model hybrid levels. Finally, the interpolated signal is subtracted from the corresponding ERA5 fields. This procedure is performed separately for each of the events analysed.

Figure 2.3 shows two maps representing the interpolated signal along hybrid levels. Specifically, panel 2.3a illustrates the spatial distribution of the temperature signal within the selected ERA5 domain at hybrid level 133, which approximately corresponds to the surface. Panel 2.3b, on the other hand, illustrate a vertical cross-section of the same signal taken along a line passing through Emilia-Romagna, which shows how the temperature perturbation changes with the vertical hybrid levels. As an example, the temperature signal is averaged over the entire duration of the May 2023 event.

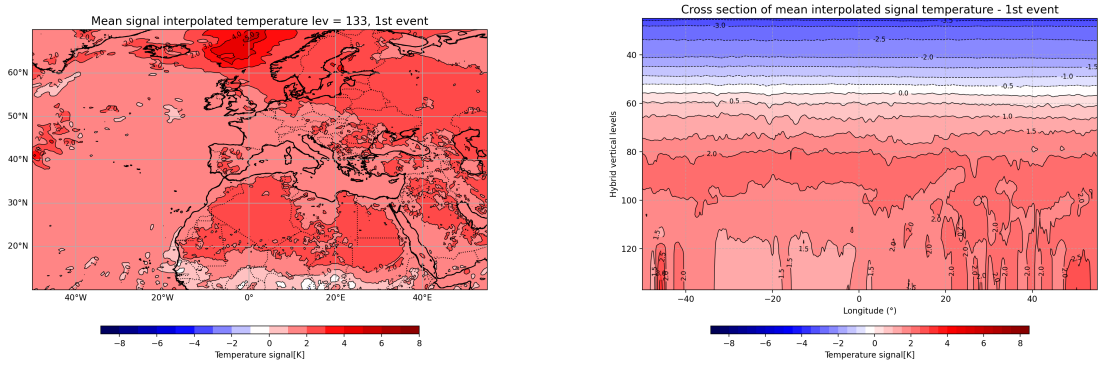

(a) (b)

Figure 2.3: Mean interpolated temperature signal for the May 2023 event: (a) spatial distribution at hybrid level 133 (near-surface) and (b) vertical cross-section along a transect passing through Emilia-Romagna.

2.2.3 Construction of ensemble simulations

In order to better isolate the signal attributable purely to the imposed warming perturbation, and thus to reduce the influence of numerical noise, an ensemble simulation was performed. The application of this methodology was deemed necessary specifically for the September 2024 event, and in particular for the analysis of the precipitation field,

as this event is characterized by the presence of numerous convective systems and is therefore difficult to reproduce accurately using a single deterministic simulation. Convective cells are relatively small-scale and highly localized phenomena; as a result, when analysing the signal, it becomes challenging to distinguish an actual climate change increase in precipitation from uncertainties related to the model's ability to accurately predict the exact location of convective development.

The fundamental concept underlying ensemble forecasting is atmospheric unpredictability, and in particular the fact that very similar initial conditions can lead to markedly different atmospheric evolutions even after only a few hours. The atmosphere is a chaotic dynamical system, meaning that its future state depends critically on the initial conditions (Buizza, 2001), with such sensitivity that even infinitesimal perturbations can result in substantially different outcomes. Ensemble simulations are therefore constructed by introducing perturbations to the initial conditions or to the model formulation itself. The divergence among ensemble members provides a quantitative measure of forecast uncertainty: a large ensemble spread indicates high indeterminacy and strong sensitivity to initial conditions, whereas a small spread suggests that the atmospheric state is more predictable. In a reliable ensemble forecasting system, the observed evolution is expected to fall within the range spanned by the ensemble members (Consorzio LaMMA, 2025).

To estimate forecast uncertainty, ECMWF has developed the Ensemble Prediction System (EPS), which consists of 51 integrations performed at a horizontal resolution of approximately 32 km with 62 vertical levels and extending up to 10 days ahead. The ensemble forecasts are initialized from a set of closely related initial conditions, designed to represent the best estimate of the atmospheric state and its associated uncertainty: one control member is initialized from the best estimate of the initial state, while 50 additional members are generated by applying small perturbations. In addition to uncertainties in the initial conditions, numerical errors inherent to the model formulation also contribute to differences among ensemble members (European Centre for Medium-Range Weather Forecasts, 2012). Forecast uncertainty and ensemble spread are not constant in time. Initial uncertainties, which typically affect the smaller spatial scales (e.g. observational errors), do not remain localized but they can rapidly amplify and propagate. Moreover, the rate at which uncertainty grows is not constant but can vary from one event to another (Buizza, 2001).

In this study, the ensemble was generated using a time-lagged approach. Specifically, the ensemble members were constructed by systematically delaying the initialization time by one-hour increments, while keeping the model configuration and the simulation period unchanged. The control member (member 0) was initialized using ERA5 data starting at 00:00 UTC, consistent with the simulation start time. Additional ensemble members were generated by progressively delaying the ERA5 input data: member 1 used ERA5 fields starting at 01:00 UTC, member 2 at 02:00 UTC, member 3 at 03:00 UTC, and member 4 at 04:00 UTC. In this way, small but physically consistent perturbations

were introduced in the initial and boundary conditions, sampling the sensitivity of the simulated event to uncertainties in the atmospheric state. The resulting ensemble consists of five members (members 0–4) and provides a framework to assess the robustness of the simulated precipitation signal and to reduce the influence of internal variability on the attribution analysis. The ensemble mean and spread were also calculated to assess the forecast uncertainty and the degree of divergence among the five members. The spread is computed as the standard deviation (σ) across the ensemble members.

2.2.4 Simulation setup and model configuration

All numerical experiments followed a two-step workflow, consisting of a preprocessing phase and a subsequent high-resolution integration of the target event. The preprocessing phase involves a short computational run (approximately 1.5 hours) aimed at defining the model configuration, including the horizontal and vertical domain, the stretching parameters for the hybrid vertical coordinate and the input datasets for initial and boundary conditions. This phase ensures internal consistency of the model setup prior to the execution of the full simulation. The main simulation phase consists of the explicit time integration of the atmospheric equations.

The total computational cost depends on both the event duration time and the computational resources employed. Simulations were carried out on two high-performance computing systems: the "BEETHOVEN" machine at CNR–ISAC and the "LEONARDO" supercomputer at CINECA. Parallelization was achieved by decomposing the horizontal domain into subdomains distributed across the available processors. On the BEETHOVEN system, simulations were performed using 48 processors distributed over three nodes, while on the LEONARDO system, the computational setup was adapted to the available computational time and processing resources (nodes). In this case, the preprocessing phase was executed serially on a single node, while the event simulations were distributed over two nodes, for a total of 96 processors. The decision to utilize both systems was driven by the need to optimize total computational time. While simulations on BEETHOVEN required approximately 6 hours each, migrating the simulation runs to LEONARDO enabled a significant reduction in execution time to 1.5 hours, which significantly accelerated the data acquisition workflow.

In the simulations conducted for this study, the model was configured with 60 vertical levels and 7 soil layers. The horizontal resolution was set to 1.8 km, using a latitude–longitude domain of fixed size for all experiments, with a grid consisting of 802 $\times$ 1154 points in the latitudinal direction. During the post-processing phase, the model output data are remapped onto a regular latitude–longitude grid with dimensions 768 $\times$ 960. The integration domain is centred over Italy and is bounded by the following geographical coordinates:

- SW = (4.0204, 35.72121)

- SE = (19.6672, 35.72121)
- NW = (4.0204, 49.28547)
- NE = (19.6672, 49.28547)

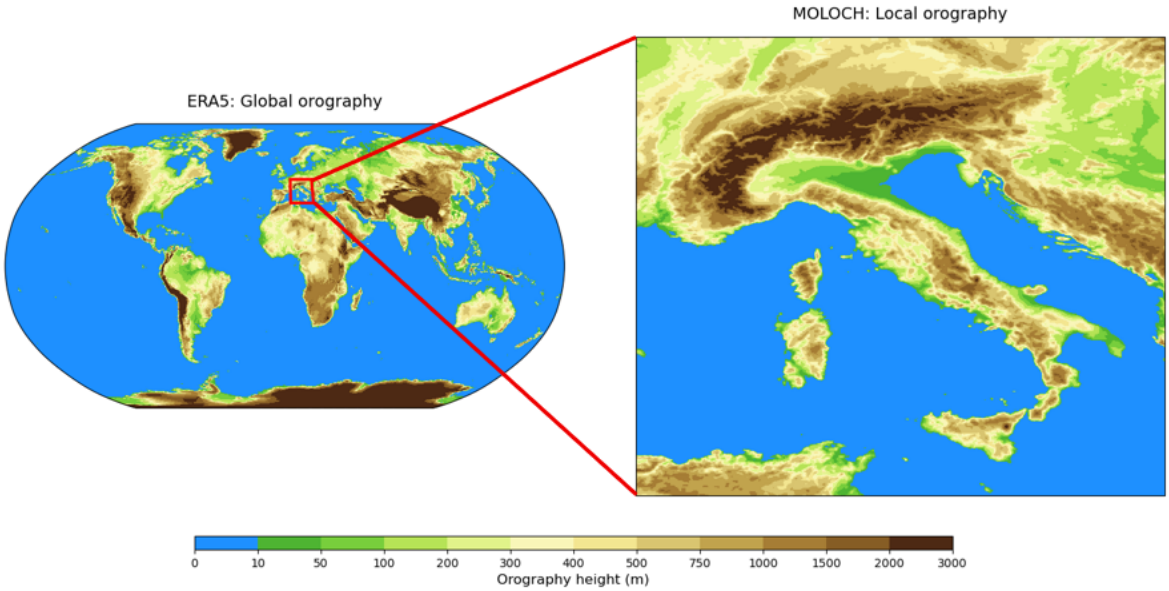

Figure 2.4: Extent of the ERA5 and MOLOCH domains of integration with orography height (m). The MOLOCH domain, inside the red box, covers Italy and surrounding areas, while the ERA5 domain is global.

The local orographic domain is illustrated in Figure 2.4, where the red box indicates the area where the direct downscaling from the global ERA5 data is performed.

The integration time step was set to 36 seconds for all simulations. This value ensured numerical stability for most configurations, while shorter time steps were tested in selected cases to address potential numerical instabilities. The duration of each simulation varied depending on the event considered. The first event was simulated from 00:00 UTC on 30 April 2023 to 00:00 UTC on 4 May 2023, for a total integration time of 97 hours. The second event covered the period from 00:00 UTC on 17 September 2024 to 00:00 UTC on 21 September 2024, again for a total of 97 hours.

The horizontal domain, grid configuration, and vertical discretization were kept identical across all simulations to ensure consistency and comparability between the different events.

2.3 Observation data

To validate the numerical simulations performed with the MOLOCH model, selected model output fields were compared with observational datasets. In particular, two reference datasets were considered: the ArCIS precipitation dataset (Archivio Climatologico per l'Italia Centro Settentrionale) and the ERA5 reanalysis produced by ECMWF.

The ArCIS dataset is a climatological archive derived from observational data collected by the regional meteorological monitoring networks maintained by the Regional Meteorological Services and/or the Regional Civil Protection Functional Centres (ArCIS, 2025). It is based on daily precipitation observations from a total of 1,762 stations located over north-central Italy and adjacent areas. These observational data are used to produce a high-resolution daily gridded precipitation analysis covering the period from 1961 to 2015. The daily precipitation observations consist of 24-hour accumulated rainfall values and are interpolated onto a latitude–longitude regular grid of dimensions 123 $\times$ 120 and with an approximate spatial resolution of 5 $\times$ 5 km. The interpolation is performed using a modified Shepard scheme, specifically adapted to account for topographic distances between observation locations.

Prior to interpolation, the input data undergo quality control procedures to ensure time consistency, synchronicity, and statistical homogeneity. Finally, the ArCIS dataset is regularly updated by the participating institutions, enabling flexible climate comparisons and supporting the continuous improvement and maintenance of the observational network (Pavan, Antolini, Barbiero, et al., 2019).

Other variables were instead compared with those provided by the ERA5 reanalysis, with particular focus on large-scale atmospheric fields. This dataset is considered as a climatological reference and is used as a benchmark for validation purposes (see Section 2.2.2). There variables are represented over a regular latitude–longitude grid of size 1440 $\times$ 721.

2.4 Diagnostic and statistical methods

2.4.1 Statistical tests

In order to provide a comprehensive overview of the performance of the MOLOCH simulations, a set of statistical indices was computed. The statistical validation was performed for the precipitation field and carried out separately for each event, using observational data from the ArCIS dataset as reference. To quantitatively assess the model outputs, two standard verification metrics for continuous forecasts were considered, namely the absolute error (AE) and the bias (as a percentage). Let S_i and O_i be the simulated and observed time-mean values, respectively, at location i, then the AE is defined as follows:

$$\mathrm{AE} = |S_i - O_i| \tag{2.9}$$

The relative bias is instead computed as:

$$\text{bias } (\%) = \left(\frac{S_i - O_i}{O_i} \right) \times 100 \tag{2.10}$$

Both metrics are evaluated for the cumulative precipitation associated with each event, applying a threshold of ≥ 30 mm in order to filter out less-relevant lower-intensity precipitation. Prior to the computation of each metric, the two datasets were made consistent by interpolating the MOLOCH-simulated fields onto the coarser ARCIS grid.

Chapter 3

Meteorological conditions and event evolution: observational and model-based analysis

This chapter provides a detailed meteorological analysis of the two selected events, namely the first phase of the May 2023 event and the September 2024 event. For each case study, the analysis begins with an overview of the large-scale atmospheric circulation that led to the occurrence of the event, based on hourly analyses of selected synoptic-scale fields using multi-level spatial maps derived from reanalysis data (ERA5). Subsequently, in order to better characterize the smaller-scale dynamics, the ERA5 analysis is complemented by results from the MOLOCH simulations, which are used to examine the moisture and water vapour fields and their vertical and horizontal distribution during key phases of each event.

3.1 Event 1: 30 April - 4 May 2023

The May 2023 event was characterized by persistent precipitation and substantial rainfall accumulations across the entire Emilia-Romagna region, leading to multiple river floods, landslides, and widespread inundations. According to the hydro-meteorological bulletin issued by ARPAE (Cardinali et al., 2023), rainfall totals exceeding 200 mm were recorded, particularly in the Bologna area, with peak accumulations observed at the Le Taverne station. Figure 3.1 presents a map of the cumulative precipitation over the entire duration of the event, derived from ARcIS observational data.
In the following sections, the atmospheric conditions responsible for this extreme precipitation event are analysed.

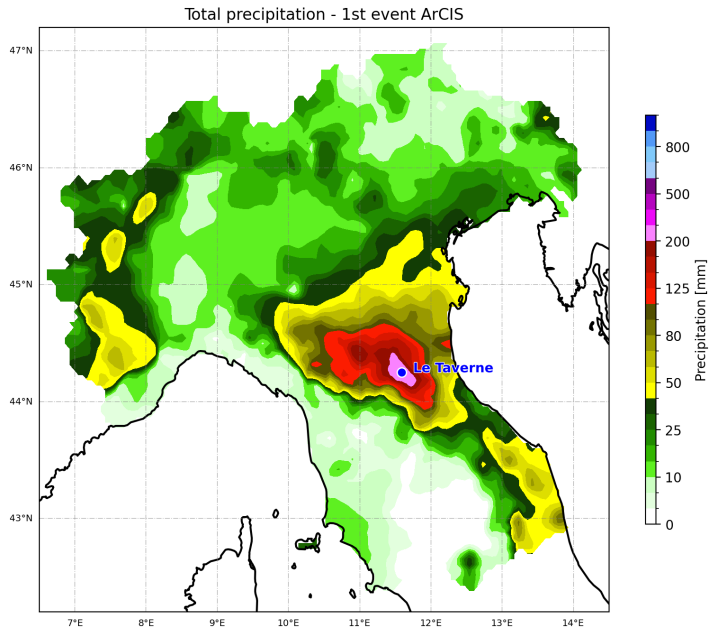

Figure 3.1: Accumulated precipitation (mm) from 1 May to 4 May 2023 derived from ArCIS observations.

3.1.1 Observed large-scale circulation and dynamical forcing

Between late April and early May 2023, a cold polar trough was present over northern Europe and progressively propagated southward toward the Mediterranean basin and the Italian Peninsula, leading to the development of a cyclonic circulation over the region. Figure 3.2 shows the mean sea level pressure (MSLP) and geopotential height at 500hPa (Z500) at different times during the event produced by ERA5.

The panel 3.2a shows the polar trough extending toward lower latitudes at 15:00 UTC on 1 May and culminating in a Rossby wave breaking and a cut-off low, which gradually favoured the formation of a cyclone over central–northern Italy (panel 3.2b). The surface low-pressure system intensified on 2 May and remained quasi-stationary, with its centre located over the Italian Peninsula through the following day. This persistence was associated with a blocking configuration, as the cut-off low remained trapped and was unable to follow its typical eastward progression due to the development of a high-pressure system over eastern Europe, as shown in panel 3.2c. Toward the end of the event the blocking situation weakened as the eastern high-pressure system decayed and displaced eastward, allowing the high-pressure system over the Iberian Peninsula to advance toward Italy (panel 3.2d).

This configuration can be further confirmed by examining the potential vorticity (PV) field at 300 hPa (Figure 3.3). The simultaneous presence of a positive PV anomaly at

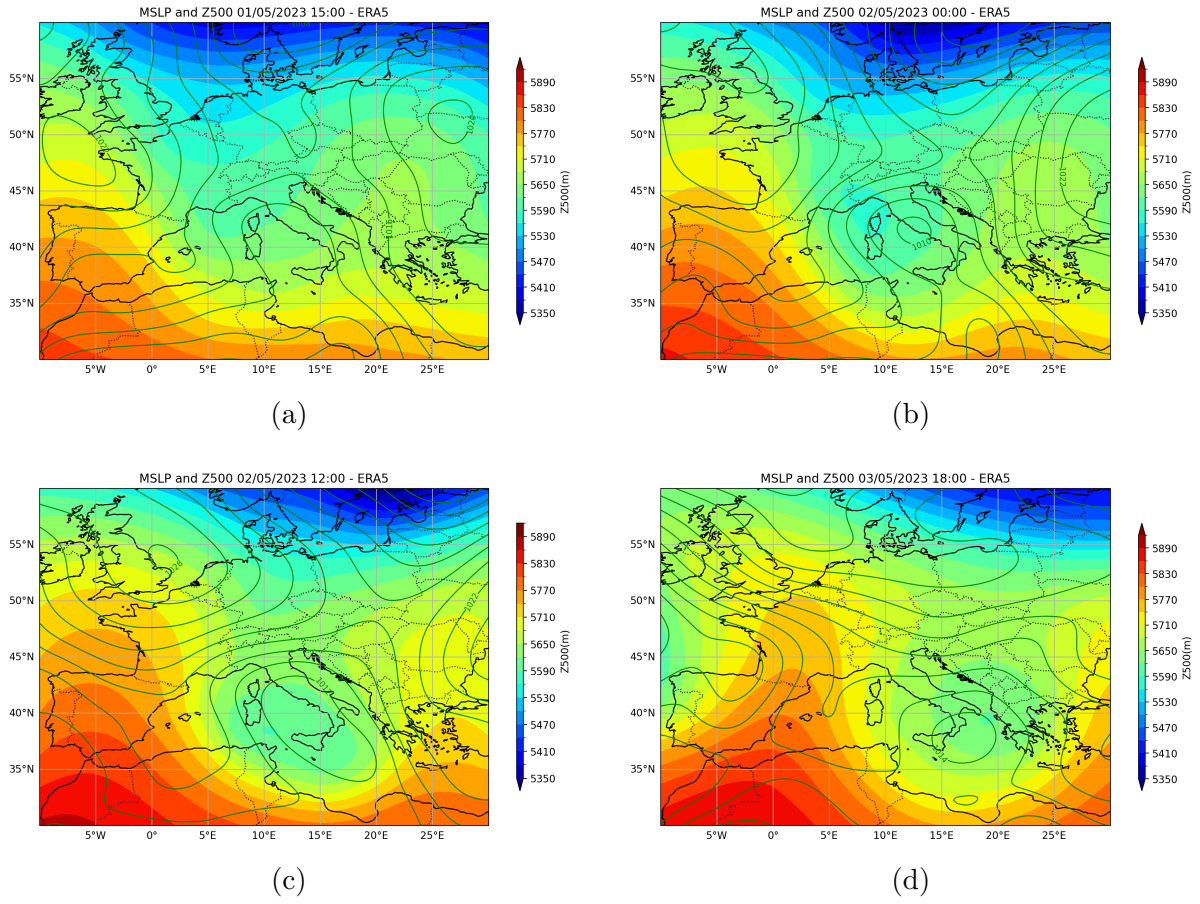

Figure 3.2: Mean sea level pressure (MSLP; contours in hPa) and geopotential height in m at 500 hPa (Z500; shading in m) from ERA5 at (a) 15:00 UTC on 1 May 2023, (b) 00:00 UTC on 2 May 2023, (c) 12:00 UTC on 2 May 2023 and (d) 18:00 UTC on 3 May 2023.

upper levels and a surface low-pressure centre indicates a strong dynamical coupling between the upper and lower troposphere, capable of sustaining cyclogenesis and enhancing upward vertical motions as well as the persistence of adverse weather conditions .

At 18:00 UTC on 1 May (panel 3.3a), a filament of positive PV descending from the polar trough is observed, associated with cold air and high potential vorticity of polar–stratospheric origin. During 2 May, this PV structure evolves into a more vortical structure, extending toward lower latitudes and moving over Sardinia toward the eastern Mediterranean and Greece (panel 3.3b). For most of the event, the PV anomaly remains located on the left flank of the surface low, contributing to the maintenance of upper-level dynamical forcing.

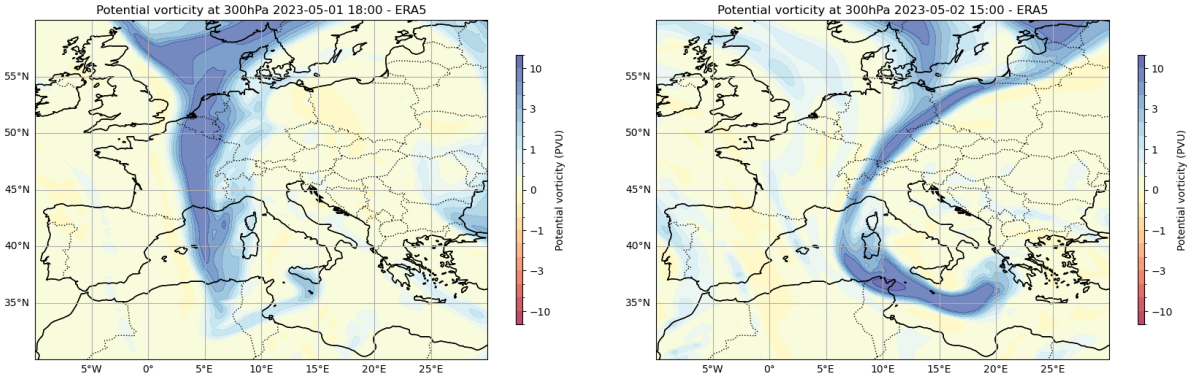

(a) (b)

Figure 3.3: Potential vorticity (PVU) at 300 hPa from ERA5 at (a) 18:00 UTC on 1 May 2023 and (b) 15:00 UTC on 2 May 2023.

3.1.2 Moisture availability and transport

One of the main drivers of this event at smaller spatial scales was the availability and transport of large amounts of atmospheric moisture. Figure 3.4 shows the total column water vapour (TCWV), expressed in $\mathrm{kg\,m^{-2}}$, derived from ERA5 and the MOLOCH simulations. TCWV represents the total amount of water vapour contained in the atmospheric column above a given location and potentially available for condensation and precipitation, independently of its dynamical transport.

Panels 3.4a and 3.4c display the time averaged TCWV over the entire event, from 00:00 UTC on 30 April 2023 to 23:00 UTC on 3 May 2023. A well defined moisture reservoir is evident over the Mediterranean basin, with mean values reaching approximately 25–30$\mathrm{kg\,m^{-2}}$ around the Italian Peninsula. The moisture distribution is not spatially uniform but organized in a manner consistent with the regional orography and this is more appreciable in the map produced by MOLOCH since it has a higher resolution.

In panel 3.4b and 3.4d, the temporal average is computed only for the rainiest day of the event, 2 May. The moisture is concentrated mostly over the Adriatic Sea before entering the Po Valley. Maximum TCWV values are observed in proximity to the Emilia-Romagna coastline, where MOLOCH daily mean exceeds 30$\mathrm{kg\,m^{-2}}$.
Despite the different resolutions of the due datasets, MOLOCH accurately reproduces the general profile shown by ERA5, with an added level of detail. The general configuration results in a high column-integrated moisture content, creating favorable conditions for the development and persistence of intense and long-lasting precipitation, particularly in the presence of orographic forcing.

In addition to assessing the availability of atmospheric moisture, it is essential to understand how water vapour is transported and whether it is advected toward specific regions. Moisture fluxes represent the primary mechanism through which humidity is

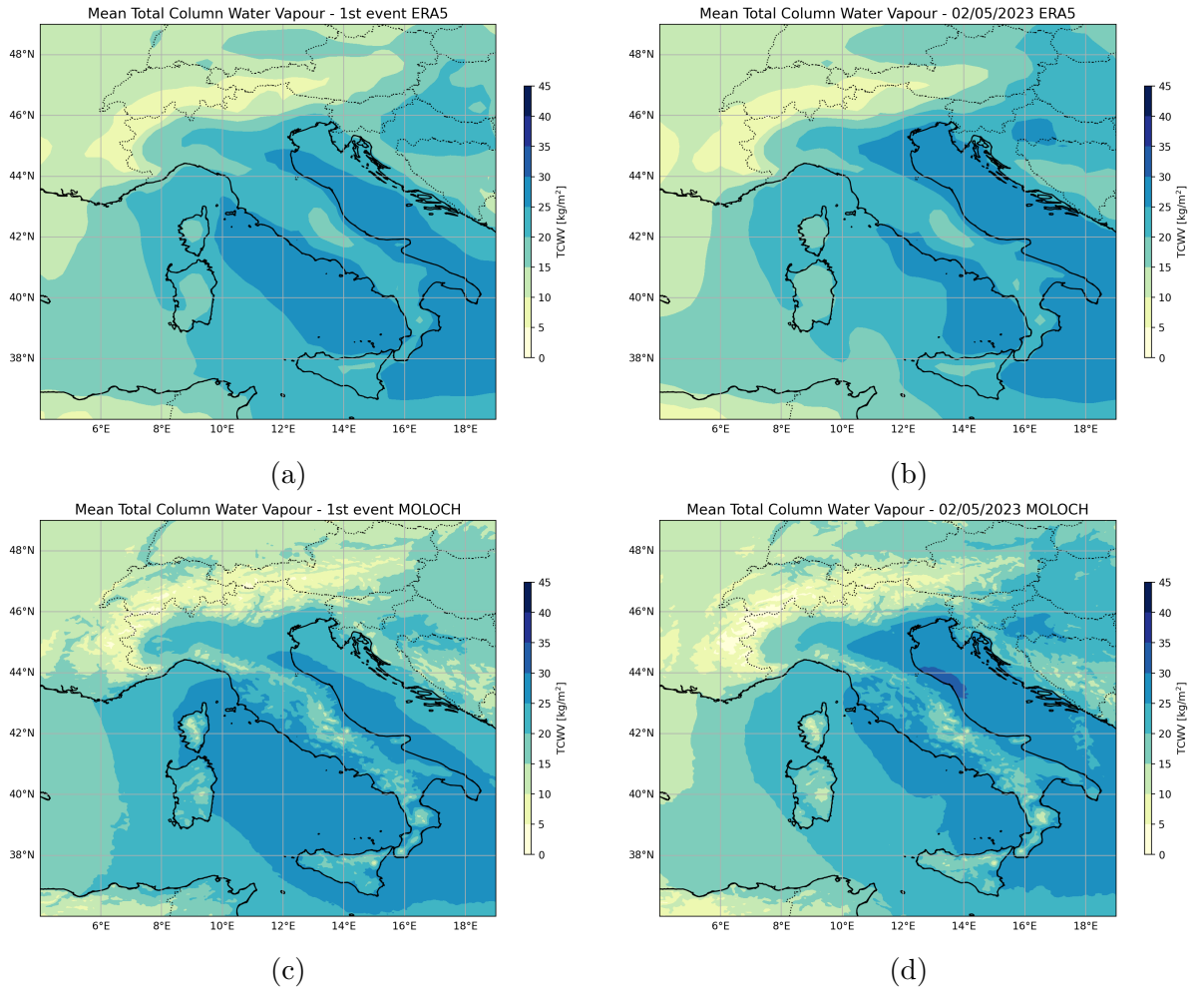

Figure 3.4: Total column water vapour (TCWV; $\mathrm{kg\,m^{-2}}$) from ERA5 (top) and MOLOCH (bottom): (a, c) TCWV averaged from 00:00 UTC on 30 April 2023 to 23:00 UTC on 3 May 2023; (b, d) TCWV averaged over the day of most intense precipitation (2 May).

supplied to extreme precipitation events in Italy, particularly over the Adriatic basin. To investigate this process, the integrated water vapour transport (IVT) field from ERA5 and MOLOCH is analysed. IVT, expressed in $\mathrm{kg\,m^{-1}s^{-1}}$, is a physical quantity that combines the vertically integrated water vapour content of the atmospheric column with the horizontal wind speed and direction. In Figure 3.5, the colour scale represents the magnitude of the IVT, computed as the modulus of the horizontal transport vector (east–west and north–south components), while the arrows indicate the wind direction, with their length proportional to the transport intensity. Panels 3.5a and 3.5c show the

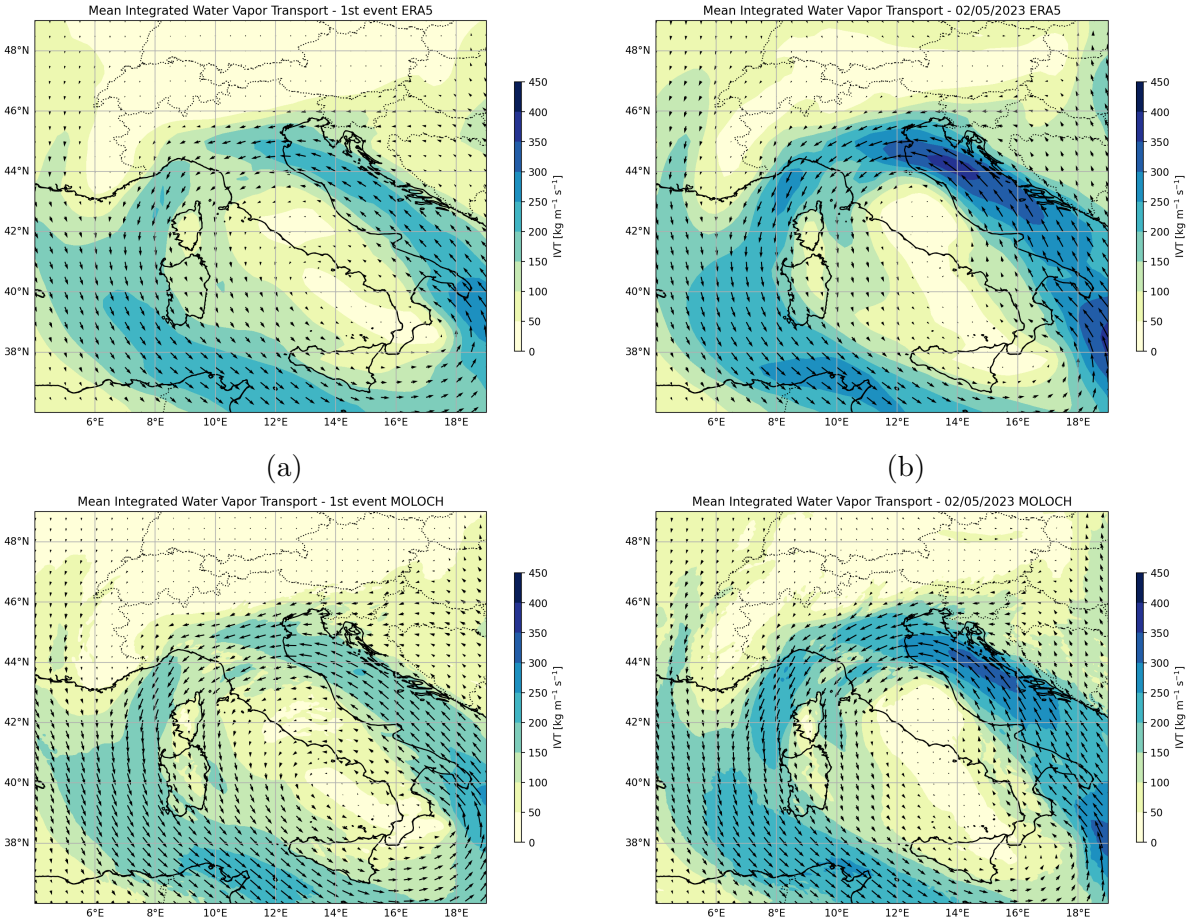

Figure 3.5: Integrated vapour transport (IVT; $\mathrm{kg\,m^{-1}s^{-1}}$) from ERA5 (top) and MOLOCH (bottom): (a, c) IVT averaged from 00:00 UTC on 30 April 2023 to 23:00 UTC on 3 May 2023; (b, d) IVT averaged over the day of most intense precipitation (2 May).

IVT averaged over the entire duration of the first event. Comparing this against the TCWV distribution reveals that not all the moisture present along the Italian coasts undergoes strong transport. On average, the strongest transport occurs over the Adriatic basin and near the Tunisian coast. MOLOCH adequately reproduces the moisture transport patterns, showing a spatial distribution consistent with ERA5, with a slight underestimation of IVT intensity over the Adriatic basin by approximately $50\mathrm{kg\,m^{-1}s^{-1}}$.

This discrepancy is further highlighted in panels 3.5b and 3.5d, which show the daily mean IVT for 2nd May and indicate a pronounced intensification of the moisture

transport. Although the overall circulation pattern remains similar, the intensity of the onshore flow along the Adriatic coast of Emilia-Romagna increases during the most intense phase of the event. In this area, vapour fluxes become more concentrated, with mean values exceeding 300kg $m^{-1}s^{-1}$ in a limited area of the Adriatic Sea in MOLOCH, whereas ERA5 locally exceeds 350kg $m^{-1}s^{-1}$. Both total and daily maps clearly indicate that the cyclonic circulation drives near-surface winds to transport substantial amounts of water vapour toward the Po Valley, where the flow weakens upon encountering the orographic barrier of the Apennines.

3.1.3 Vertical structure and atmospheric stability

After analysing the atmospheric circulation in the horizontal plane, it is useful to investigate the atmospheric stability along the vertical axis. To this end, Figure 3.6 shows a Skew T-ln P diagram, with on the x-axis the temperature expressed in degrees Celsius referring to isotherms tilted 45 degrees to the right, while on the y-axis the pressure in hPa on a logarithmic scale. The diagram is derived from radiosonde data recorded by the University of Wyoming and referred to 12:00 UTC on May 2nd at the San Pietro Capofiume (BO) location.

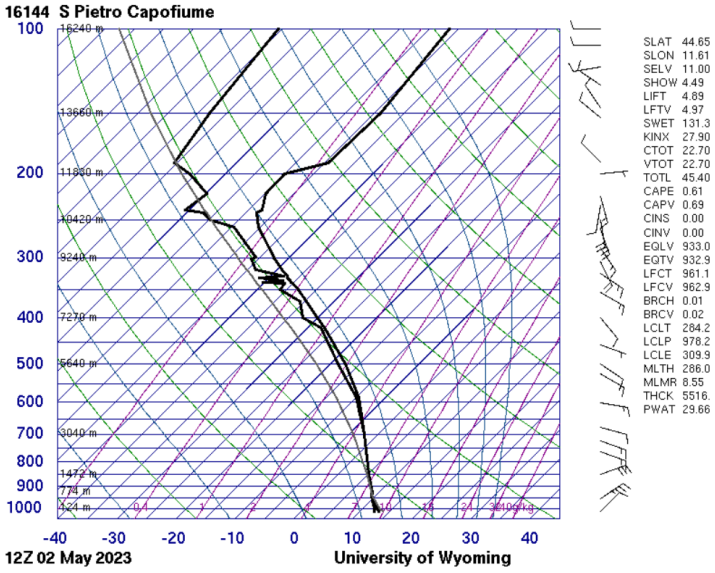

Figure 3.6: Skew T-lnP thermodynamic diagram in San Pietro Capofiume (BO) at 12:00 on May 2, 2023. The black line on the right refers to temperature of the environment, while the one on the left refers to the dew point temperature. The blue curves show moist adiabatic transformations, while green lines the dry adiabatic. The grey line shows the uplift of a surface parcel.

To interpret the moisture state of the atmospheric column, we observe the state curve,

which is the ambient temperature curve (the rightmost curve), and the dew point curve (the curve on the left), which are the two thick black lines in the figure. The former represents the actual observed air temperature at various altitudes, while the dew point curve indicates the temperature to which the air must be cooled to become saturated. The distance between these two curves indicates how far the air is from saturation, and thus how dry the air is. In this case, two curves are observed to be practically overlapping up to approximately 600 hPa, indicating a saturated air column up to this altitude and, therefore, a very humid atmosphere. This is also confirmed by the Precipitable Water for entire sounding index, which is equal to 29.66 mm (PWAT). Winds near the surface originate from the northeast and are of moderate intensity, while in the upper levels they weaken and become more easterly. This implies that in such a moisture-rich atmosphere the low levels dynamical forcing was sufficient to produce orographic lifting and the subsequent development of persistent precipitation.

The analysis of stability is based on the comparison between the environmental temperature profile and the parcel trajectory (the thin grey line), which represents the path of an hypothetical air parcel lifted from the surface under these atmospheric conditions. The trajectory of the lifted parcel remains consistently to the left of the environmental temperature curve. This indicates that throughout the atmospheric column the parcel would be colder than the surrounding environment, thereby implying stable conditions. Convective Available Potential Energy (CAPE) is also very low (0.61), as is Convective Inhibition (CIN) which is null, confirming that the atmospheric conditions on 2 May 2023 were highly stable and not conducive to the development of convective systems. This stability further confirms that the primary driver of the event was orographic lifting within a saturated atmospheric layer.

3.2 Event 2: 17 -20 September 2024

The event of September 2024 was marked by high-intensity, short-duration rainfall generated by localized convective cells, whose development was significantly favored by unusually high sea surface temperatures. According to the ARPAE hydro-meteorological report, several areas experienced rainfall totals equivalent to three to four times the average for the entire month of September. A record-breaking accumulation of 288.2 mm in a single day was documented at the San Cassiano sul Lamone station (Ravenna) (Foraci et al., 2024). The spatial distribution of these cumulative totals, derived from ARcIS observational data, can be visualized in Figure 3.7. In the following sections, the specific atmospheric drivers that triggered this extreme convective episode are analyzed.

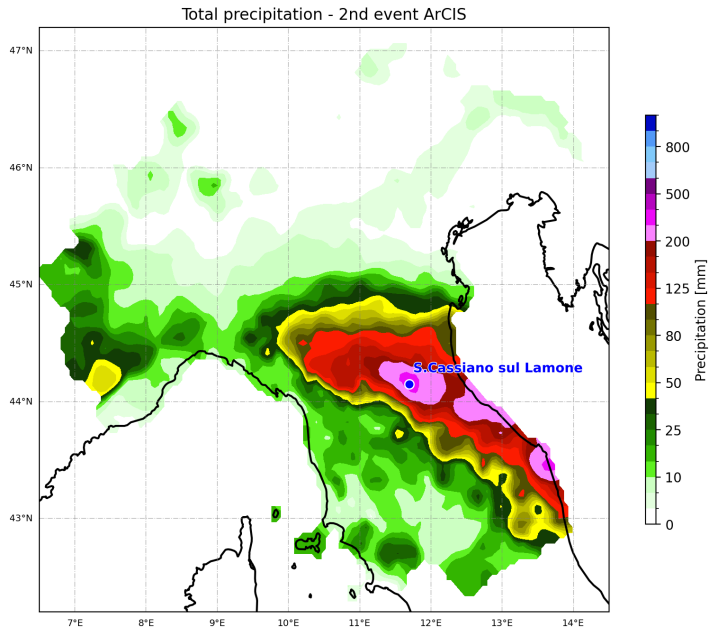

Figure 3.7: Accumulated precipitation (mm) from 17 September to 20 September 2024 derived from ArCIS observations.

3.2.1 Observed large-scale circulation and dynamical forcing

During the first half of September 2024, a cyclone named Boris affected large parts of Europe. According to the hydro-meteorological bulletin issued by ARPAE, the system followed a trajectory typical of Vb cyclones, which generally originate over the Gulf of Genoa on the lee side of the Alpine chain and are often associated with enhanced moisture transport leading to extreme precipitation over central Europe (Messmer, Raible, and Gómez-Navarro, 2020).

Figure 3.8 presents selected snapshots of mean sea level pressure (MSLP) and geopotential height during the evolution of the storm. At 06:00 UTC on 13 September (panel 3.8a), an upper-level Atlantic trough is seen over the Alps, with the associated surface low-pressure centre (Boris) already formed over the Balcans. This surface cyclone initially moved toward eastern Europe. As shown in panel 3.8b, the flow became blocked, and its eastward progression was slowed by the development of a high-pressure system over Russia leading to extensive precipitation over several countries, such as Poland, Czech Republic and Austria. In the following hours, the depression underwent a retrograde motion and moved back toward the Mediterranean basin. Between 17 and 18 September, an upper-level low remained quasi-stationary over the area (panel 3.8c), generating the most intense precipitation phase over Emilia-Romagna. Finally, panel 3.8d shows conditions at 15:00 UTC on 19 September, when the low-pressure system began

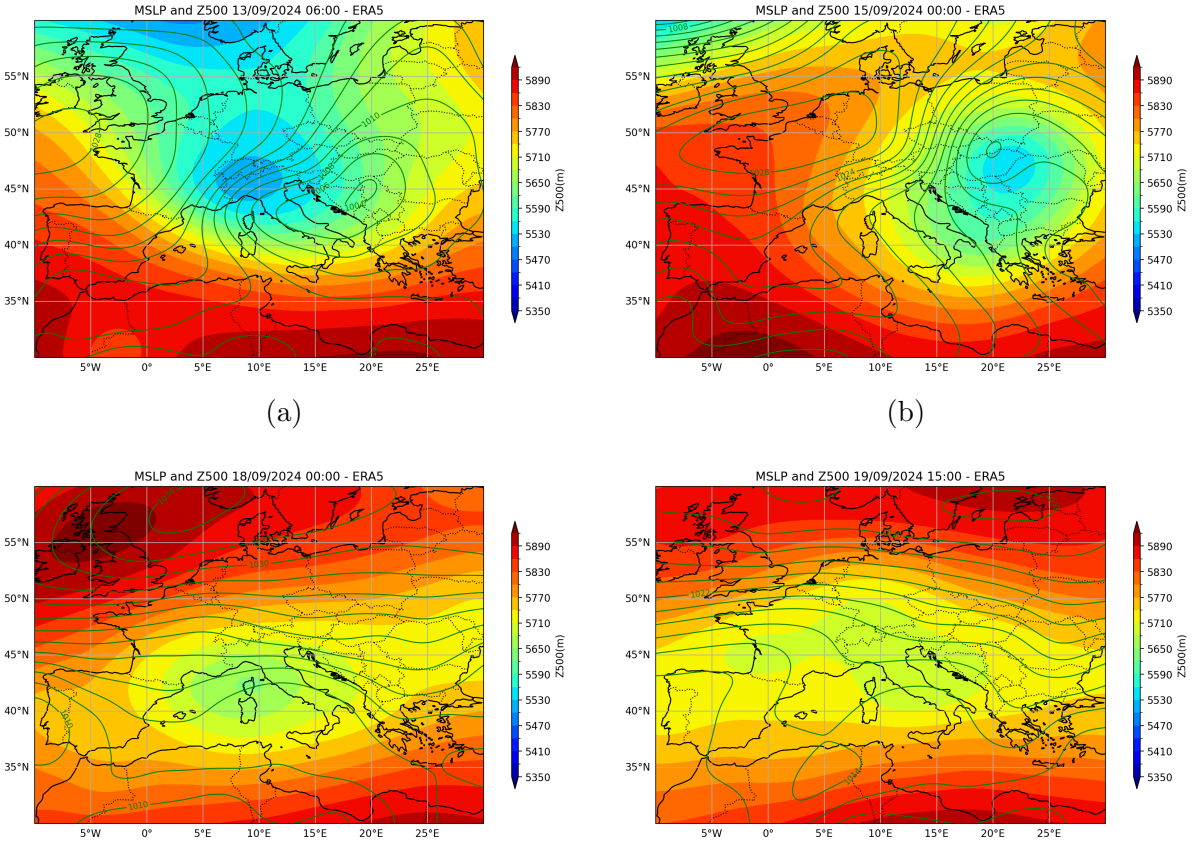

(a) (b)

(c) (d)

Figure 3.8: Mean sea level pressure (MSLP; contours in hPa) and geopotential height at 500 hPa (Z500; shading in m) from ERA5 at (a) 06:00 UTC on 13 September 2024, (b) 00:00 UTC 15 on September 2024, (c) 00:00 UTC on 18 September 2024 and (d) 15:00 UTC on 19 September 2024.

to weaken, marking the end of the extreme event.

The most intense phase over Italy was primarily associated with the upper-level depression and its persistence over the region. The event was initially driven by an upper-level potential vorticity (PV) cut-off, i.e., the isolation of cold and unstable air from the main mid-tropospheric flow (panel 3.9a). This vortical structure remained quasi-stationary over northern Italy before following a characteristic retrograde trajectory that also influenced the lower-level cyclone. Overall, the system can be described as a slow-moving upper-level PV streamer, which maintained an unstable flow configuration and favoured strong upward vertical motions (Riboldi et al., 2025). From 17 September onward, the slow displacement of the isolated PV core over central–northern Italy (panel 3.9b) created favourable conditions for the ascent of moist air from the Adriatic Sea.

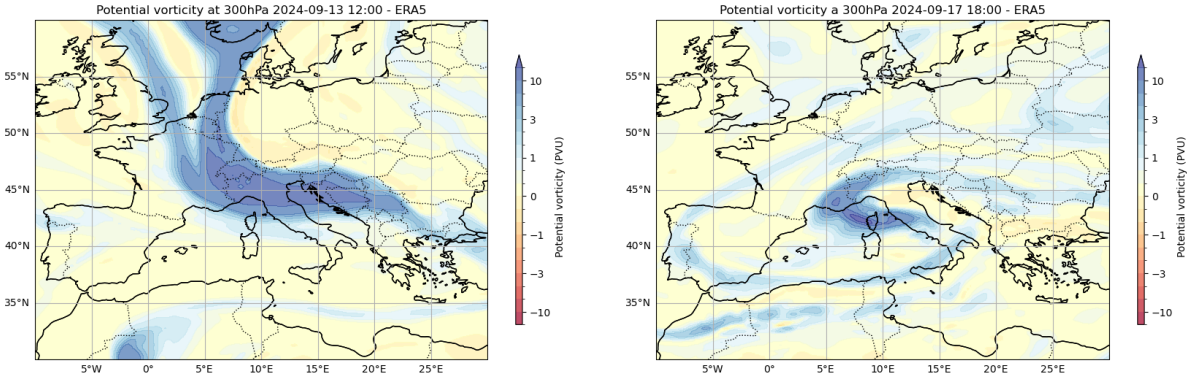

(a) (b)

Figure 3.9: Potential vorticity (PVU) at 300 hPa from ERA5 at (a) 12:00 UTC on 13 September 2024 and (b) 18:00 UTC on 17 September 2024.

3.2.2 Moisture availability and transport

Following the same approach adopted for the previous event, this section describes the moisture fields associated with the September 2024 case. Starting from the analysis of the available atmospheric water content, Figure 3.10 presents the time-averaged TCWV over the entire event from 00:00 UTC on 17 September 2024 to 23:00 UTC on 20 September 2024 (panel 3.10b and 3.10c), and subsequently for the day of most intense precipitation, 18 September 2024 (panel 3.10b and 3.10d) in both ERA5 and MOLOCH.

The event-mean TCWV reveals a substantially higher mean column-integrated water vapour content compared to the previous event. This difference can be attributed to seasonal effects, as the event occurred shortly after the summer season, as well as to the anomalously high sea surface temperatures observed in 2024 (Foraci et al., 2024). While mean TCWV values stay below $20\,\mathrm{kg\,m^{-2}}$ near main mountain ranges —with MOLOCH providing a finer representation of orographic influences —they peak at almost $40\,\mathrm{kg\,m^{-2}}$ over the Ionian and Adriatic Seas. Notably, MOLOCH tends to estimate higher precipitable water levels over the Adriatic basin than ERA5.

The daily mean shown in panel 3.10b and 3.10d highlights a further increase in TCWV over the Adriatic basin, suggesting the presence of moisture fluxes transporting humid air from southern regions and converging toward the Po Valley. This configuration provides a physical explanation for the large precipitation amounts recorded over Emilia-Romagna on that day. Moreover, although the May 2023 event was characterized by more persistent rainfall, the late September 2024 episode featured a markedly higher atmospheric moisture content, with a mean TCWV difference of nearly $10\,\mathrm{kg\,m^{-2}}$, thereby creating more favourable thermodynamic conditions for the development of intense precipitation. Compared to ERA5, MOLOCH shows high consistency in reproducing the total column water vapor patterns; it provides finer spatial resolution, although it slightly underesti-

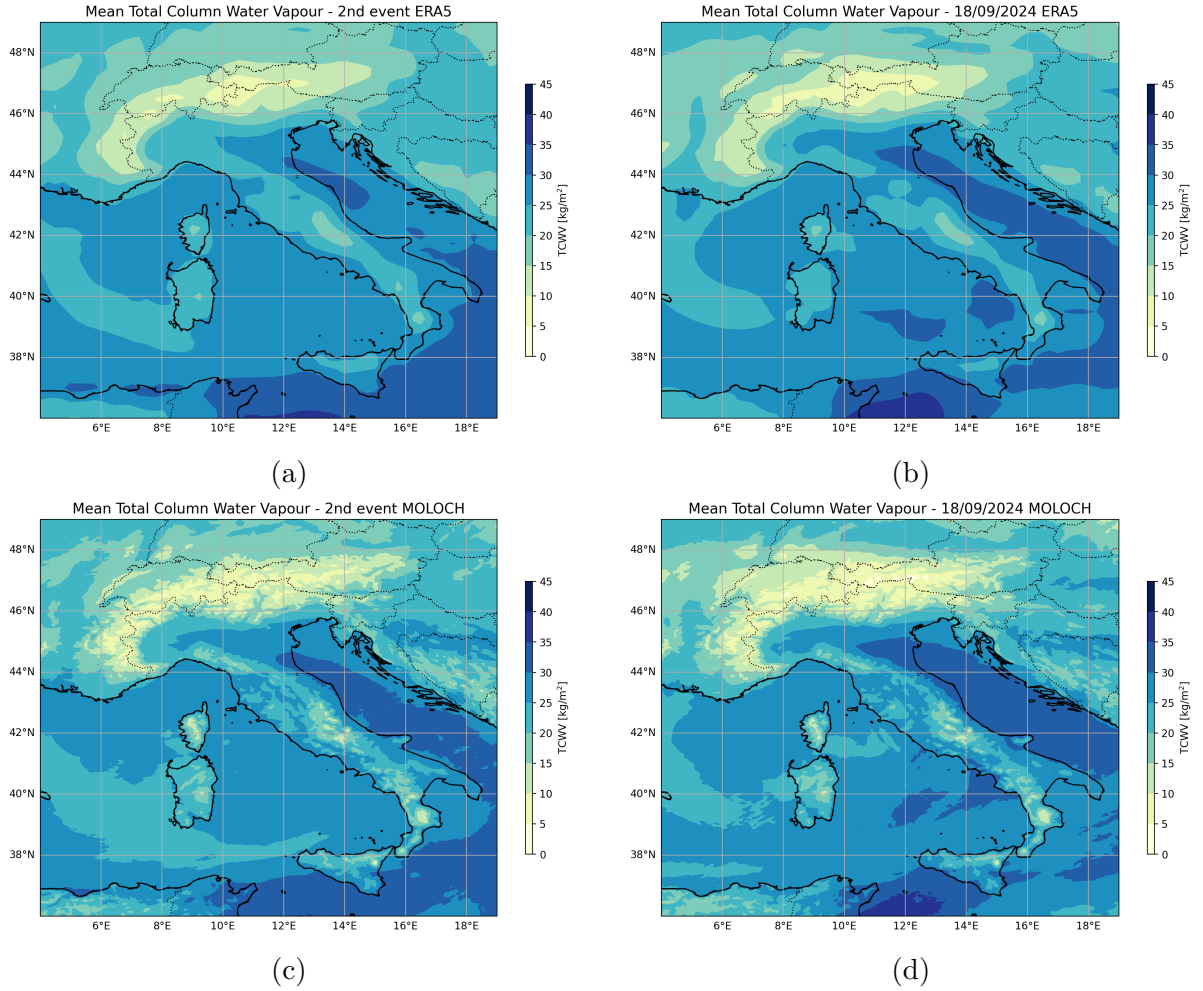

Figure 3.10: Total column water vapour (TCWV; $\mathrm{kg\,m^{-2}}$) from ERA5 (top) and MOLOCH (bottom): (a, c) TCWV averaged from 00:00 UTC on 17 September 2024 to 23:00 UTC on 20 September 2024; (b, d) TCWV averaged over the day of most intense precipitation (18 September).

mates the water content over the Ionian Sea.

The horizontal transport of moisture is illustrated in Figure 3.11. The event-mean IVT (panels 3.11a and 3.11c), in contrast to the May 2023 case, exhibits a more pronounced and spatially extensive transport over northern Italy, extending from the northern Adriatic basin toward the Po Valley and also affecting the Gulf of Genoa. This configuration indicates a well-organized and persistent moisture transport, associated with intensified low-level winds and enhanced by orographic channeling in the vicinity of the Alps and the Apennines. The structure is dynamically supported by the marked

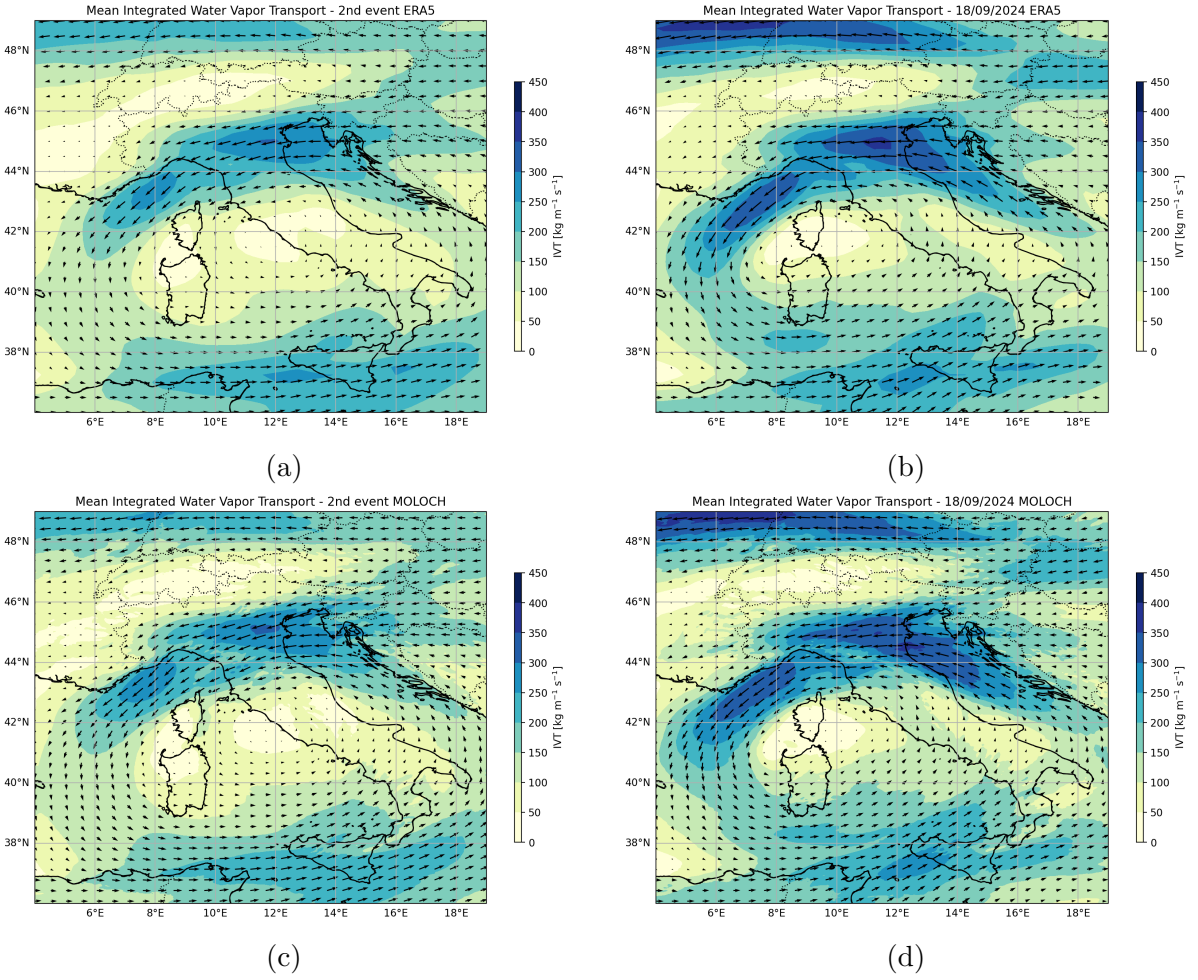

Figure 3.11: Integrated vapour transport (IVT; $\mathrm{kg\,m^{-1}s^{-1}}$) from ERA5 (top) and MOLOCH (bottom): (a, c) IVT averaged over the entire event; (b, d) IVT veraged over the day of most intense precipitation (18 September).

horizontal pressure gradient and the presence of a depression centred near Corsica (see Figure 3.8c).

The daily mean IVT shown in the panels on the right hand side retains the same overall flow configuration but displays a clear intensification of the transport on 18 September. This case is characterized by a predominant west–east flow component, with a well-defined IVT corridor extending from the western Mediterranean and North Africa toward the Adriatic basin, where values locally exceed $400\mathrm{kg\,m^{-1}s^{-1}}$ in both ERA5 and MOLOCH depictions. During the most intense phase of the event, the moisture transport becomes significantly strengthened and more focused over the northern Adriatic,

thereby creating highly favourable conditions for the development of intense convective cells.

Overall, compared to the May 2023 case, MOLOCH shows a better agreement with ERA5, reproducing the same transport pattern and accurately capturing the location of the intensity peaks both in event-mean and the daily-mean.

3.2.3 Vertical structure and atmospheric stability

The Skew T–ln P diagram shown in Figure 3.12a allows the investigation of the vertical structure of the atmosphere on 18 September 2024 at 12:00 UTC, again at the San Pietro Capofiume station.

In this case as well, a saturated atmospheric column is observed in the lower layers, with the environmental temperature profile overlapping the dew point curve. At higher levels, the two curves are no longer superimposed but remain close up to approximately 250 hPa, indicating a very moist atmosphere extending nearly to the tropopause. This is consistent with the findings discussed in the previous section and is further confirmed by the Precipitable Water for entire sounding index, which is very high (33.02 mm), exceeding the value recorded in 2023. This is consistent with the higher sea surface temperatures. Low-level winds originate again from the northeast and gradually veer to southwesterly directions at higher altitudes. However, wind intensity is stronger throughout the entire column compared to 2 May, suggesting a deeper and more vertically coherent moisture transport.

With regard to stability, the diagram appears to suggest that the 2024 event occurred under stable conditions, as both CAPE and CIN are again negligible and the lifted parcel remains colder than the environmental temperature throughout the troposphere. However, several aspects must be considered when classifying this event, which justify the fact that it has been documented as being characterized by convection (Foraci et al., 2024). First, the thermodynamic diagram highlights a steeper environmental temperature gradient compared to the 2023 case, i.e., a more inclined temperature profile. This indicates that air cools more rapidly with height, a condition that can more readily favour the development of convective motions. Moreover, it is important to acknowledge a source of uncertainty arising from the fact that the diagram discussed above refers to a single location in the Bologna area; this does not exclude the presence of instability over the sea, where sea surface temperatures were particularly high. Indeed, substantial rainfall accumulations were recorded along the Romagna and Marche coasts. In addition, the ARPAE bulletin reports the presence of thunderstorm cells based on mesoscale analyses conducted over the regional territory (Foraci et al., 2024). In particular, Figure 3.12b shows the radar reflectivity map at 18:50 UTC on 18 September, where convective precipitation (dark orange and red colours) can be observed over the central-eastern hilly belt and near the Marche coast.

Taken together, these elements indicate that the event under investigation was not

characterized by purely instability-driven deep convection, but rather by embedded convective potential. This implies that precipitation developed within a generally stable atmosphere and was predominantly stratiform in nature, similarly to the May 2023 event, although convective cores with intense rainfall peaks could develop locally. This type of convection typically forms within extensive precipitation areas, where warm and moist air is forced to ascend; thus, it does not represent isolated convection but rather convective elements embedded within stratiform cloud systems.

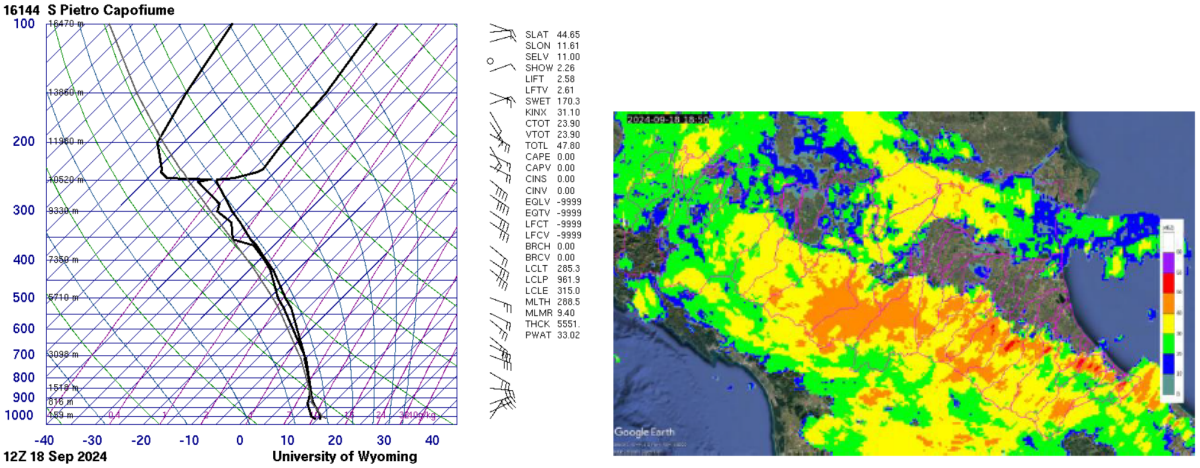

(a) (b)

Figure 3.12: (a) Skew T-lnP thermodynamic diagram in San Pietro Capofiume (BO) at 12:00 on September 18, 2024. (b) Composite radar reflectivity map dated on the same day at 18:50 UTC. Source: Arpae Emilia-Romagna - Struttura Idro-Meteo-Clima

Chapter 4

Precipitation analysis and model evaluation in the factual scenario

This chapter is devoted to a detailed examination of the rainfall field, focusing on its main characteristics and on the differences identified between the two case studies. To this end, extensive analyses were conducted using the results of the high-resolution, convection-permitting MOLOCH simulations, together with the precipitation outputs from the Destination Earth spectrally-nudged storyline simulations. Finally, in order to assess the capability of MOLOCH to accurately reproduce the spatial and temporal structure of the rainfall patterns, a model validation is presented. This includes a qualitative comparison with ArCIS observational datasets through spatial maps, as well as a quantitative assessment based on selected statistical metrics.

4.1 Event 1: 30 April - 4 May 2023

4.1.1 Model-observation intercomparison: MOLOCH, Destination Earth and ArCIS

The quasi-stationary behaviour of the cyclonic system described in the previous chapter resulted in a precipitation event predominantly driven by orographic forcing, with substantial rainfall accumulations across the entire region and particularly over the windward slopes of the Apennines.

Figure 4.1 illustrates the spatial distribution of accumulated precipitation over central–northern Italy from 1 May to 4 May 2023 (left panels) and for the most intense rainfall day on 2 May (right panels) in different datasets. Panels 4.1a and 4.1b present the observed precipitation derived from ArCIS over central–northern Italy. The cumulative rainfall map for the entire event shows totals exceeding 200 mm over the hilly areas of the Bologna and Ravenna provinces (purple shading), with a maximum of 274.4

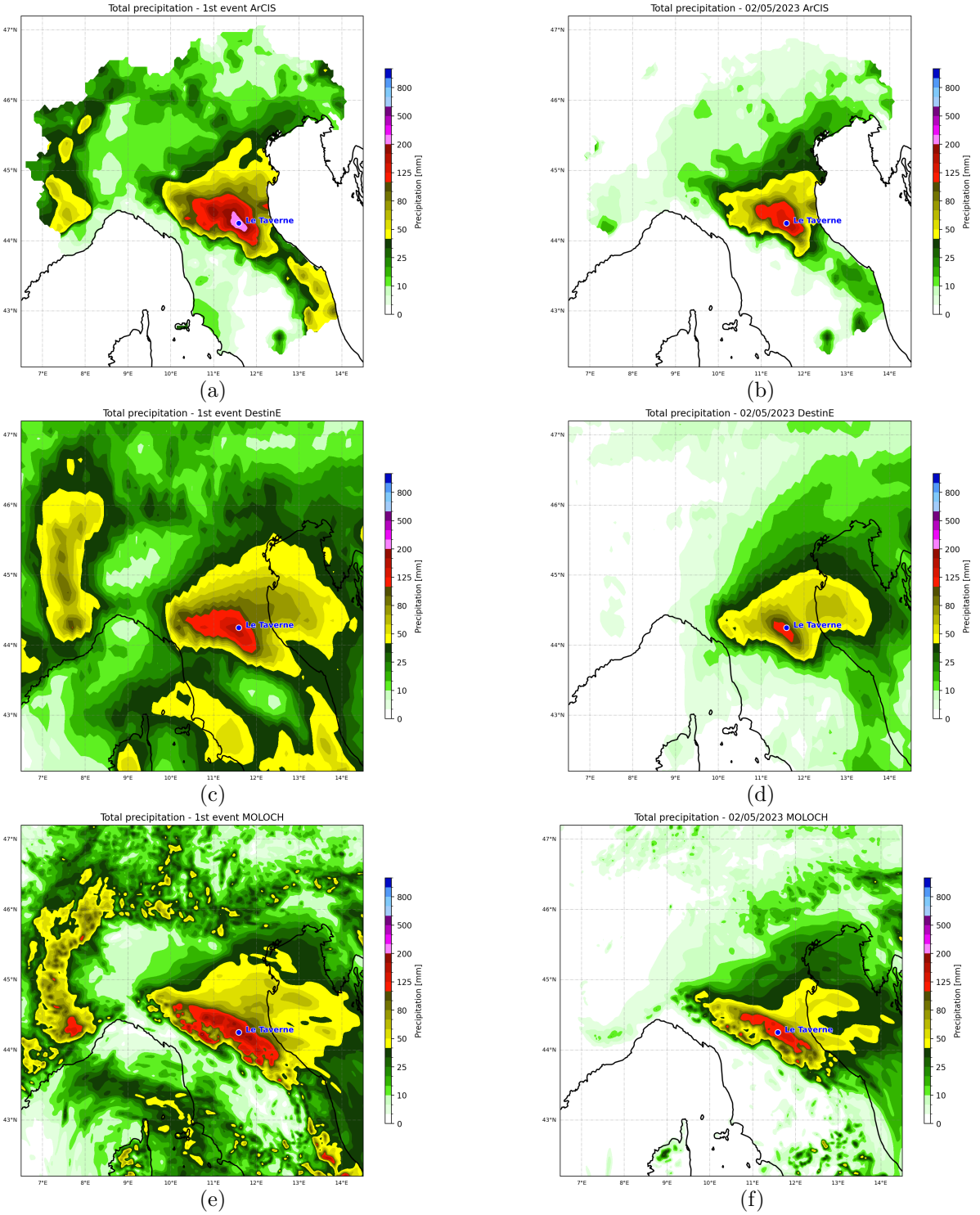

Figure 4.1: Spatial distribution of total (left) and peak daily (May 2nd, right) accumulated precipitation (mm) during the 2023 event. Comparison between (a-b) ArCIS observations, (c-d) Destination Earth, and (e-f) MOLOCH simulations.

mm recorded at the Le Taverne station (Fontanelice, BO; 44°14′56.4″N, 11°35′16.8″E). Across most of the region, cumulative totals exceeded 50 mm (yellow to red shading). Although precipitation was predominantly of moderate intensity, 2 May was marked by exceptionally high and spatially widespread daily accumulations, reaching 206 mm at the Le Taverne station. The highest totals were concentrated along the Adriatic-facing slopes, contributing to river flooding in hilly areas and severe inundations across the adjacent lowlands.

A comparison between the observed rainfall and the simulated precipitation provides insight into the capability of the models to reproduce the severity of the event. In particular, the accumulated precipitation simulated by Destination Earth (DestinE; panels 4.1c and 4.1d) and by MOLOCH (panels 3.1 and 4.1f) can be directly compared with the observations. Although the added spatial detail provided by the higher resolution of MOLOCH is clearly evident, both simulations reproduce the observed precipitation pattern reasonably well, with only limited differences. This suggests that the benefit of employing a convection-permitting configuration is relatively modest in the case of a predominantly orographic event, where even coarser-resolution simulations are able to capture the main precipitation features.

In comparison with ArCIS, MOLOCH appears to more accurately concentrate precipitation along the Adriatic slopes, while DestinE produces higher rainfall amounts also on the leeward Tyrrhenian side, where weaker showers were reported on 1 May according to the ARPAE bulletin. At the same time, MOLOCH tends to overextend precipitation northward and southward along the Apennine ridge, a feature evident in both the total (panel 4.1e) and daily (panel 4.1f) accumulations, whereas ARcIS observations indicate a more spatially distributed filed.

A more quantitative assessment highlights that the differences between MOLOCH and DestinE are most evident in the extreme values, and that both models clearly underestimate the observed precipitation. In particular, MOLOCH simulates a maximum cumulative rainfall of 202.29 mm near Mount Cimone, whereas DestinE reaches 166.22 mm in the vicinity of Fontanelice (BO).

This underestimation becomes even more apparent when examining the hourly evolution of precipitation during the event at the Le Taverne station. Figure 4.2 presents the time series of precipitation from 00:00 UTC on 1 May to 00:00 UTC on 4 May. The black line represents the observed rainfall recorded hourly by the rain gauge at the Le Taverne station and provided by ARPAE. The three coloured lines correspond to precipitation simulated by MOLOCH, DestinE, and ERA5.

Overall, the general temporal evolution of the event over the three-day period is well reproduced by all models. As expected, ERA5 (blue line) exhibits the poorest performance, as its coarser resolution does not allow it to adequately resolve local-scale processes, resulting in an underestimation of the total accumulated precipitation by approximately 100 mm compared with observations. DestinE (green line) and MOLOCH (red line) show very close agreement during the initial phase of the event; however, during

the morning of 2 May, MOLOCH begins to better capture the observed precipitation trend, more closely following the measured profile. By the end of the most intense rainfall period — corresponding to the steepest slopes of the curves — the three simulations level off at different cumulative values, maintaining mutual differences below 50 mm, while the underestimation relative to the observed total becomes more pronounced.

Discrepancies between observations and models may arise from differences in spatial sampling: observed data are point-based, whereas models resolve variables on a grid. In this study, model data were extracted using the "nearest neighbor" interpolation method; therefore, the underestimation of peak values also depends on the grid cell's inability to fully represent the intensity of precipitation measured locally by the station.

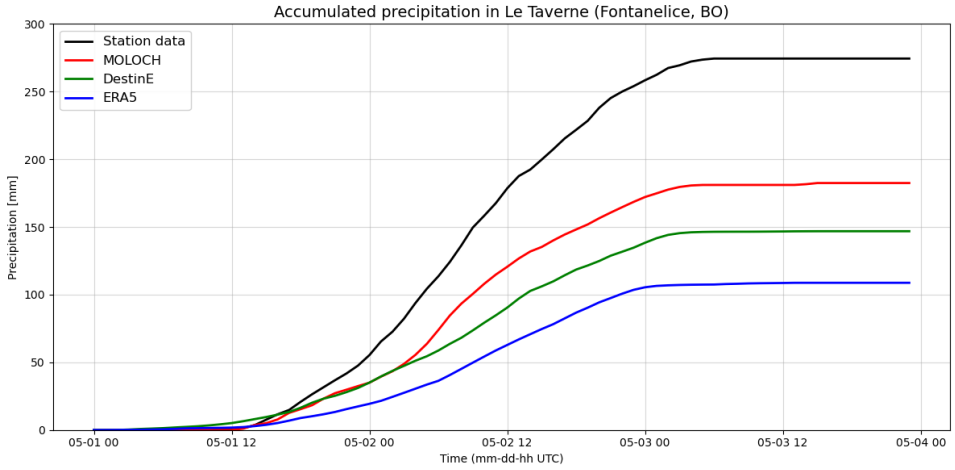

Figure 4.2: Time series of hourly accumulated precipitation (mm) throughout the 2023 event in the Le Taverne station. The plot compares observed data from ARPAE (black line) with simulations from MOLOCH, Destination Earth (DestinE), and ERA5.

4.1.2 Statistical validation of MOLOCH simulations

This paragraph provides a further quantitative assessment of the performance of MOLOCH in reproducing the accumulated precipitation field. Figure 4.3 presents maps of the spatial distribution of the absolute error (AE) and the relative bias, both computed exclusively for precipitation amounts exceeding 30 mm in order to isolate errors strictly associated with the event.

The maps illustrate how model performance is influenced by orographic features. The absolute error quantifies the overall discrepancy between the two datasets, expressing the magnitude of the difference in millimeters between forecast and observation, regardless of underestimation or overestimation. It is plotted in panel 4.3a, which indicates a very good agreement between the two datasets over the Po Valley, with differences generally

below 10 mm. In the same area, the relative bias (panel 4.3b) remains below 30% in cases of overestimation and above -30% in cases of underestimation. The largest absolute errors are observed along the north-central Apennine belt, reaching values of approximately 100 mm. In correspondence with these AE maxima, the bias indicates that the model underestimated precipitation by about 50%. In areas where accumulated precipitation exceeded 200 mm, the agreement is relatively good. For instance, at the Le Taverne station, the bias is $19,6\%$ and the AE is about 44 mm.

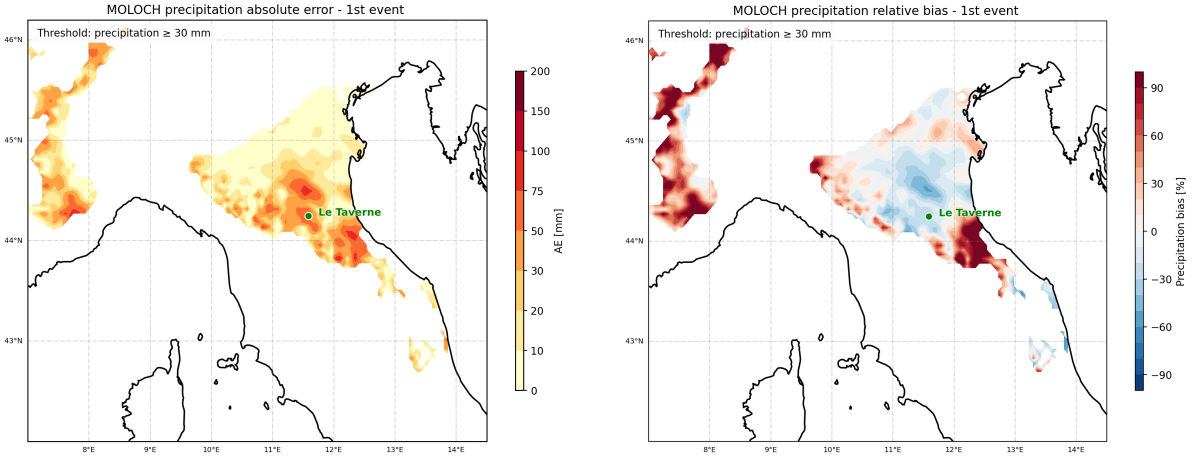

(a) (b)

Figure 4.3: Statistical comparison between MOLOCH simulated precipitation and ArCIS observations for the 2023 event. Panel (a) displays the Absolute Error (mm), while panel (b) shows the Relative Bias (%).

MEAN bias	**MEAN relative bias**	**MEAN AE**
4,42 mm	15,57%	19,33 mm

Table 4.1: Mean spatial values of bias, relative bias and absolute error for the first event; they are computed for observed and modeled precipitation $\geq 30mm$.

These results indicate that, overall, the model was able to reproduce the precipitation peaks satisfactorily, whereas the most significant errors concern the spatial distribution of precipitation. In particular, MOLOCH substantially overestimated precipitation along the Apennine ridge (bias $> 90\%$), as already evident from the maps discussed in the previous paragraph. Furthermore, the presence of small dipoles of positive and negative bias in proximity to the mountainous areas suggests a slight displacement error in the positioning of the precipitation cores. Table 4.1 reports the spatially averaged values (again considering a cumulative precipitation threshold of 30 mm) of bias, relative bias,

and mean absolute error. These metrics confirm the findings discussed above, indicating good overall agreement between simulated and observed precipitation on average across the domain, with MOLOCH accurately capturing the spatial extent of the event but exhibiting an overall wet bias due to an exaggerated orographic enhancement.

4.2 Event 2: 17 -20 September 2024

4.2.1 Model-observation intercomparison: MOLOCH, Destination Earth and ArCIS

While exhibiting similar dynamical characteristics to those described in the previous section, the September 2024 event resulted in markedly more intense precipitation. Higher sea surface temperatures, greater atmospheric moisture availability, and stronger horizontal moisture fluxes contributed to very high rainfall accumulations occurring within relatively short time intervals. Unlike the May 2023 case, this episode was not dominated by weak and persistent rainfall, but rather by intense and highly localised convective downpours. According to the regional hydrometeorological bulletin, cumulative rainfall over three days reached amounts equivalent to three to four times the climatological mean precipitation for September (Foraci et al., 2024).

The maps shown in Figure 4.4 illustrate the spatial distribution of total accumulated precipitation from 17 September to 20 September 2024 (left panels) and during 18 September (right panels), corresponding to the most intense phase.

The observed data produced by ArCIS (panels 4.4a and 4.4b) show that precipitation was predominantly distributed along the windward slope of the Apennines, exceeding 300 mm of cumulative rainfall in the hilly areas of the Bologna and Ravenna provinces. The most severely affected station was San Cassiano sul Lamone (RA), located at $44°08'52.8''\text{N}, 11°41'27.6''\text{E}$ (blue marker in the maps). At this site, during 18 September, rainfall intensity exceeded the threshold of 30mm h^{-1} for three consecutive hours, reaching a peak hourly value of 51.8 mm (Foraci et al., 2024). A comparison between Figures 4.1a and 4.4b indicates that, on 18 September, daily precipitation totals approached values comparable to the total accumulation recorded during the 2023 event, with a maximum daily total of 288.2 mm observed precisely at San Cassiano.

Panels 4.4c and 4.4d, 4.4e and 4.4f present the precipitation simulated by DestinE and MOLOCH, respectively. In contrast to the first case study, MOLOCH appears substantially more realistic than DestinE in reproducing both the intensity and the spatial distribution of the rainfall field. In this event, the benefit of employing a convection-permitting model becomes evident: explicitly resolving convective processes allows a more accurate representation of intense and localized precipitation, whereas coarser resolution and the parameterization of convection tend to smooth and weaken this signal. From the maps, the precipitation field simulated by MOLOCH exhibits organized struc-

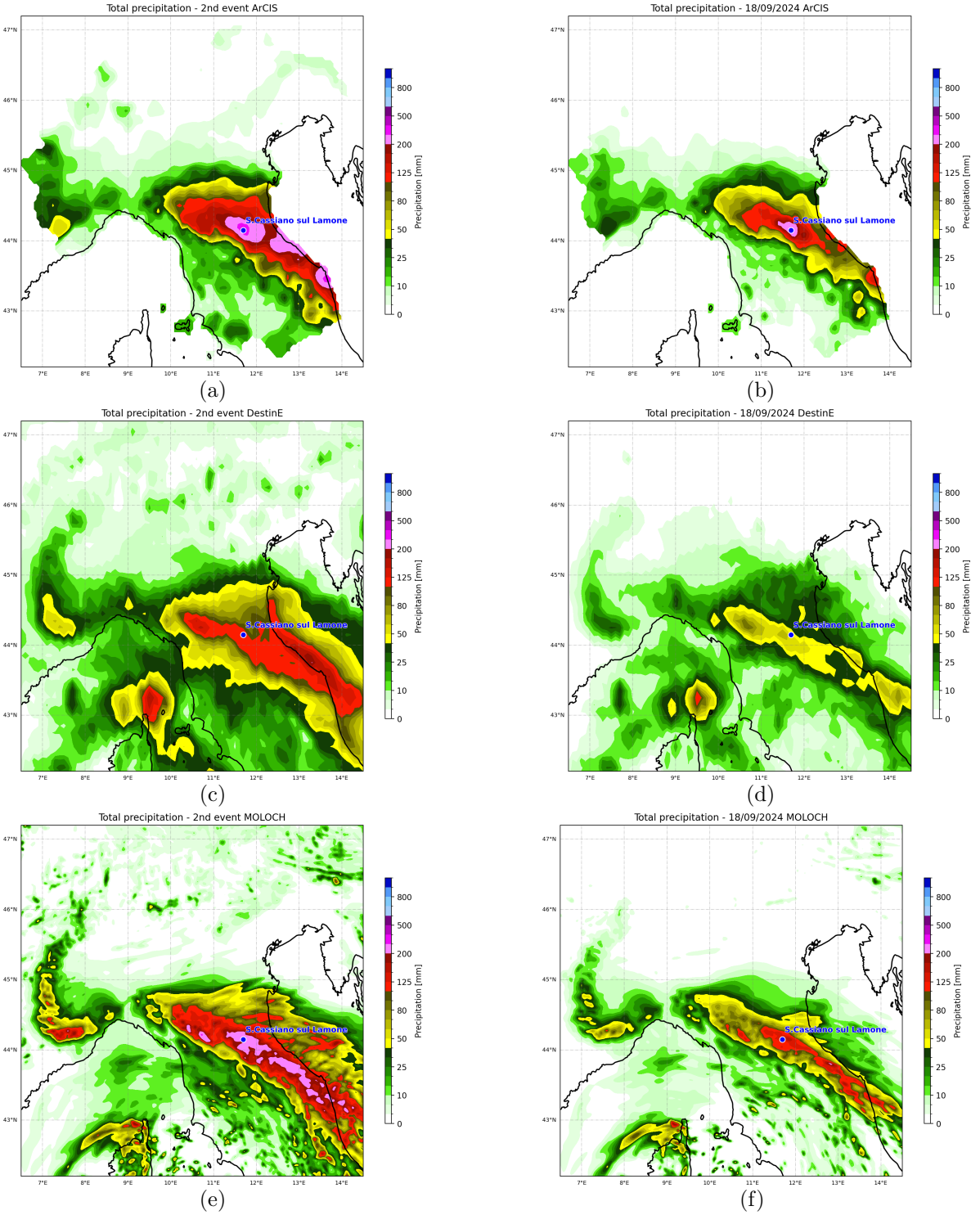

Figure 4.4: Spatial distribution of total (left) and peak daily (18 September, right) accumulated precipitation (mm) during the 2024 event. Comparison between (a-b) ARCIS observations, (c-d) Destination Earth, and (e-f) MOLOCH simulations.

tures extending from the Adriatic Sea toward the coastline and the Apennine ridge; the spatial continuity between marine and inland precipitation areas suggests the development of dynamically coherent convective features interacting with coastal and orographic forcing. Such behaviour is consistent with what is typically observed in convection-permitting simulations, where mesoscale organization can emerge explicitly.

The underestimation of precipitation by DestinE is already apparent in the spatial maps; however, a more detailed analysis allows the differences relative to MOLOCH to be quantified. MOLOCH simulates a maximum total accumulated precipitation of 270.3 mm near Monte Cimone, whereas DestinE reaches 202.12 mm along the Marche coast near Ancona. The added value of higher resolution becomes even more evident when considering daily maxima. In Figure 4.4d, DestinE reproduces a maximum of 114.57 mm over the Corsican Sea, while over the area most affected by the event daily accumulated precipitation remains below 100 mm.

Figure 4.5 presents the time series of hourly precipitation recorded at the San Cassiano sul Lamone station from 00:00 UTC on 17 September to 23:00 UTC on 20 September.

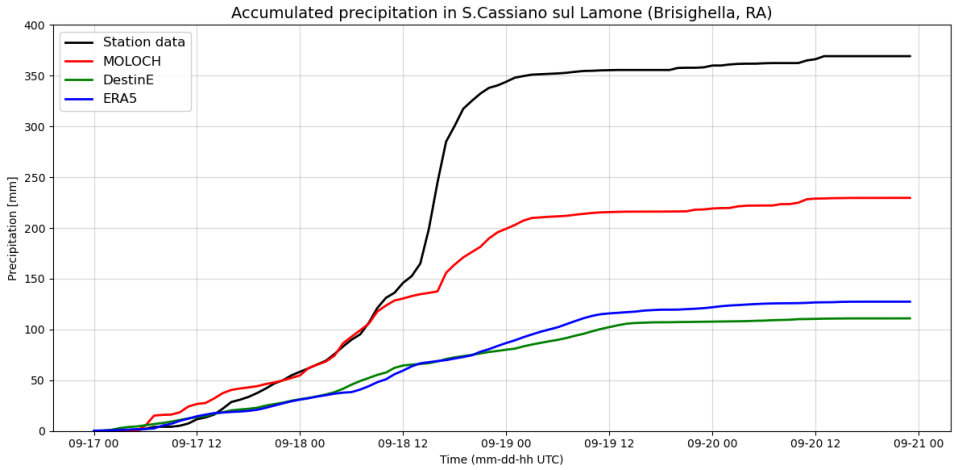

Figure 4.5: Time series of hourly accumulated precipitation (mm) throughout the 2024 event in the S.Cassiano sul Lamone station. The plot compares observed data from ARPAE (black line) with simulations from MOLOCH, Destination Earth (DestinE), and ERA5.

The rainfall evolution simulated by MOLOCH closely follows the gauge observations until the first half of 18 September. During the subsequent hours, however, MOLOCH does not fully capture the intensity of the peak cumulative precipitation. In contrast, the blue and green curves, corresponding to ERA5 and DestinE respectively, show a much more gradual increase in precipitation and substantially underestimate the observed rainfall. It is noteworthy that, in this case study, the ERA5 and DestinE profiles are very

similar, and ERA5 even appears to perform slightly better in reproducing the maximum peak. This suggests that increasing horizontal resolution from 30 km to 10 km is not sufficient, by itself, to adequately represent convective processes.

4.2.2 Statistical validation of MOLOCH simulations

Although MOLOCH was able to reproduce the precipitation field much more accurately than DestinE in this case study, the statistical analysis through bias and Absolute Error (AE) reveals a much more severe point-wise error. The AE map in Figure 4.6 shows intense and localized error peaks. While the error in the first case was spatially more diffuse, here sharp and dark patches are shown (high values, exceeding 100-150 mm), particularly in the areas with the highest rainfall. Specifically, at the S. Cassiano sul Lamone station, the AE reaches 130.45 mm.

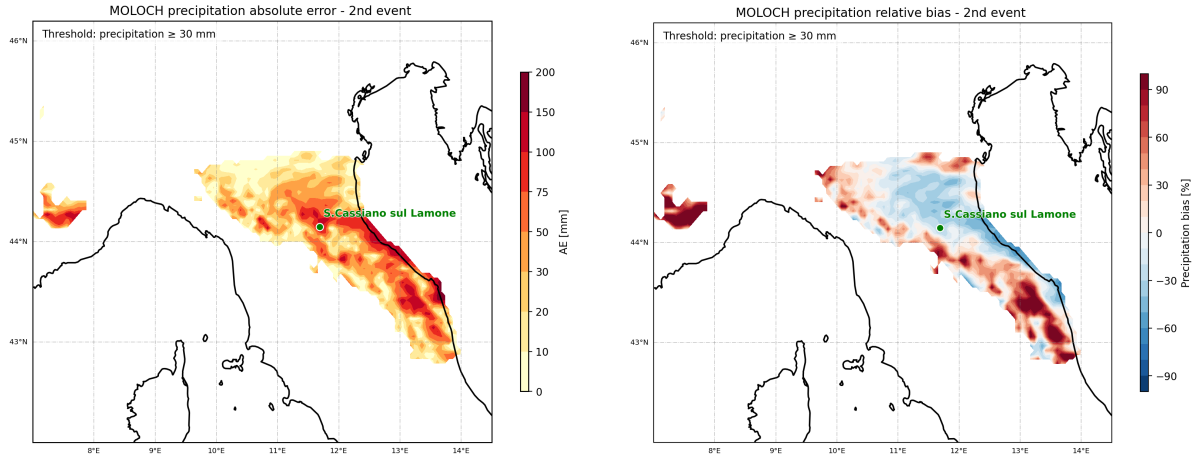

(a) (b)

Figure 4.6: Statistical comparison between MOLOCH simulated precipitation and ArCIS observations for the 2024 event. Panel (a) displays the Absolute Error (mm), while panel (b) shows the Relative Bias (%).

MEAN bias	MEAN relative bias	MEAN AE
-1,19 mm	11,04%	36,10 mm

Table 4.2: Mean spatial values of bias, relative bias and absolute error for the second event; they are computed for observed and modeled precipitation $\geq 30mm$.

Analyzing the bias in panel 4.6b, the same fragmented error pattern is evident, mainly affecting the Apennine ridge and the Marche region. Most of the affected area shows a

band of negative bias, indicating a model underestimation of extremes. The relative bias at the S. Cassiano sul Lamone station is -36.62%.

It is important to note the presence of extreme positive bias cores in close proximity to underestimated zones. This suggests that while the model correctly simulated the general violent nature of the event, slight spatial displacements of the most intense precipitation structures occurred. Such misplacements are expected in convection-permitting simulations due to the intrinsically chaotic nature of convective processes (Kendon et al., 2021) and do not indicate a systematic error in intensity. This interpretation is further supported by Table 4.2, which shows a sharp contrast between a Mean Bias near zero and a Mean AE that has almost doubled compared to the first event. In particular, the very small bias indicates that, on average, the model's overestimations and underestimations nearly cancel each other out. This is a clear sign of spatial compensation between areas of overestimation and underestimation, typical of a spatial shift of cells. Therefore, the high average error serves as an indicator of misplacement rather than incorrect intensity.

Chapter 5

Atmospheric changes between factual and counterfactual simulations

This chapter presents the results of the counterfactual simulations of the two events, in which a thermodynamic climate perturbation has been removed from the ERA5 boundary conditions used in the initialisation of MOLOCH, in order to assess the contribution of climate change to the intensity of the observed signals.

Sections 5.1.1 and 5.2.1 discuss the comparison between precipitation simulated under present and past climate conditions for each event, through the analysis of the signal expressed as a percentage difference. A comparison between the MOLOCH and DestinE simulations is also carried out in order to evaluate the added value of higher resolution modelling. Subsequently, the same comparative analysis is extended to the horizontal and vertical spatial distribution of the moisture fields simulated by MOLOCH in the two climate states. In addition, for the September 2024 event, results from the factual and counterfactual ensemble simulations are also discussed. Finally, Section 5.3 provides a comparison of the signal obtained for the two events.

5.1 Event 1: 30 April - 4 May 2023

5.1.1 Precipitation changes and inter-model differences

The counterfactual simulations performed with MOLOCH and DestinE produced a precipitation field that is visually different from that discussed in the previous chapter. Figure 5.1 presents the spatial distribution of accumulated precipitation simulated by DestinE (left) and MOLOCH (right) under present-day climate conditions (panels 5.1a and 5.1b) and pre-industrial conditions (panels 5.1c and 5.1d). The lower panels show

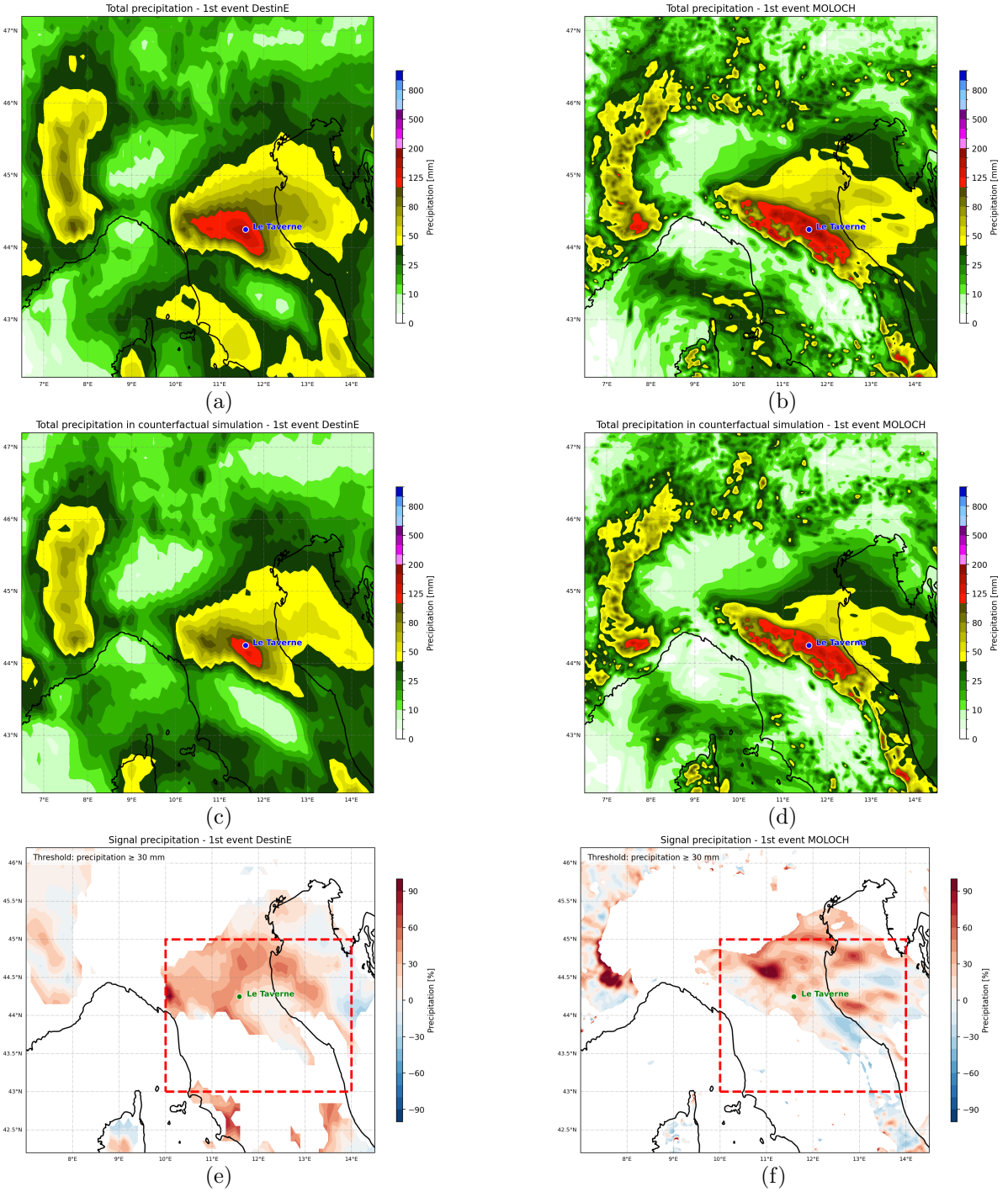

Figure 5.1: Spatial distribution of total precipitation (mm) simulated by DestinE (left) and MOLOCH (right) durign the 2023 event. Panels (a) and (b) display precipitation in the factual simulation, (c) and (d) refer to the counterfactual simulations. Panel (e) and (f) represent the relative precipitation signal (%) with a threshold applied to consider only precipitation $\geq$ 30 mm and a box (43–45°N, 10–14°E) indicating the averaging area.

the signal, computed as the percentage increase of factual relative to counterfactual precipitation, excluding cumulative precipitation values below 30 mm in order to prevent negligible rainfall amounts from generating unrealistically large percentage anomalies. The maps refer to total precipitation accumulated between 1 and 4 May 2023.

Comparing the two DestinE simulations and the associated signal reveals a clear intensification of the precipitation event under factual climate conditions. This is evident in the signal map (Figure 5.1e), where the predominantly red-shaded area indicates positive relative differences. Under present-day conditions, DestinE simulates more spatially widespread precipitation compared to the past scenario (Figure 5.1c), with accumulated rainfall exceeding 100 mm extending over a larger area (red shading). This area includes the station of Le Taverne, the most severely affected location, where the relative increase amounts to 34.20%. The largest increase over the affected region is found in the Po Valley; in particular, a peak of approximately 50–60% is observed over the Bologna plains and along the northern Romagna coast (Figure 5.1e). Despite the 30 mm threshold, slight noise associated with weak precipitation remains visible over the northwestern Apennine sector, where increases close to 100% are locally simulated, while over the southeastern Apennines a slightly negative signal of around 10% is detected. When averaging the cumulative rainfall signal over the entire Emilia-Romagna region, DestinE predicts an overall increase of 13.91%.

Examining panels 5.1b and 5.1d in light of the previous discussion, confirms the conclusions drawn in the earlier chapter regarding the performance of MOLOCH in reproducing a predominantly stratiform precipitation event associated with large-scale dynamical forcing and enhanced by orographic uplift. The precipitation change signal between factual and counterfactual simulations generated by MOLOCH exhibits a spatial pattern broadly consistent with that simulated by DestinE. This confirms that, for this type of phenomenon, the large-scale thermodynamic perturbation dominates the response, with limited sensitivity to convection-permitting resolution. Nevertheless, differences can be identified in the magnitude of local precipitation changes and in the spatial localisation of peak variations.

A comparison of the two MOLOCH simulations highlights an increase in the spatial extent of precipitation over the Emilia region, with a more pronounced signal over the plains, where cumulative amounts around 50 mm (yellow shading) expands. A marked increase, approaching 100%, is simulated over the Modena area, where accumulated rainfall rises from approximately 50–60 mm to 100–120 mm. A positive signal is again visible along the northern Adriatic coast and a negative one in the southern sector, with magnitudes locally exceeding 30%. Along the Apennine ridge, the signal remains weaker, consistent with the relatively uniform precipitation distribution simulated by MOLOCH under both climate conditions. Quantitatively, MOLOCH predicts an average regional increase of 8.84%, compared to 28.02% in DestinE within the defined maritime box (43–45°N, 10–14°E). At the Le Taverne station, the simulated increase amounts to 13.15%.

Finally, the smaller magnitude of the signal in MOLOCH suggests a certain model-dependent sensitivity of the attribution response. Nevertheless, both modelling frameworks consistently indicate a positive thermodynamic contribution to precipitation intensification across several areas of Emilia-Romagna.

5.1.2 Changes in moisture-related variables and vertical structures

In support of the precipitation signal, this section discusses the signal in total column water vapour (TCWV). Figure 5.2 presents the percentage change in the time-mean TCWV over the entire period of interest, derived from the DestinE (panel 5.2a) and MOLOCH (panel 5.2b) simulations.

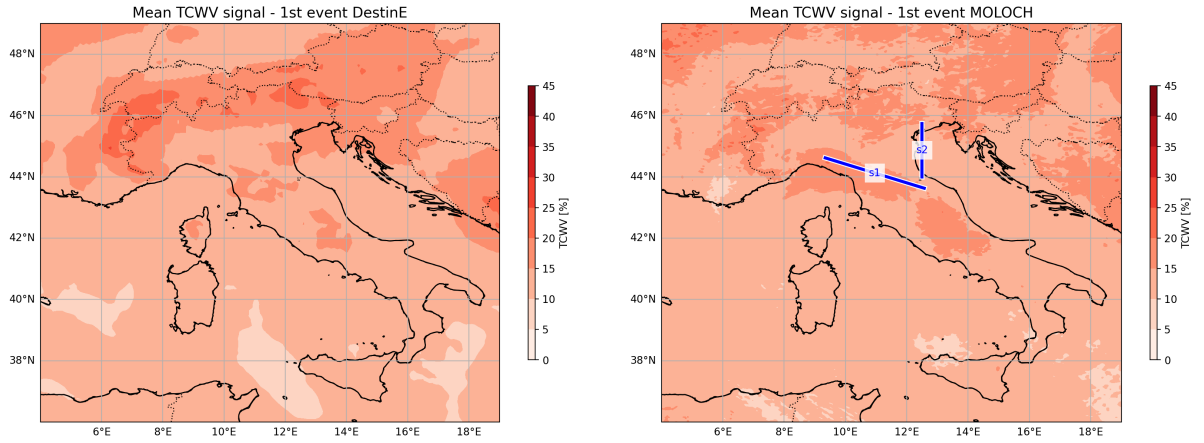

(a) (b)

Figure 5.2: Total column water vapour (TCWV) signal, computed as the relative difference (%) between the mean values over the entire period of the 2023 event in the factual and counterfactual world; panel (a) and (b) refer to DestinE and MOLOCH simulations respectively. The blue lines in panel (b) represent the location of the two cross sections.

A comparison of the two maps confirms the findings previously discussed for the precipitation increase. Both simulations show a general rise in precipitable water across the entire Mediterranean domain, primarily as a consequence of the way the perturbation applied to the factual simulation was constructed. Over the sea, an increase in TCWV between 10% and 15% is observed. Notably, DestinE predicts a pronounced increase in precipitable water over the Alps, approaching 30%, which is less evident in the MOLOCH simulation. Regarding the area of interest, DestinE simulates an increase between 15% and 20% over the Gulf of Venice and part of the Romagna coast, whereas MOLOCH

localises this increase along the Tyrrhenian slope of the Apennines. On average, over the Emilia-Romagna region, the two simulations agree on an increase of approximately 15%, confirming the good agreement between the two simulations in reproducing this case study.

The investigation of the moisture field continues with an analysis of two strategic cross-sections positioned to intercept the moisture inflow reaching the affected area. The orientation of the two sections is shown in Figure 5.2b: the first, s_1, is defined along the Tuscan-Emilian Apennines (defined by the points by the points 43.63 °N, 12.57 °E and 44.62 °N, 9.34 °E), while the second, s_2, is located directly off the Romagna coast (at longitude 12.5°E, extending from latitude 44.0 °N to 45.74 °N).

Figure 5.3a-f shows selected hourly time steps of integrated water vapour transport ($\mathrm{kg\,m^{-1}s^{-1}}$) across the cross sections simulated by MOLOCH in counterfactual (left panels) and factual (right panels) simulations. Shading depicts the IVT associated with the component normal to the cross-section plane. Yellow colours indicate positive values of inflow from east to west, i.e., onshore advection from the Adriatic Sea towards the Apennines, whereas blue colours denote negative outflow from west to east. Contours represent the wind component normal to the cross-section and are used to highlight where and how strongly the flow crosses the section. The black shaded area represents the Apennine topography.

As shown in Chapter 3, the present case study was characterized by a uniform and moist, yet stable, vertical column, where the primary dynamical driver resided specifically in the moisture transport. Panels 5.3a-5.3b, 5.3c-5.3d, 5.3e-5.3f and 5.3g-5.3h refer to the IVT evolution along s_2. The inflow flux at the coast shows a substantial increase in the present-day scenario (factual), with peak values approximately 30% higher than those of the past (counterfactual). This flux, particularly intense along the southern coastline, exhibited remarkable persistence throughout the event in both scenarios. The flux is uniformly distributed throughout the first 4 km of the atmosphere, especially in the factual scenario, characterized by a wider moisture inflow corridor. Furthermore, the wind magnitude remains relatively constant across the entire latitudinal extent of the coastal section in this scenario. Interestingly, MOLOCH simulates stronger influx winds closer to the surface in the factual simulation. This seems to contribute substantially to the enhanced transport in the first km, where atmosphere is not nudged, so winds are free to change in response to the warming. Although the maps display only specific timestamps, the peaks observed during the night and morning of May 2nd confirm a significantly greater availability of water vapor in the current climate scenario.

This increased moisture availability translates, with a delay of a few hours, into an impinging flux on the Apennines of comparable intensity, showed in panels 5.3i-5.3j and 5.3k-5.3l. The flux normal to the ridges is uniformly distributed, suggesting a structurally stable transport; notably, in the factual scenario, higher IVT values extend toward higher altitudes. In this current scenario, the transport reaches 140 $\mathrm{kg\,m^{-1}s^{-1}}$, compared to

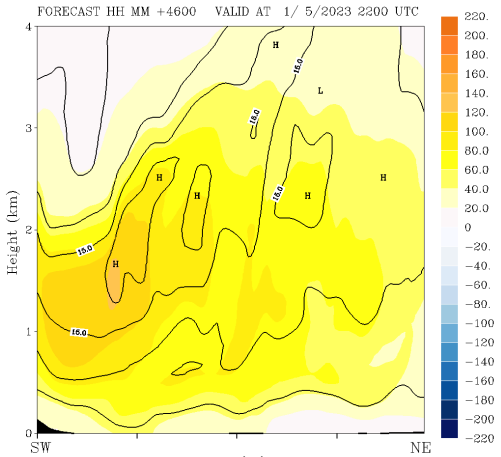
FORECAST HH MM +4600 VALID AT 1/ 5/2023 2200 UTC
Height (km)
SW
NE

(a)

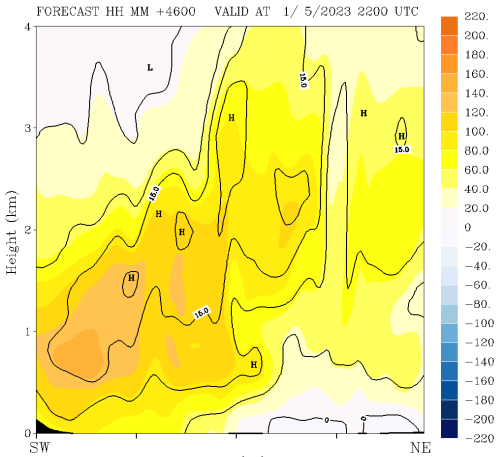
FORECAST HH MM +4600 VALID AT 1/ 5/2023 2200 UTC
Height (km)
SW
NE

(b)

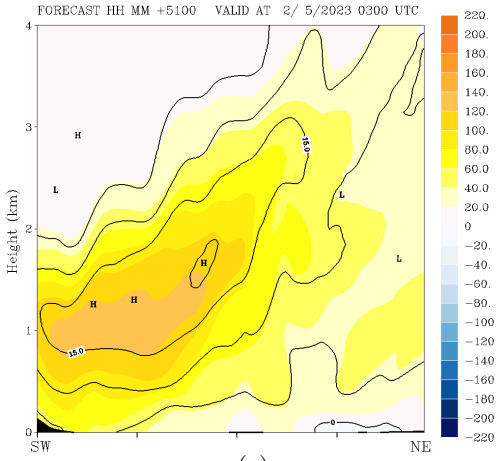
FORECAST HH MM +5100 VALID AT 2/ 5/2023 0300 UTC
Height (km)
SW
NE

(c)

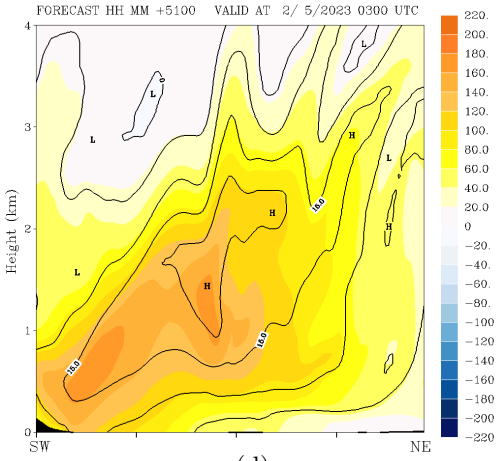
FORECAST HH MM +5100 VALID AT 2/ 5/2023 0300 UTC
Height (km)
SW
NE

(d)

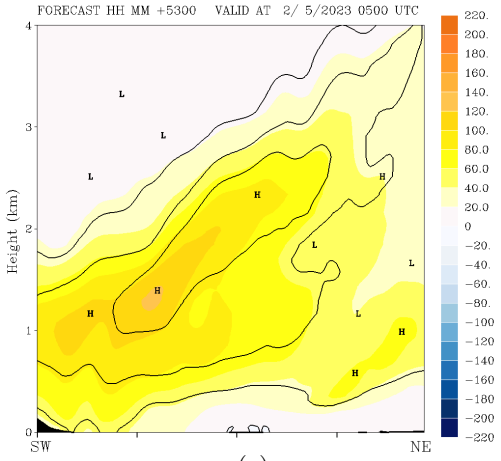
FORECAST HH MM +5300 VALID AT 2/ 5/2023 0500 UTC
Height (km)
SW
NE

(e)

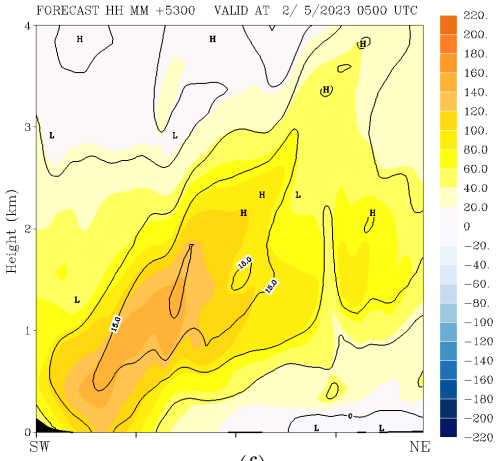
FORECAST HH MM +5300 VALID AT 2/ 5/2023 0500 UTC
Height (km)
SW
NE

(f)

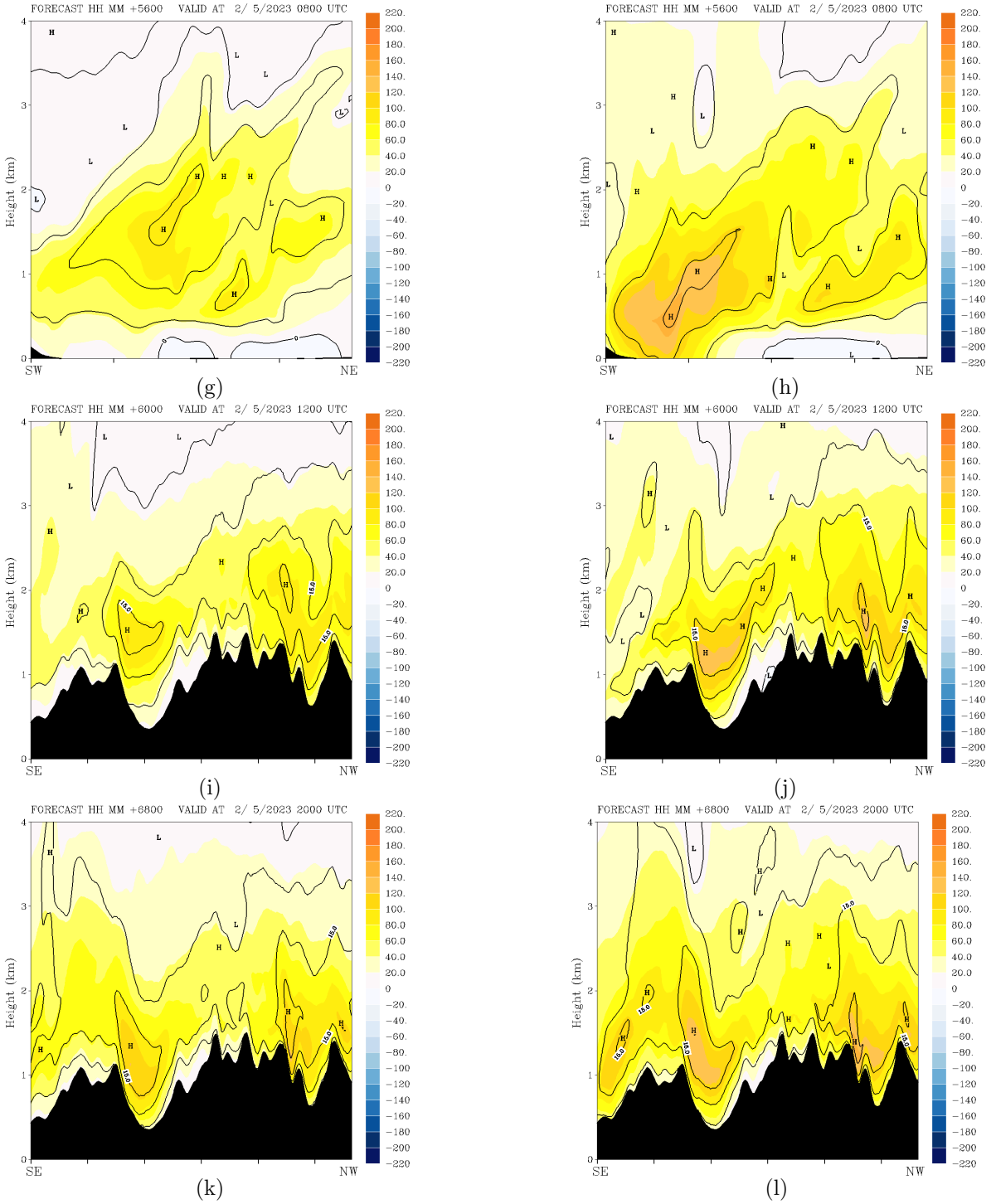

Figure 5.3: Cross-sections of IVT (shading; $\mathrm{kg\,m^{-1}s^{-1}}$) and normal component of wind (contours) simulated by MOLOCH in counterfactual (left panels) and factual (right panels) scenario at some instant of the 2023 event. The cross sections are defined along the Romagna coast (panels a-h) and along the Appenines (panels i-l); See Fig. 5.2b.

120 $\mathrm{kg\,m^{-1}s^{-1}}$ in the counterfactual one. It is therefore evident how the intensification of the coastal inflow in the present-day climate provides the necessary fuel to enhance orographic lifting, leading to more severe and persistent precipitation over the ridges.

5.2 Event 2: 17 -20 September 2024

5.2.1 Precipitation changes and inter-model differences

For the September 2024 event, the analysis of the climate signal is not expressed as a spatially coherent intensification across the region. Inspection of the maps in Figure 5.4 immediately indicates the absence of a clear increase in precipitation in the factual simulation relative to the counterfactual one.

Panels 5.4a and 5.4c show the total accumulated precipitation over the entire duration of the event simulated by DestinE under past and present climate conditions, respectively, while panel 5.4e displays the relative signal derived from these simulations. The percentage signal map shows predominantly negative values over most of the area affected by the event, indicating a decrease in precipitation under present-day climate conditions, with a regional mean of -8.02%. In particular, a negative signal emerges over the hilly and plain sectors of the region, with a decrease of -13.53% at the San Cassiano sul Lamone station. visually, this is consistent with a less extensive red-shaded (representing cumulative precipitation $< 100mm$) accumulation area in the factual map compared with the counterfactual map. A notable increase in the factual scenario, both in terms of intensity and spatial extent of precipitation, occurs over the Adriatic Sea and the southern Romagna coast, extending towards the Marche coastline, with values ranging between 10% and 50%. When spatially averaging the signal over the rectangular domain showed in Fig. 5.4e, this coastal positive contribution offsets much of the inland negative signal, resulting in a mean increase of about 3%, consistent with the dipole-like pattern in the signal map, characterised by adjacent red and blue patches. Overall, these features suggest that DestinE is capturing, at least in part, a displacement of precipitation maxima rather than a uniform weakening/strengthening of rainfall intensity.

Furthermore, it had previously been shown that MOLOCH, by explicitly resolving convection, led to an improvement in the representation of these phenomena. The signal map shown in panel 5.4f reveals a much more patchy and fragmented structure across a large portion of the domain, exhibiting a much stronger fine-scale variability. In particular, the larger precipitation amounts simulated by MOLOCH, with accumulations exceeding $100mm$, remain distributed along the Apennines in both the factual and counterfactual scenarios, as evidenced by the signal map, which displays very low percentage values in this area; consistently, at the San Cassiano sul Lamone station, MOLOCH predicts a negligible decrease of -3.77%. Within the rectangular box, by contrast, the

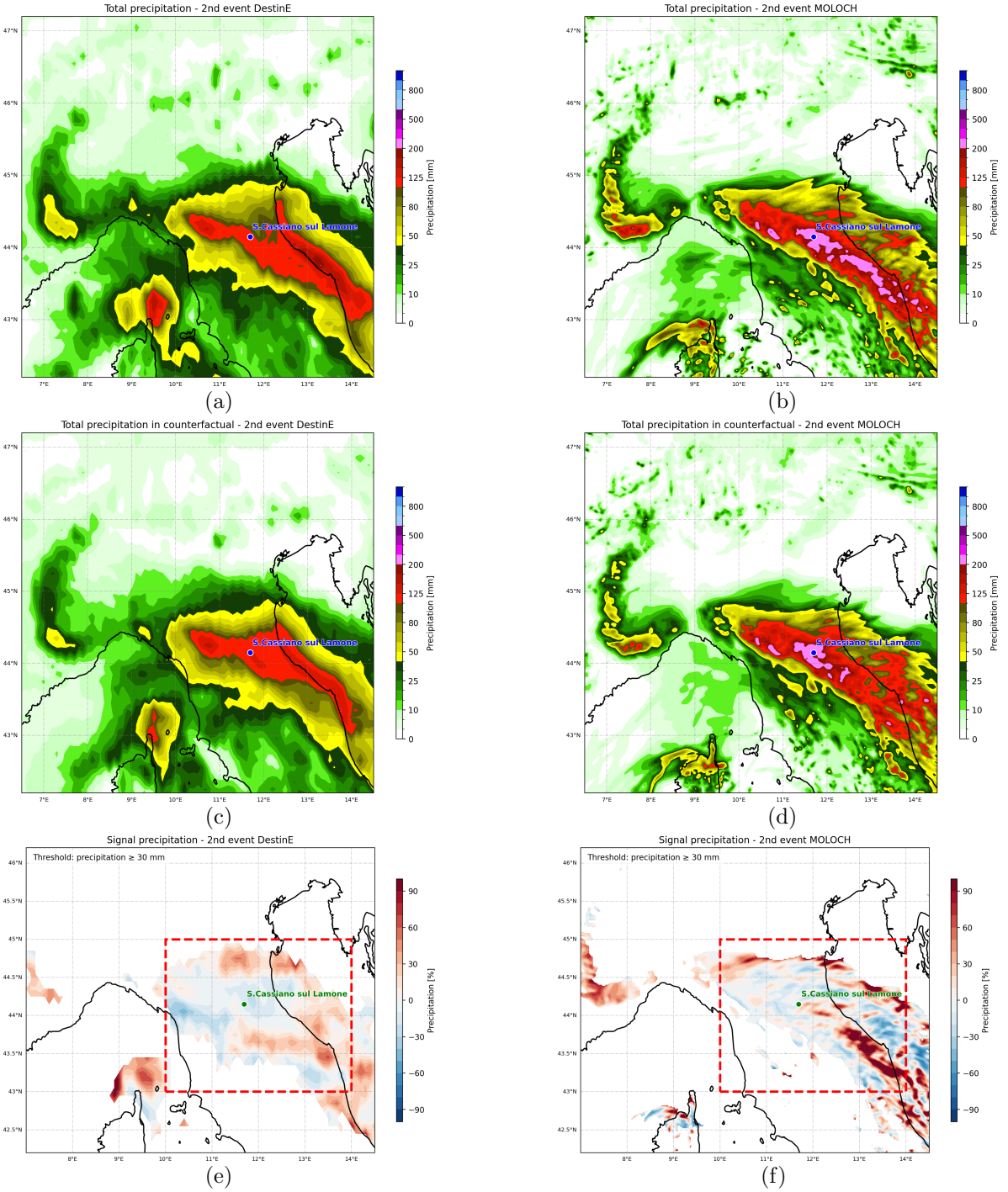

Figure 5.4: Spatial distribution of total precipitation (mm) simulated by DestinE (left) and MOLOCH (right) during the 2024 event. Panels (a) and (b) display precipitation in the factual simulation, (c) and (d) refer to the counterfactual simulations. Panel (e) and (f) represent the relative precipitation signal (%) with a threshold applied to consider only precipitation $\geq$ 30 mm and a box (43–45°N, 10–14°E) indicating the averaging area.

signal doubles relative to that predicted by DestinE, with an increase of 6.69%, primarily driven by a substantial rise in precipitation outside the regional boundaries. Indeed, greater accumulated precipitation is observed in the factual scenario along the Marche coastline, with percentage signal values reaching 100%. Both its magnitude and its lack of correspondence in the DestinE simulation make this signal a focal point of interest for this specific analysis.

Considering the average over the entire region, the signal amounts to 3.70%, thus remaining very small, because the widespread patchwork of positive and negative anomalies largely compensates in the mean. These dipoles may appear negligible over inland areas, where a comparison of the spatial distributions of accumulated precipitation in the two scenarios (5.4d and 5.4b) does not reveal visible differences. However, signal peaks are considerably more intense over coastal areas and offshore regions, where adjacent increases approaching 100% and decreases below -50% are observed, indicating that differences in the spatial positioning of convective cells between the two climates dominate the local signal.

This suggests that even with a high-resolution, convection-permitting model, it remains challenging to isolate a uniform signal of intensification attributable purely to warming. Rather, the detectable climate signal in precipitation totals appears tightly linked to shifts in the location and organization of convective precipitation, which can produce large local changes but small regional means due to spatial compensation. Such behavior may also be associated with a possible marine instability, warranting further investigation, which could give rise to isolated convective events.

5.2.2 Changes in moisture-related variables and vertical structures

The analysis of humidity fields, with particular reference to TCWV (Total Column Water Vapor), allows for different considerations compared to those formulated for the previous event. Figure 5.5 presents the maps of the percentage signal of the temporal mean TCWV over the entire period of interest, derived from the DestinE (panel 5.5a) and MOLOCH (panel 5.5b) simulations.

First, it is evident that the increase signal is generally more pronounced in both simulations relative to the first case study. This finding can be attributed to the initial thermodynamic conditions of the factual simulation: as discussed in the previous chapters, 2024 recorded unprecedented sea surface temperatures, resulting in a marked difference in terms of available moisture between the two events already under the present-day scenario.

Both MOLOCH and DestinE converge in predicting an increase in precipitable water of approximately 30% over the Alpine arc. However, in this second episode—unlike what was observed in May 2023—MOLOCH estimates a more substantial increase in TCWV

over the Mediterranean basin, reaching peaks of around 40% over central Italy. Although a visual inspection suggests that MOLOCH exhibits a generally stronger signal (with values ranging between 15% and 25% over the event area), these discrepancies diminish when considering spatial averages: when computed over the Emilia-Romagna region or over the rectangular domain extended to the Adriatic basin, the values predicted by the two simulations are closely aligned, ranging between 18% and 20%. However, it is important to note from the two maps that MOLOCH simulates a greater TCWV increase along the Marche coast compared to DestinE, consistent with the precipitation increments simulated by the two models.

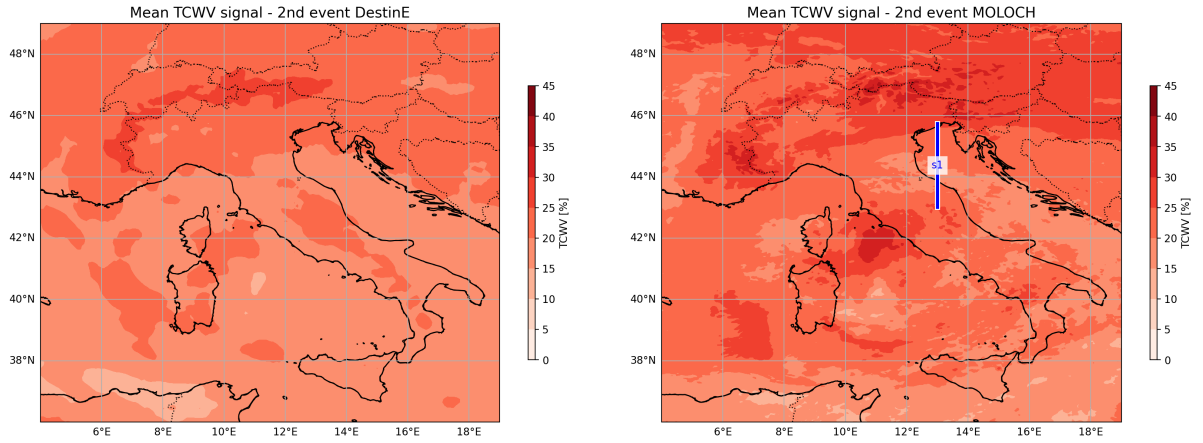

(a) (b)

Figure 5.5: Total column water vapour (TCWV) signal, computed as the relative difference (%) between the mean values over the entire period of the 2024 event in the factual and countefactual world; panel (a) and (b) refer to DestinE and MOLOCH simulations respectively. The blue line in panel (b) represents the location of the cross section.

For the study of vertical profiles in this event, a cross-section was chosen along the Romagna coast at longitude 13.0°E, extending into the Marche region to capture phenomena associated with the increased precipitation signal in this area. Figure 5.5b shows the section layout, from latitude 43.0 °N to 45.74 °N.

In Figure 5.6 selected hourly frames of IVT ($\mathrm{kg\,m^{-1}s^{-1}}$) along the defined cross section are showed. Compared with the colder climate experiment (left panels of the figure), the present-day simulation (panels on the right) exhibits a more persistent low-tropospheric inflow both during 17 September (panels 5.6b-5.6d) and throughout the 18 September intensification phase (panels 5.6f-5.6h). The flux in the factual experiment appears deeper, with a broader vertical extent and sustained IVT maxima impinging on the southern side of the section. In this area, local maxima increments of about 40% are observed, with IVT values increasing from approximately 120$\mathrm{kg\,m^{-1}s^{-1}}$ in the counterfactual scenario

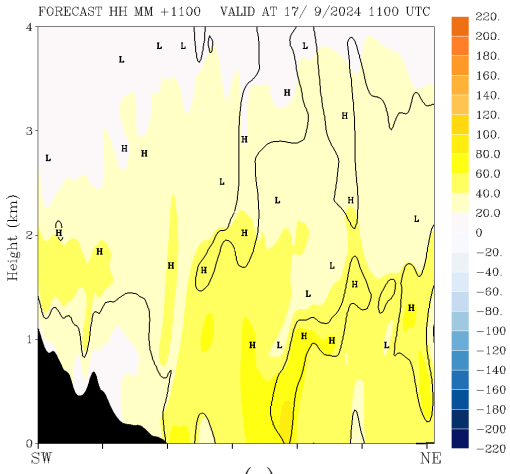
FORECAST HH MM +1100 VALID AT 17/ 9/2024 1100 UTC
Height (km)
SW
NE

(a)

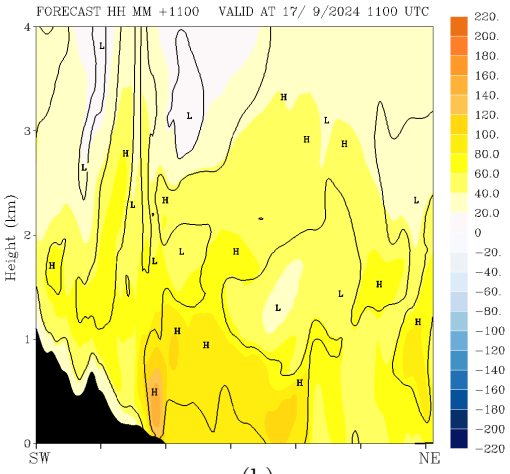
FORECAST HH MM +1100 VALID AT 17/ 9/2024 1100 UTC
Height (km)
SW
NE

(b)

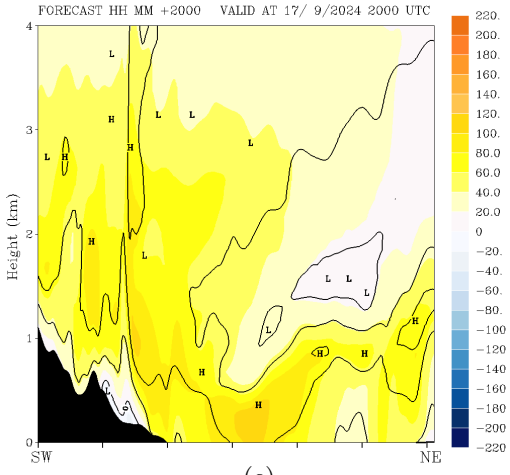
FORECAST HH MM +2000 VALID AT 17/ 9/2024 2000 UTC
Height (km)
SW
NE

(c)

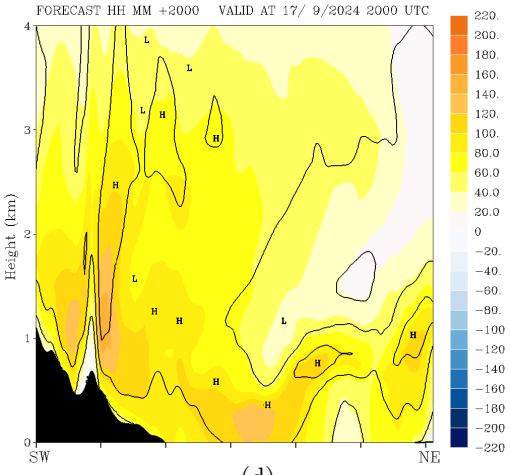
FORECAST HH MM +2000 VALID AT 17/ 9/2024 2000 UTC
Height (km)
SW
NE

(d)

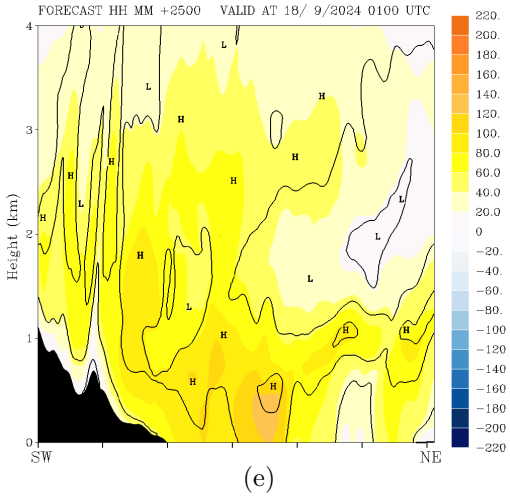
FORECAST HH MM +2500 VALID AT 18/ 9/2024 0100 UTC
Height (km)
SW
NE

(e)

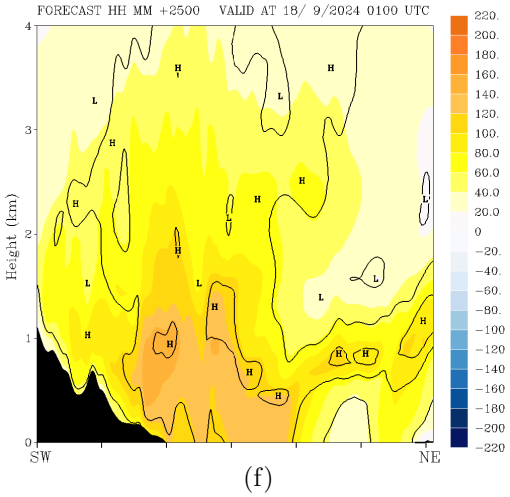
FORECAST HH MM +2500 VALID AT 18/ 9/2024 0100 UTC
Height (km)
SW
NE

(f)

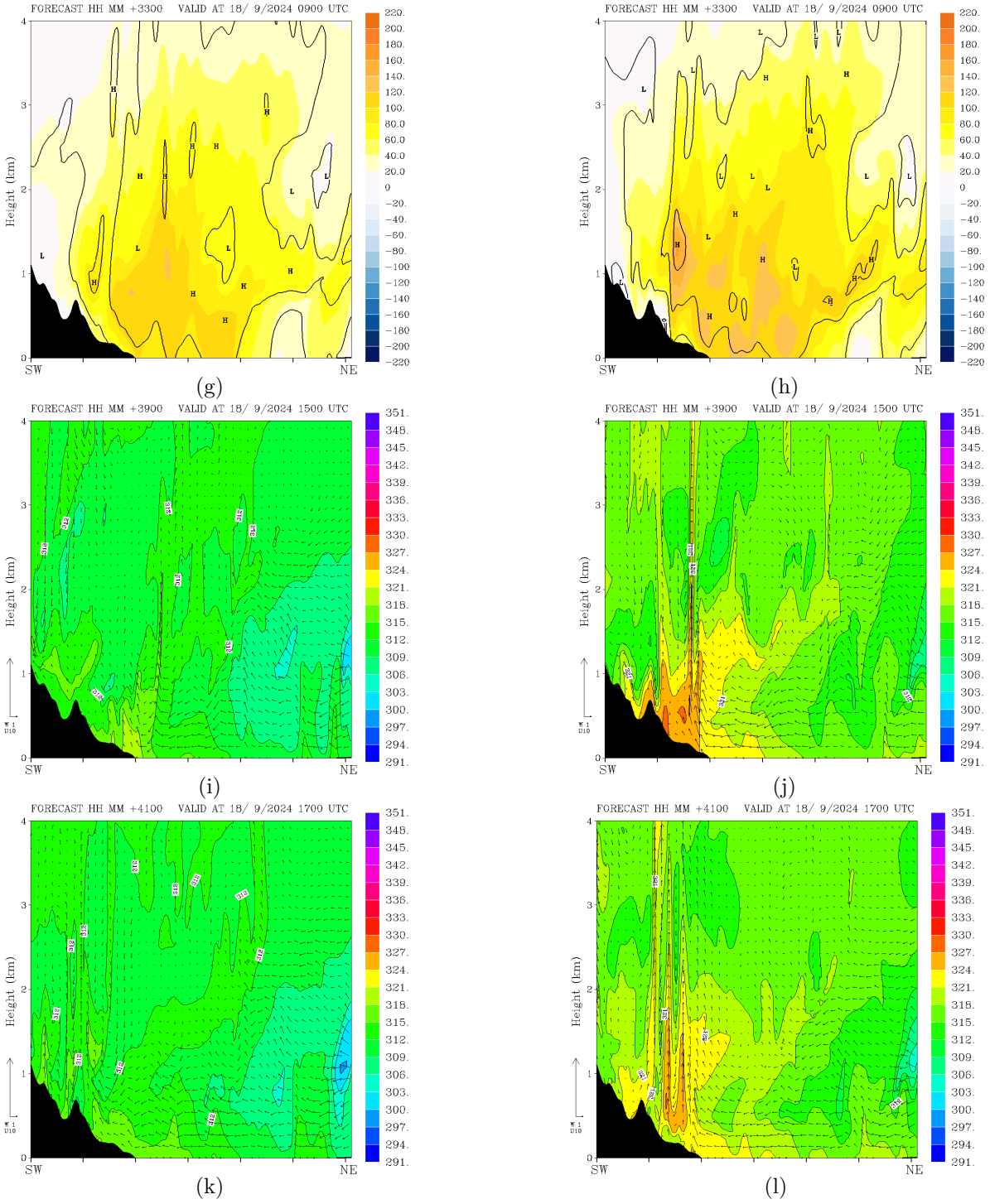

Figure 5.6: Cross sections of normal IVT (panels a–h; $\mathrm{kg\,m^{-1}s^{-1}}$) and θ_e (i–l); K) simulated by MOLOCH in counterfactual (left) and factual (right) scenarios for the 2024 event. Cross sections are defined along the Romagna coast; see Fig. 5.5b.

to 160kg m^{-1}s^{-1} in the factual one. This behaviour is consistent with a more effective Adriatic moisture supply towards inland areas and with environmental conditions more conducive to intense and long-lasting precipitation. Notably, the vertical wind shear within this inflow is deeper in the present climate, indicating structured variation in wind speed and direction with height, which can influence convective organization and precipitation efficiency. In contrast, the counterfactual simulation tends to show a more vertically confined structure, with shear concentrated within a shallower layer and less persistent moisture transport towards the orographic barrier (panels 5.6a to 5.6g).

Additional thermodynamic insight is provided by cross-sections of equivalent potential temperature (θ_e) in panels 5.6i, 5.6j, 5.6k and 5.6l. The wind component tangential to the cross-section is also represented with arrows, which identifies the advection component along the Adriatic coast. Because θ_e depends on both temperature and moisture, it is commonly used as a diagnostic to identify warmer, moister air masses, and θ_e maxima (plumes) may be more favourable to convection when a lifting mechanism is present. During the intense phase on 18 September (at 15:00 and 17:00 UTC), the factual simulation shows distinct high-θ_e plumes near the Apennine sector that extend vertically up to about $3 - 4km$, whereas in the counterfactual scenario the same feature is strongly reduced or absent. This indicates that the air feeding the event is warmer and moister in the factual scenario. This creates potentially higher thermodynamic support, which can lead to more intense interaction with the orography. It can be argued that this scenario seems to favour the triggering of more extreme convective phenomena.

5.2.3 Ensemble-based evaluation of the signal

Given the the role played by convective cells in MOLOCH and DestinE simulations, particularly along the Romagna and Marche coasts, it was considered worthwhile to analyze the precipitation signal produced by an ensemble simulation for this case study. In convection-permitting frameworks, small perturbations can lead to substantial differences in convective timing and cell placement, which motivates assessing the robustness of the inferred signal using ensemble mean and spread.

Figure 5.7 shows the time evolution of cumulative precipitation at the San Cassiano sul Lamone station for five ensemble members (labeled member 0 to 4) ((see Section 2.2.3 for the technique used for their initialization). Specifically, the two panels allow for a comparison between the ensemble simulations performed under the counterfactual (panel 5.7a) and factual (panel 5.7b) scenarios. The five colored curves represent the precipitation simulated by each member, the red curve denotes the ensemble mean, and the black curve in panel 5.7b represents the observed data. Finally, the gray shaded area represents the ensemble spread. In the factual scenario, member trajectories remain close until the early hours of 18 September and then diverge sharply, yielding a total-accumulation spread exceeding 50 mm by the end of the event; notably, member 3 acts as an outlier, falling outside the spread while moving closer to the observed values. In

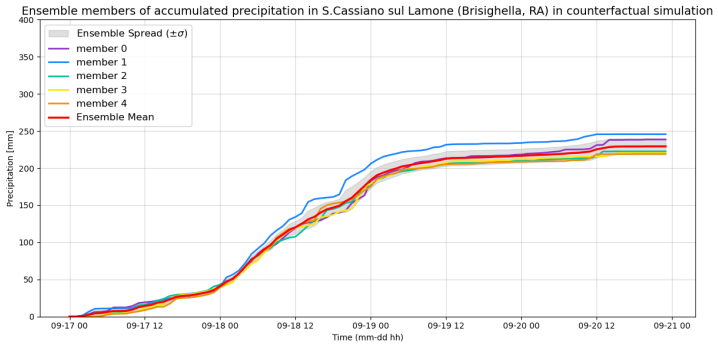

(a)

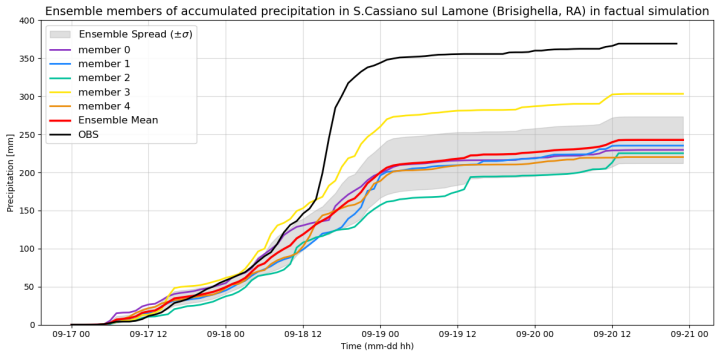

(b)

Figure 5.7: Time series of hourly accumulated precipitation (mm) throughout the 2024 event in the S.Cassiano sul Lamone station. The plot compares 5 members of ensemble simulation conducted with MOLOCH model in counterfactual (a) and factual (b) scenario. In both panels, the red line denotes the ensemble mean, the gray shaded area represents the ensemble spread ($\pm\sigma$), and the individual colored lines represent the five ensemble members. In panel (b), the black line indicates the observed data (OBS).

contrast, in the counterfactual scenario, the spread is much narrower: all members follow a similar evolution, producing final totals in the range 200–250 mm, with only a modest deviation by member 1. These point-based results suggest higher intrinsic uncertainty in the factual experiment, consistent with enhanced sensitivity of convective precipitation to small perturbations.

These observations, while referring to a single point in the domain, reflect broader trends across the entire area, as shown in the maps in Figure 5.8. Panel 5.8a illustrates the spatial distribution of cumulative ensemble-mean precipitation during the event in the counterfactual scenario. Comparing this map with the single-member simulation (Figure 5.4d) reveals a high degree of similarity in peak localization over all the domain. This reflects the high predictability of the event, consistent with the spaghetti plot where

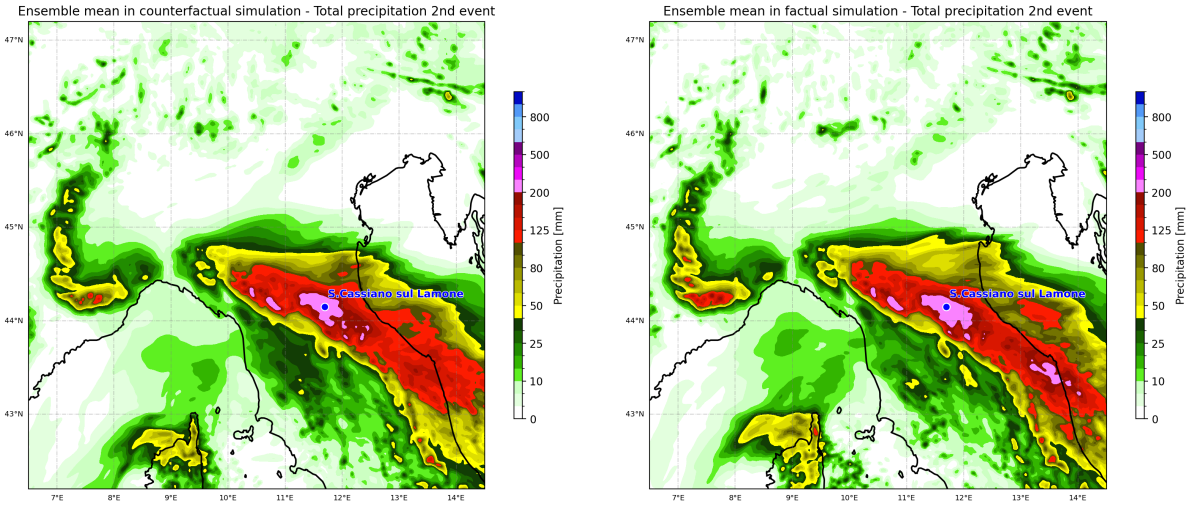

(a) (b)

Figure 5.8: Spatial distribution of ensemble mean accumulated precipitation (mm) during the 2024 event in counterfactual (a) and factual (b) scenario.

the reduced spread indicates strong model convergence.

In contrast, in the factual scenario the ensemble-mean precipitation map in panel 5.8b appears markedly different from the single-member simulation previously seen in Figure 5.4b. The primary difference is located in the coastal hinterland extending from the Emilia-Romagna and Marche border down to Macerata, where the wide band of cumulative rainfall exceeding 200 mm, is reduced in the ensemble mean. This indicates that the contributions of members simulating less precipitation in that area offset those simulating more, pointing to substantial event-to-event variability in the placement/intensity of coastal and near-coastal convective structures.

In terms of climate change, the analysis highlights that an ensemble approach is essential for quantifying variations. Figure 5.9 displays the spatial distribution of the precipitation signal, calculated as the percentage difference between the ensemble mean in the factual and counterfactual scenarios, using a 30 mm threshold. The resulting signal pattern remains similar to the broadly consistent with the single-member estimate (Fig. 5.4f) across much of the region, with a regional average increase of 4.29%. In the rectangular box covering the sea and part of the Marche coast, the increase remains nearly unchanged at 6.28%, while at the San Cassiano sul Lamone station, an increase of approximately 5.87% is recorded. Interestingly, however, the signal is significantly reduced across the entire Marche coastal area when using the ensemble mean, as expected when averaging over members with differing convective placement. Nevertheless, a signal is still present, with local increases ranging from 10% to 60%.

This evidence, combined with the absence of a similar signal in the DestinE simu-

lation, suggests that small-scale convective structures developing over the Adriatic and propagating inland can strongly modulate the local precipitation response and its apparent climate signal. MOLOCH is able to represent these localized features, while the ensemble spread highlights their intrinsic forecast uncertainty and the resulting sensitivity of the inferred signal to convective positioning.

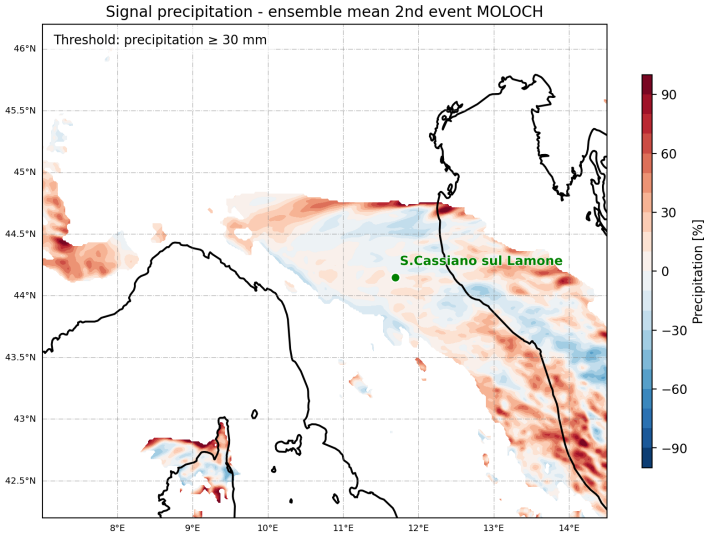

Figure 5.9: Spatial distribution of precipitation signal (%) computed for ensemble mean of the 2024 event. A threshold was applied to consider only precipitation $\geq$ 30 mm.

5.3 Summary and discussion

This section provides a final consolidated comparison of the climate-change increments diagnosed for the May 2023 and September 2024 events, highlighting both the magnitude of the simulated changes and their spatial structure. Table 5.1 summarizes the mean increments calculated both in the regional domain and inside a rectangular box (10-14°E, 43-45°N) (see Figure 5.1f) designed to capture the coastal and offshore contribution over the Adriatic. For accumulated precipitation and precipitable water, a comparison between the increments simulated by MOLOCH and DestinE is provided, whereas the increments of IVT and its components were evaluated only for MOLOCH.

For the May 2023 event, the response is comparatively consistent across variables and models. Both MOLOCH and DestinE simulate an increase in accumulated precipitation, with differences in magnitude (ranging from 8.84% to 28.02%) likely reflecting model-dependent differences in the reproduced precipitation field. However, this precipitation increase is accompanied by coherent increases in moisture availability and

transport. Specifically, the IVT increase of approximately 12–13% aligns with the increments observed in the cross-sections, particularly the 17.94% increase in the east-west flux component originating primarily from the sea.

In contrast, the September 2024 event does not exhibit the same linearity or consistency across the increments of the different variables. The mean regional precipitation increase is less than 5%, even when using the MOLOCH ensemble approach, while DestinE actually predicts a decrease. Importantly, the maps indicate that the most pronounced signal is not a uniform inland intensification, but is concentrated along the Romagna–Marche coastal sector and adjacent offshore areas, where MOLOCH shows markedly larger local changes and a dipole structure consistent with shifts in the location of convective maxima. Consistently, when considering the signal observed on the maps over the coast and the sea, the precipitation increment rises modestly, reaching a maximum of 6.69% in the MOLOCH deterministic simulation; in the ensemble analysis, the regional mean signal is 4.29% and the box-mean increase remains 6.28%, while local increases along the Marche coastal sector persist on the order of 10–60%. This confirms that substantial local changes can coexist with small domain-mean increments due to spatial compensation. At the same time, precipitable water shows a greater increase compared to the first case, which is consistent on average between the models, indicating enhanced moisture availability in the present-day configuration. Even more strikingly, IVT increases strongly in MOLOCH, with a regional increment of 14.44% rising to 18.10% in the box, highlighting the enhanced role of sea-to-land moisture transport during this event. Taken together, these results suggest that, for September 2024, increases in moisture availability and transport do not translate into a proportional increase in regional-mean precipitation totals; rather, the precipitation response is strongly modulated by mesoscale and convective organization—especially near the coast and offshore—so that shifts in convective placement can produce large local signals while yielding small regional means.

Mask on Emilia-Romagna region

First event: May 2023

Variable	Moloch	DestinE
Precipitation*	+8.84%	+13.91%
Mean TCWV	+14.98%	+16.10%
Mean IVT (Module)	+12.07%	
E-W Flux	+13.11%	

Mask on box lon 10-14°E, lat 43-45°N

First event: May 2023

Variable	MOLOCH	DestinE
Precipitation*	+13.78%	+28.02%
Mean TCWV	+14.22%	+14.93%
IVT (Module)	+13.50%	
E-W Flux	+17.94%	
S-N Flux	+4.29%	

Mask on Emilia-Romagna region

Second event: September 2024

Variable	Moloch	DestinE	Ensemble
Precipitation*	+3.70%	-8.02%	+4.29%
Mean TCWV	+19.92%	+18.10%	
IVT (Module)	+14.44%		
E-W Flux	+13.84%		

Mask on box lon 10-14°E, lat 43-45°N

Second event: September 2024

Variable	MOLOCH	DestinE	Ensemble
Precipitation*	+6.69%	+3.2%	+6.28%
Mean TCWV	+20.84%	+19.07%	
IVT (Module)	+18.10%		
E-W Flux	+17.91%		
S-N Flux	+15.80%		

*Threshold: precipitation $\geq$ 30 mm.

Table 5.1: Comparative summary tables of the percentage increments for the analyzed variables during the first and second events, calculated for the Emilia-Romagna region and the specific rectangular box (lon 10-14°E, lat 43-45°N).

Conclusions and open questions

Summary

The Emilia-Romagna region was struck by two extreme precipitation events, occurring between 1 and 4 May 2023 and 17 and 20 September 2024, which caused widespread flooding and hydrogeological instability. The two analyzed events were governed by a substantially similar large-scale dynamic configuration, with cyclonic currents that transported large amounts of moisture toward the area of interest, resulting in orographic lifting. However, the two events showed a different precipitative response and hydrological impacts. The May 2023 episode was characterized by low-intensity but long-persistent precipitation, which affected a territory already predisposed to saturation, determining severe damages. In contrast, the September 2024 event featured more intense precipitation with a convective component, yet was more spatially and temporally localized, occurring within a different seasonal context that resulted in less extensive hydrological consequences.

The intensity of these precipitation events and the magnitude of the associated damage raised the central research question of this thesis: to what extent these episodes may have been influenced by climate change, and whether their intensity can be attributed to it. In particular, comparing two extreme events with distinct precipitation patterns and impacts provides a framework to examine whether the climate change signal manifests uniformly, or if it differentially modulates events based on their physical and dynamical characteristics.

To address these questions, this thesis developed a novel methodological approach that integrates the strengths of the storyline approach with spectral nudging and the Pseudo-Global Warming (PGW) framework. Specifically, spectral-nudged storyline simulations from the Destination Earth project were used to derive event-specific thermodynamic perturbations induced by climate change. High-resolution simulations of the events, initialised by ERA5, were conducted with the convection-permitting model MOLOCH at a resolution of 1.8 km. The setup aimed to represent the event in factual (present-day) climate conditions, with the additional implementation of spectral nudging. Subsequently, the Destination Earth perturbation was applied to ERA5 data, in order to initialize MOLOCH simulations and reconstruct counterfactual scenario, effectively simulating the same event in a past pre-indutrial climate in absence of global warming. This

is done by subtracting the thermodynamic temperature and humidity signal from the initial and boundary conditions. This approach allowed for quantifying the thermodynamic contribution to the events' intensity by employing a convection-permitting model, all while preserving the consistency of the ERA5 large-scale circulation. Furthermore, the use of the MOLOCH model served to investigate the extent to which the direct representation of convective processes can improve the simulation of the analyzed extreme events compared to coarser-resolution (9km) Destination Earth simulations, with particular reference to the September 2024 episode where the convective component played a decisive role. Furthermore, in the context of this specific event, an ensemble-based approach adopted with MOLOCH allowed for overcoming the limitations of the single member available in Destination Earth.

Key results

A preliminary analysis of the dynamics of both events identified the atmospheric conditions and the primary dynamic drivers responsible for the precipitation peaks. In both cases, the dynamic forcing of orographic lifting acting on a large amount of moisture was a determining factor. This was the main driver of the May 2023 event, which was predominantly orographic in nature, with persistent flows maintaining a constant moisture supply toward the Po Valley. In September 2024, the mechanism was similar, but with higher sea surface temperatures and a more pronounced lapse rate, resulting in a component of embedded convection within the stratiform precipitation.

The analysis primarily focused on the precipitation fields in the factual and counterfactual scenarios, as simulated by both MOLOCH and the global IFS-FESOM model used within the Destination Earth project. A comparison between the two simulations in the factual scenario highlights how the added value of high resolution varies significantly between the two case studies, depending on the physical nature of each event. Regarding the May 2023 event, both models showed good spatial accuracy, capturing the general precipitation pattern well, however, slightly underestimating the maximum observed values. In general, MOLOCH was more precise in concentrating the precipitation along the windward Apennine slope, with an exaggerated orographic enhancement along the Apennine ridge. Destination Earth, instead, simulated high accumulations also on the Tyrrhenian slope, where observations indicated weaker precipitation. In this case, the benefit derived from the convection-permitting approach appeared modest, however, as the mechanism is already well represented even at lower resolution. Since it was an event with predominantly orographic rather than convective forcing, the precipitation pattern was overall well captured also by Destination Earth.

In the second case study (September 2024), characterized by a convective component and high-intensity peaks, the performance of the models showed much more marked differences compared to the first one. Indeed, the use of the convection-permitting model MOLOCH provided clear added value, delivering a substantially more realistic result

than Destination Earth in terms of both intensity of the peaks and their spatial distribution. The model successfully simulated the multiple convective cell structure along the Apennines and the coast, although a slight misplacement of the convective cells emerged from the statistical validation. The Destination Earth simulation results showed a significant underestimation of precipitation, especially at the highest peaks. This occurred because the convective component was dominant in the event, and the 9 km resolution of IFS-FESOM wasn't sufficient to correctly capture it through parameterizations or to identify its intensity and positioning. In this case study, high resolution and the direct resolution of convection proved necessary for an accurate representation of the fine-scale nature of this phenomenon.

Analyzing the two events in a counterfactual scenario allowed for a direct comparison of the precipitation fields, confirming earlier observations regarding model-specific sensitivities. The event-based perturbation applied to both simulations highlighted how global warming influenced precipitation intensity differently across the two cases.

Regarding the May 2023 event, the analysis showed a clear signal of precipitation intensification due to the thermodynamic contribution, visible in both the MOLOCH and Destination Earth simulations. Since the event is driven by large-scale dynamics, the results from both models agreed in confirming that anthropogenic warming amplified the stratiform precipitation and that its intensity has been greater than that would have occurred if the same large scale unfolded in the climate of the 1950s. Destination Earth estimated a mean regional precipitation increase of 13.91%, with local peaks between 50% and 60% in the Bologna plains. The MOLOCH model detected a more contained but consistent signal, with a mean regional increase of 8.84%. A local analysis at the station recording the highest precipitation totals during the event, Le Taverne (BO), showed an increase of 34.20% according to Destination Earth, while MOLOCH reported 13.15%. Thus, the observed increase is somewhat variable depending on the model and the area, but it remains present and very evident. This signal can be considered highly robust, especially given the linearity of the physical processes characterizing this event. Examining the dynamic drivers, it is clear that precipitation increased consistently with moisture levels and transport flux. Indeed, the precipitation increase relative to the pre-industrial scenario is supported by an increase in Total Column Water Vapor (TCWV) of approximately 15% and Integrated Vapor Transport (IVT) of about 12% on a regional scale. Furthermore, the vertical distribution of moisture flux revealed a 15–30% increase in the component perpendicular to the coast, which subsequently impacts the Apennines, creating more favorable conditions for orographic lifting and the development of stratiform precipitation.

The attribution analysis for the September 2024 event is inherently more intricate, arising from the complex nature of the phenomenon itself, thus is primarily based on the ensemble-mean results, which provide a more robust physical signal compared to individual simulations. At the San Cassiano sul Lamone station, the ensemble signal indicates a 5.87% increase, while it remains modest over the rest of the region. However, these av-

erage values mask substantial ensemble spread, particularly regarding coastal convective structures. Relying on a single deterministic member can lead to highly misleading conclusions: for instance, the deterministic MOLOCH simulation predicts localized increases approaching 100% along the coast of the Marche region. In contrast, the ensemble-mean shows a much more contained increase in the same area, ranging between 10% and 60%. This discrepancy highlights the value of the ensemble methodology introduced here: it allows to isolate the true response to thermodynamic perturbation from numerical noise and event-to-event variability in convective placement. Nevertheless, the robustness of this signal remains uncertain, as the same linearity observed in the other case study was not found. The average regional rainfall increase is not consistent with the observed increases in Total Column Water Vapor (TCWV) of approximately 20% and Integrated Vapor Transport (IVT) of about 15%. In this case study, the identification of drivers is less immediate. This event was certainly driven by a more intense and vertically deeper low-level inflow. However, an increase in thermodynamic energy and a more pronounced vertical shear were also observed, which favored the organization of persistent convection more significantly in the factual scenario.

In summary, the clear distinction between the nature of the two events is also reflected in the robustness of the climate signal attribution. The May 2023 event exhibited a highly linear character, with a clear dynamic and orographic forcing that allows for a robust assertion that the extreme precipitation event was intensified by global warming. Driven primarily by the thermodynamic contribution and vapor fluxes, the signal remains solid and consistent in the Destination Earth and MOLOCH simulations, regardless of their resolution. In the September 2024 event, however, embedded convection represented a crucial aspect of the meteorological phenomena. It was demonstrated that the use of a convection-permitting model and an ensemble approach is necessary to accurately reproduce this event and the increase in precipitation from the thermodynamic perturbation. Nevertheless, the complexity of the dynamics driving this event made the attribution more challenging. Although the climate signal detected by MOLOCH appears robust, this case requires further quantitative analysis to physically understand how the development of the convective cells is responding to the climate perturbation.

Open questions and future perspectives

The study presented in this thesis could be further explored through more quantitative analyses. First, it is necessary to more precisely quantify the relative weights of dynamic contributions (mass convergence) versus thermodynamic ones, such as moisture and atmospheric instability, for both events. Furthermore, the instability observed in the September 2024 event requires a rigorous calculation of instability indices—such as CAPE, CIN, or LFC—to support what has been qualitatively inferred from the equivalent potential temperature profiles.

Building on these results, future investigations should upgrade the ensemble-based

methodology. This includes significantly increasing the ensemble membership to provide more robust statistics on extreme convective peaks, and also applying an ensemble approach to the first May 2023 event for consistency.

Moreover, it is essential to study additional events with strong convective components, similar to September 2024, to verify if they exhibit a consistent response to thermodynamic perturbations, extending the analysis to hourly precipitation peaks in addition to the daily accumulations examined here.

Finally, comparison with the Destination Earth results was limited by the absence of certain diagnostic variables, which prevents an exact quantification of the smoothing of vertical gradients. Nonetheless, MOLOCH superior representation of the convective event remains a strong argument with reliable results; this may also be linked to a greater capacity to represent atmospheric instability and convection-triggering processes that Destination Earth may only partially capture. This motivates future in-depth studies, particularly regarding the September 2024 event, to understand the relative importance of thermodynamic contributions versus modeling capabilities in its representation.

References

Andersson, Erik and Jean-Noël Thépaut (2008). "ECMWF's 4D-Var data assimilation system – the genesis and ten years in operations". In: *ECMWF Newsletter* 115. Meteorology section, Spring 2008, pp. 8–12.

ArCIS (2025). *Analisi piogge: monthly precipitation analysis*. Archivio Climatologico per l'Italia Centro Settentrionale (ArCIS). URL: https://www.arcis.it/wp/2025/11/analisi-piogge/.

Athanase, Mélanie, Adrián Sánchez-Benítez, Elisa Monfort, et al. (2024). "How climate change intensified storm Boris' extreme rainfall, revealed by near-real-time storylines". In: *Communications Earth & Environment* 5, p. 676. DOI: 10.1038/s43247-024-01847-0.

Barriopedro, David et al. (2025). "A Multimethod Attribution Analysis of Spain's 2024 Extreme Precipitation Event". In: *Bulletin of the American Meteorological Society*, E2440–E2460. DOI: 10.1175/BAMS-D-25-0049.1.

Buizza, Roberto (2001). "Chaos and weather prediction: A review of recent advances in numerical weather prediction". In: *Il Nuovo Cimento C* 24.2, pp. 273–297. DOI: 10.1007/BF02559565.

Campos, Diego A. et al. (2025). *The October 2024 Extreme Precipitation Event over Valencia: Storyline Attribution of the Synoptic-Scale Thermodynamic Drivers*. EGUsphere preprint. DOI: 10.5194/egusphere-2025-5929. URL: https://doi.org/10.5194/egusphere-2025-5929.

Cardinali, Chiara et al. (June 3, 2023). *Rapporto degli eventi meteorologici di piena e di frana dell'1-4 maggio 2023*. Bologna, Italy: Arpae Emilia-Romagna – Struttura Idro-Meteo-Clima.

CIMA Foundation (2025). *Flooding in Emilia-Romagna: Scientific analysis by CIMA Research Foundation*. Accessed: 2025-10-17. URL: https://www.cimafoundation.org/en/news/flooding-in-emilia-romagna-scientific-analysis-by-cima-research-foundation/.

Consorzio LaMMA (2025). *Le previsioni probabilistiche*. Consorzio LaMMA. URL: https://www.lamma.toscana.it/meteo/le-previsioni-probabilistiche.

Copernicus Climate Change Service (2024). *European Ocean*. European State of the Climate 2024. Copernicus Climate Change Service. URL: https://climate.copernicus.eu/esotc/2024/european-ocean.

Davolio, Silvio, Alberto Buzzi, and Paolo Malguzzi (2006). "Orographic influence on deep convection: case study and sensitivity experiments". In: *Meteorologische Zeitschrift* 15.2, pp. 215–223. DOI: 10.1127/0941-2948/2006/0118.

Destination Earth (2024). *Digital Twins and the Digital Twin Engine*. Accessed: 2025-11-13. Destination Earth. URL: https://destination-earth.eu/destination-earth/destines-components/digital-twins-digital-twin-engine/.

European Centre for Medium-Range Weather Forecasts (2012). *The ECMWF Ensemble Prediction System*. ECMWF informational brochure. Reading, United Kingdom: European Centre for Medium-Range Weather Forecasts. URL: https://www.ecmwf.int.

— (2015). *IFS Documentation CY41R2, Part III: Dynamics and Numerical Procedures*. Reading, United Kingdom: European Centre for Medium-Range Weather Forecasts. URL: https://www.ecmwf.int/en/elibrary/79696-ifs-documentation-cy41r2-part-iii-dynamics-and-numerical-procedures.

European Centre for Medium-Range Weather Forecasts (ECMWF) (2025). *ECMWF official website*. European Centre for Medium-Range Weather Forecasts. URL: https://www.ecmwf.int.

European Digital Twin Earth (DESTINe) (2024). *Replaying Extreme Weather: How Storyline Simulations Help Us Prepare for Climate Change*. Accessed: 2025-11-13. European Digital Twin Earth (DESTINe). URL: https://destine.ecmwf.int/news/replaying-extreme-weather-how-storyline-simulations-help-us-prepare-for-climate-change/.

Faranda, Davide et al. (2024). "ClimaMeter: contextualizing extreme weather in a changing climate". In: *Weather and Climate Dynamics* 5, pp. 959–983. DOI: 10.5194/wcd-5-959-2024.

Foraci, Rosanna et al. (Dec. 2, 2024). *Rapporto degli eventi meteorologici di piena e di frana del 17–19 settembre 2024*. Bologna, Italy: Arpae Emilia-Romagna – Struttura Idro-Meteo-Clima.

Garderen, Lisette van, Frank Feser, and Theodore G. Shepherd (2021). "A methodology for attributing the role of climate change in extreme events: a global spectrally nudged storyline". In: *Natural Hazards and Earth System Sciences* 21, pp. 171–186. DOI: 10.5194/nhess-21-171-2021.

Giorgi, Filippo (2019). "Thirty years of regional climate modeling: Where are we and where are we going next?" In: *Journal of Geophysical Research: Atmospheres* 124, pp. 5696–5723. DOI: 10.1029/2018JD030094.

Holton, James R. and Gregory J. Hakim (2012). *An Introduction to Dynamic Meteorology*. 5th ed. Burlington, MA: Academic Press.

Intergovernmental Panel on Climate Change (IPCC) (2023). *Climate Change 2021 – The Physical Science Basis: Working Group I Contribution to the Sixth Assessment*

Report of the Intergovernmental Panel on Climate Change. Cambridge: Cambridge University Press.

ISAC-CNR (2012). *Moloch: Short Description*. Institute of Atmospheric Sciences and Climate – National Research Council (ISAC-CNR). URL: https://www.isac.cnr.it/dinamica/projects/forecasts/moloch_short_description_2012.htm.

John, Amal, Sebastian Beyer, Marylou Athanase, et al. (2026). *Global Kilometre-Scale Climate Storylines Using Spectral Nudging*. Preprint. DOI: 10.22541/essoar.173160166.64258929/v2.

Kendon, E. J. et al. (2021). "Challenges and outlook for convection-permitting climate modelling". In: *Philosophical Transactions of the Royal Society A: Mathematical, Physical and Engineering Sciences* 379.2195, p. 20190547. DOI: 10.1098/rsta.2019.0547.

Koo, M.-S. and S.-Y. Hong (2013). "Double Fourier series dynamical core with hybrid sigma-pressure vertical coordinate". In: *Tellus Series A: Dynamic Meteorology and Oceanography* 65.1, p. 19851. DOI: 10.3402/tellusa.v65i0.19851.

Lenderink, Geert et al. (2025). "A pseudo global warming based system to study how climate change affects high impact rainfall events". In: *Weather and Climate Extremes* 49, p. 100781. ISSN: 2212-0947. DOI: https://doi.org/10.1016/j.wace.2025.100781. URL: https://www.sciencedirect.com/science/article/pii/S2212094725000398.

Malguzzi, Paolo et al. (2006). "The 1966 "century" flood in Italy: A meteorological and hydrological revisitation". In: *Journal of Geophysical Research* 111, p. D24106. DOI: 10.1029/2006JD007111.

Mariani, Simone et al. (2015). "A new high-resolution BOLAM–MOLOCH suite for the SIMM forecasting system: assessment over two HyMeX intense observation periods". In: *Natural Hazards and Earth System Sciences* 15, pp. 1–24. DOI: 10.5194/nhess-15-1-2015.

Messmer, Michael, Christoph C. Raible, and Juan J. Gómez-Navarro (2020). "Impact of climate change on the climatology of Vb cyclones". In: *Tellus A: Dynamic Meteorology and Oceanography* 72.1, pp. 1–18. DOI: 10.1080/16000870.2020.1724021.

O'Gorman, Paul A. (2015). "Precipitation Extremes Under Climate Change". In: *Current Climate Change Reports* 1.2, pp. 49–59. DOI: 10.1007/s40641-015-0009-3.

Pavan, Valentina, Gabriele Antolini, Roberto Barbiero, et al. (2019). "High resolution climate precipitation analysis for north-central Italy, 1961–2015". In: *Climate Dynamics* 52, pp. 3435–3453. DOI: 10.1007/s00382-018-4337-6.

Riboldi, Jacopo et al. (2025). *Storm Boris (2024) in the current and future climate: a dynamics-centered contextualization, and some lessons learnt*. EGUsphere preprint. DOI: 10.5194/egusphere-2025-3599. URL: https://doi.org/10.5194/egusphere-2025-3599.

Scoccimarro, Enrico, Alessandro Borrelli, Luca Sangelantoni, et al. (2025). "A cul-de-sac effect makes Emilia-Romagna more prone to floods in a changing climate". In: *Scientific Reports* 15, p. 36823. DOI: 10.1038/s41598-025-24486-7.

Shepherd, Theodore G. (2016). "A Common Framework for Approaches to Extreme Event Attribution". In: *Current Climate Change Reports* 2, pp. 28–38. DOI: 10.1007/s40641-016-0033-y.

Wu, Hsiao-Ting, Kai Hartmuth, and Heini Wernli (2026). "Performance of the operational ECMWF ensemble in predicting heavy rain associated with the Emilia-Romagna flood in May 2023". In: *Weather*. DOI: 10.1002/wea.70017.